NTNU – Trondheim
Norwegian University of
Science and Technology

Biosimilar Mucus as a Model System for Small Intestinal Mucus

-Evaluating the Applicability for Nanoparticle
Drug Delivery Studies

Frida Sandvik Våset

Biotechnology (5 year)
Submission date: May 2014
Supervisor: Kurt Ingar Draget, IBT
Co-supervisor: Catherine Taylor Nordgård, IBT

Norwegian University of Science and Technology
Department of Biotechnology

Preface

This master thesis was conducted at the Norwegian Biopolymer Laboratory (NOBIPOL), Institute of Biotechnology at the Norwegian University of Science and Technology (NTNU) from September 2013 to May 2014. The thesis was written in collaboration with a research group led by Professor Kurt Ingar Draget, which is part of the EU-project COMPACT. The main objective of COMPACT is to "reduce delivery and targeting bottlenecks for developing novel innovative biopharmaceutical based medicines".

First of all I would like to thank my supervisors, Professor Kurt Ingar Draget and Dr. Catherine Taylor Nordgård for great support and guidance through the project, both regarding theoretical and practical challenges. They have been very patient with me and my questions, but have also at times challenged me to think by myself, which has taught me a lot. Through the project I have learned how scientific research works in practise, the process of writing a thesis, and also things about myself. I would also like to thank Morten Johnsen Dille, Magnus Hattrem and Astrid Bjørkøy for guidance and help in the laboratory, and Camilla Marstrander Reehorst for great moral support. And last, but not least, I would like to thank my amazing family and friends, which has supported me and believed in me through the process.

NTNU, Trondheim
May 2014

_____

Frida Sandvik Våset

Abstract

Biopharmaceuticals are due to low stability often administered though injections, but for several reasons it is desirable to deliver them orally, via the gastrointestinal tract. It is possible to shield the biopharmaceuticals from the harsh environment of the gastrointestinal tract by utilizing nanoparticles as drug delivery systems (NDDS). The mucus lining the intestines creates a significant barrier for the delivery of nanoparticles to the epithelial cells. More information and knowledge on how nanoparticles interact with mucus is still needed to create NDDS that efficiently transverse this mucus barrier. Caco-2 cells, the common cell line utilized in drug absorption studies, are not compatible with native mucus. A biosimilar mucus has recently been developed that is compatible with Caco-2 and has potential as an intestinal mucous model system in drug absorption studies.

In this master thesis it was attempted to characterize the adhesion and distribution of nanoparticles on and in mucus. By running replicate experiments on pig small intestinal mucus (PSIM) and biosimilar mucus, the applicability of biosimilar mucus as an intestinal mucous model system for drug absorption studies was evaluated. It was attempted to develop a new throughput method, the plate method, which would characterize the adhesion of nanoparticles on mucus, and also allow for the testing of different variables on the mucoadhesion of the particles. The distribution of nanoparticles in and on mucus was characterized by confocal microscopy of fluorescent nanoparticles in and on the two mucous systems. Furthermore, the rheological profiles of biosimilar mucus and PSIM were investigated and compared.

The plate method looked promising up until it was detected that PSIM and biosimilar mucus gave a lot of unwanted background fluorescence, possibly due to Raman scattering. The further development of the method was terminated. The results of the distribution studies suggested that bisoimilar mucus might be an applicable mucous model system in drug absorption studies. They showed that nanoparticles distribute in biosimilar mucus and PSIM in a comparable manner, and that the biosimilar mucus did not significantly aggregate or alter the nanoparticles, which might prevent the intestinal epithelial cells from nanoparticle uptake. The nanoparticle distribution showed no specific patterns relating to the size or charge of different nanoparticles. Neither the biosimilar mucus or the PSIM were robust enough for the experimental conditions of studying nanoparticle distribution and adsorption of nanoparticles on top of the mucus, and were also too dense for the laser of the confocal microscope to penetrate properly. The rheological profile of biosimilar mucus was broadly comparable to the rheological profile of PSIM.

Sammendrag

"Biopharmaceuticals" er på grunn av en generell lav stabilitet administrert via injeksjoner, men av flere grunner er det ønskelig å levere de oralt, via mage-tarmkanalen. Det er mulig å skjerme "biopharmaceuticals" fra det tøffe miljøet i mage-tarm-kanalen ved å anvende nanopartikler som medisin-leverings-systemer (NDDS). Slimlaget i tarmen skaper en betydelig barriere for levering av nanopartikler til epitelcellene. Det er stadig behov for informasjon og kunnskap om hvordan nanopartikler samhandler med slimet for å skape NDDS som effektivt trenger gjennom slimbarrieren. Caco-2 celler er den celle-linjen som vanligvis benyttes i opptaksstudier av medisiner over tarmbarrieren, men den er ikke kompatibel med naturlig slim. Nylig har det blitt utviklet et "biosimilar slim" som er kompatibelt med Caco-2, og som har potensiale som et modellsystem for tarmslim i opptaksstudier.

I denne masteroppgaven ble adhesjonen og distribusjonen av nanopartikler på og i tarmslim forsøkt karakterisert ved å gjennomføre gjentatte forsøk på tynntarmsslim fra gris (PSIM) og biosimilar slim. Anvendelsen av biosimilar slim som et modellsystem for opptaksstudier ble vurdert. Det ble forsøkt å utvikle en ny metode, platemetoden, som karakteriserer adhesjonen av nanopartikler på slim, og som også gir muligheten til å teste hvordan ulike variabler påvirker adhesjonen til nanopartiklene. Distribusjonen av nanopartikler i og på slim ble karakterisert ved konfokalmikroskopi av fluorescerende partikler i og på de to slimsystemene. Videre ble de rheologiske profilene av biosimilar slim og PSIM sammenliknet.

Platemetoden virket lovende før det ble oppdaget at PSIM og biosimilar slim ga mye uønsket bakgrunnsfluorescence, som trolig skyldes "Raman scattering". Videre utvikling av metoden ble da terminert. Resultatene fra distribusjonsstudiene antydet av biosimilar slim kan være et brukbart slim-modellsystem i opptaksstudier av nanopartikler, da de viste at nanopartikler distribuerer seg på tilsvarende måte i biosimilar slim og PSIM. Det ble også vist at det biosimilare slimet ikke aggregerer nanopartiklene i noen stor grad, noe som kan føre til redusert partikkel-opptak av epitelcellene i tarmen. Nanopartikkel-distribusjonen viste ingen spesielle mønstre knyttet til størrelsen eller ladningen av de ulike partiklene. Verken biosimilar slim eller PSIM var robust nok for det eksperimentelle oppsettet der distribusjonen av nanopartikler ble studert på toppen av slim, og var så tett at laseren på konfokalmikroskopet hadde problemer med å trenge igjennom hele slimprøven. Den rheologiske profilen til biosimilar slim var stort sett sammenliknbar med den rheologiske profilen til PSIM.

Contents

1. Introduction

1.1 Scientific introduction

1.1.1 Biopharmaceuticals and challenges of drug delivery via the gastrointestinal tract

The pharmaceutical industry is frequently working on developing new, more efficient and safe drugs and pharmaceuticals. The last two decades there has been a growth in the interest of biopharmaceuticals, which differ from conventional medicines in several ways. Biopharmaceuticals originate from living organisms such as cells, animals or plants, and are high molecular proteins and/or nucleic acids. The majority of the market is comprised of protein products with various substituents (Crommelin et al., 2003) (Guiochon and Beaver, 2011). Insulin, for treatment of different types of diabetes mellitus, is considered the "original" biopharmaceutical (Walsh, 2005). Though still a small part of the pharmaceutical industry, biopharmaceuticals constitutes the fastest expanding sector of the market, and is likely to comprise half of the new US Food and Drug Administration (FDA) approved drugs in the near future (Staub et al., 2011). In 2012, 18 out of 44 new FDA approved drugs were biopharmaceuticals (Rader, 2013).

The advantage of biopharmaceuticals over conventional drugs is a highly selective mode of action towards the pathological target and increased safety. In general, the body handles its' own molecules better than the foreign molecules of conventional drugs, and induce less toxicity and side effects (D'Haens, 2007) (Sekhon, 2010). Even so, biopharmaceuticals generally have low solubility and low stability, which complicates the drug delivery (Ensign et al., 2012) (Grazú et al., 2012). The most common route of administration of biopharmaceuticals is through painful injections (Crommelin et al., 2003). For convenience, patient compliance and lower costs, it is desirable to deliver biopharmaceuticals via the gastrointestinal (GI) tract (Grazú et al., 2012) (Kwon et al., 2013).

1

There are however several significant hurdles to overcome in deliverance of biopharmaceuticals via the GI tract. The main function of the GI tract is digestion of food, which is not a good fit with the natural proteins and nucleic acids that biopharmaceuticals are made up of. The major challenge is the harsh environment in the stomach and intestines. The pH of the stomach is 1-2.5, while the pH in the small intestines is 6.6-7.5 (Galindo-Rodriguez et al., 2005). Furthermore, the gastric fluids of the stomach contain hydrochloric acid and pepsin, which degrade proteins. The small intestines contain bile salts and pancreatic juices that contain an array of enzymes that degrade proteins, fats and carbohydrates (Galindo-Rodriguez et al., 2005).

In addition, the mucus layer lining the epithelial surfaces of the GI tract creates a considerable barrier to the delivery of biopharmaceuticals, conventional drugs and nanoparticle drug delivery systems (NDDS) (Ensign et al., 2012) (Grazú et al., 2012). Mucus has a constant turnover rate, which means that pharmaceuticals have to diffuse "upstream" in the mucus layer. This contributes to low bioavailability of many drugs (MacAdam, 1993) (Bhat et al., 1995). Mucus and its' properties will be discussed next, before returning to the challenge of delivering biopharmaceuticals via the GI tract.

1.1.2 Mucus

Mucus is a biological secretion consisting of water (~95 %), mucin glycoproteins, other proteins, lipids, inorganic salts, carbohydrates, antibodies, bacteria and cellular debris (Smart, 2005) (Ensign et al., 2012). Mucus covers the epithelium of all the organs and surfaces of the body that is exposed to the external environment, and is often the first contact point when pharmaceuticals are entering the body (Bansil and Turner, 2006) (Kwon et al., 2013). Mucus is synthesized by goblet cells in single layer epithelia, or salivary glands in multi-layered/stratified epithelia, which secretes mucus onto the epithelial surface (Smart, 2005).

The main function of mucus in the GI tract is to serve as a semipermeable barrier. It protects the exposed epithelial surfaces by trapping pathogens, and clears them out through faecal elimination (Ensign et al., 2012) (Kwon et al., 2013). At the same time the mucus barrier in the intestines allows rapid passage of selected ions, gasses, nutrients and some proteins (Lai et

2

al., 2009b). Furthermore, the mucus layer is an excellent lubricant, as it enables the transit of digestive material, protects the epithelia from mechanical stress and keeps it hydrated (Atuma et al., 2001) (Bansil and Turner, 2006).

In one day a human being secretes almost 10 litres of mucus into the GI tract, where most of it is digested and reused (Cone, 2009) (Kwon et al., 2013). The composition of mucus is continuously regulated, which in turn affects physiological and protective properties of the mucus (Cone, 2005). The thickness of the mucus in the GI tract varies from 50-300 µm (Ensign et al., 2012), where the thickest layer can be found in the stomach and the colon (Lichtenberger, 1995).

1.1.2.1 Mucins and the mucus gel network

The main components of mucus are the mucin glycoproteins, which make up about 2-5 % of the wet weight of mucus (Bansil and Turner, 2006). So far there has been found at least 20 different genes coding for different mucin glycoproteins, expressed in different tissues of the body. These constitute the *MUC* gene family (Bansil and Turner, 2006). Normal GI tract mucus contains mucins coded by MUC2, MUC5AC, MUC5B, MUC6 and MUC19 (Antoni et al., 2013). Different mucins are classified by their protein backbone (Rose and Voynow, 2006).

Mucin monomers have a long and flexible protein backbone, consisting of tandem repeats of proline, threonine and/or serine residues. The backbone is heavily glycosylated through O-glycosylation of short hydrophilic glycans (Cone, 2009) (Lai et al., 2009a), which contains sialic acids and sulphate groups, giving the mucins an overall negative charge (Lichtenberger, 1995). The regions coated with negatively charged glycans are interspersed by naked hydrophobic regions rich in cysteins, which gives the naked regions a globular shape (Cone, 2005) (Lai et al., 2009b). The terminal ends of the mucin monomers are also rich in cysteins, enabling polymerization of mucin monomers via disulphide bonds (Cone, 2009). The mucin polymers range from 10 to 40 MDa in size (Lai et al., 2009a). The structure of mucins is illustrated in Figure 1.1.
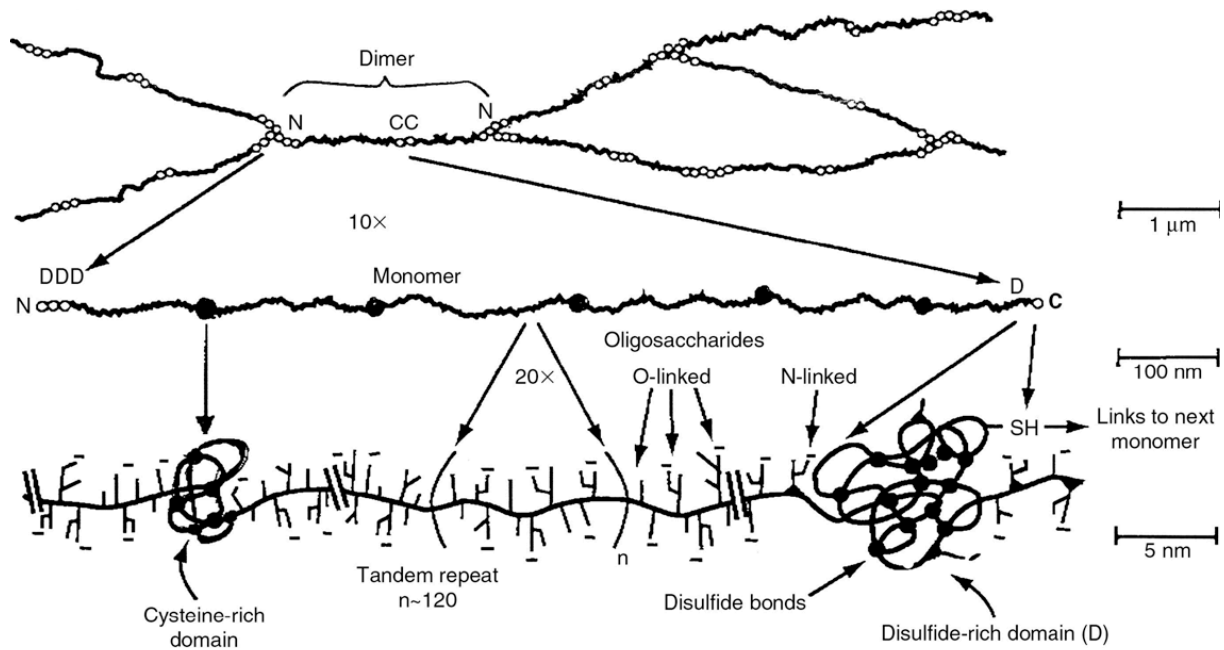
Figure 1.1 The structure of mucin at different magnifications, indicated to the right (Cone, 2009).

In the presence of water mucins starts to overlap, interpenetrate and form a mesh network, which leads to gelation (Kočevar-Nared et al., 1997). Although several models have been suggested, the exact structure of the gel matrix of mucus is still not clear. Mucins are assumed to be the main contributors to the structure of the gel matrix (Sellers et al., 1991) (Taylor et al., 2005a), but the non-mucin components of the mucus, like other proteins, lipids and nucleic acids are also thought to play a role (Taylor et al., 2003). The mechanism behind this is somehow uncertain. An array of various interactions that flicker on and off is assumed to contribute to the formation of the mucus gel structure, like hydrophobic bonds, electrostatic and ionic interactions, H-bonds and van der Waals interactions. These are assumed to occur both between the carbohydrate side chains and the hydrophobic regions of the mucin molecules (Kočevar-Nared et al., 1997) (Cone, 2009). Taylor and colleagues (Taylor et al., 2003) showed that the gel network consists of both transient and non-transient interactions. It was also indicated that an equilibrium exists between molecules or parts of molecules involved in gelation, and molecules or part of molecules not involved in gelation, leading to "dangling chain ends" (Taylor et al., 2003).

The interactions of the mucin polymers and the non-mucin components of the mucus not only contribute to the gelling of the mucus, but also contribute to physical properties like adhesiveness (mucoadhesion) and viscoelasticity. Adhesiveness makes mucus stick to most

surfaces and small particles due to the range of low affinity bonds that flicker on and off between the mucin fibres and surface/particle(Cone, 2005) (Bansil and Turner, 2006).

The various interactions in the mucin mesh resists flow, and contributes to giving mucus rheological viscoelastic properties (Kočevar-Nared et al., 1997), which means is has both viscous and elastic behaviour in response to an applied force (Girod et al., 1992) (Smidsrød and Moe, 2008). Appropriate viscoelastic properties are crucial for the functions of GI tract mucus. Dominant viscoelastic behaviour maintains the protective barrier the mucus layer constitutes, and rheological reversibility makes sure that mucus can be reused. Rheological reversibility includes shear thinning, where the rheological properties are dependent on strain or shear, and thixotropy, where the rheological properties in addition to being dependent on strain or shear, also are dependent on time (Girod et al., 1992) (Barnes, 1997) (Moller et al., 2006) (Ensign et al., 2012). The viscoelastic properties are regulated primarily by the mucin content, but also by the ion, lipid and water content of the mucus (Ensign et al., 2012).

1.1.3 Nanoparticles and nanoparticle drug delivery systems

The mucus lining the GI tract is a complex material, and constitutes a significant hurdle in the oral delivery of biopharmaceuticals. One solution that might overcome this hurdle, and at the same time deal the challenge of the harsh environment in the GI tract, could be utilization of nanoparticles (Ensign et al., 2012).

Nanoparticles are particles in the size range of 10^{-9}-10^{-7} meters, and they have been thoroughly studied as potential drug delivery systems (NDDS) the past few decades (Orive et al., 2004). The first nanoparticle drug delivery system was approved on the market in 1995, and since then numerous others have been accepted (Grazú et al., 2012). Nanoparticle drug delivery systems come in many designs; from organic liposomes, polymer-drug conjugates and dendrimers to inorganic nanoparticles such as carbon nanotubes, metals, silica and semiconductor quantum dots. Nanoparticles for medical applications are defined as particles with a size between 1 and 1000 nm (Grazú et al., 2012).

Nanoparticle drug delivery systems have great potential as vectors of biopharmaceuticals because of the many advantages they offer. They have better bioavailability than most pharmaceuticals because of enhanced water solubility and small size, which enhance interactions with cell membranes and proteins in the same size range. Nanoparticles are very applicable, and can be engineered with coatings or ligands that e.g. prolong circulation in the blood system, target the particle to a specific organ, cell or organelle, or enhance drug release control at the target site. As a result of the specific targeting the drug dose can be lowered, which reduces side effects and is more cost-efficient (Orive et al., 2004), (Grazú et al., 2012) (Laroui et al., 2012).

Regarding the obstacles of biopharmaceutical delivery via the GI tract, polymer and lipid nanoparticle carriers could be designed to entrap the biopharmaceutical. Entrapment in a suitable nanocarrier would protect the pharmaceutical from the harsh environment and degradable enzymes in the GI tract (Wong, 2010) (Ensign et al., 2012). Different coatings could also target the nanoparticles to the small intestine (Grazú et al., 2012).

Assuming the nanoparticles are shielded from the harsh environment of the GI tract, there are three possible routes they can take (Florence, 1997) (Ponchel and Irache, 1998); (i) Direct transit through the system, ending in faecal elimination. (ii) Adherence of particles to the mucin molecules (mucoadhesion), followed by mucus clearance and faecal elimination. (iii) Transport or diffusion across the mucus barrier (through the mucin matrix) where uptake of the particles takes place through the M-cells in the Peyers patches, isolated follicles of the gut-associated lymphoid tissue and/or via the normal intestinal enterocytes (Florence, 1997). Transport across the mucus layer and particular uptake is affected by factors like particle size, ionization/surface charge, hydrophobicity and the presence or absence of surface ligands (Florence, 1997) (Norris and Sinko, 1997). The majority of nanoparticles typically undergo direct transit through the GI tract (Lai et al., 2009a).

To avoid immediate clearance the nanoparticles has to interact with the mucus surface. This increase the residence time at the mucosal surface and increase the NDDS concentration gradient over the mucus layer (Ponchel and Irache, 1998) (Lai et al., 2009a). Some of the obstacles currently being worked with are designing nanoparticle drug delivery systems that can diffuse faster through the mucus mesh, or break the mucus barrier (Ensign et al., 2012).

1.1.4 Absorption studies and mucous model systems

The faith of nanoparticles in the intestines is studied in nanoparticle drug delivery studies, or more generic; absorption studies. Caco-2 is a cell line that cultured under specific conditions, resembles the enterocytes that lines the small intestines, and is the standard cell line utilized in absorption studies of drugs over the epithelial surfaces of the intestines (Hidalgo et al., 1989) (Boegh et al., 2014). Caco-2 cells do not produce mucus, and has to be supplemented with mucus in order to get a representative *in vivo* small intestine situation (Boegh et al., 2014).

The mucins and mucus of pig stomachs has been widely studied as a mucous model system, because of the similarities in anatomy and physiology between pigs and human stomachs. Furthermore, there is a similarity in the sequence of the pig gastric mucin and the human gastric mucin MUC5AC (Celli et al., 2005). It has also been shown that mucus from the stomach and the small intestine has similar viscoelastic behaviour and properties (Sellers et al., 1991) (Lai et al., 2009b). Consequently, extracted mucus from the stomachs or intestines of pigs could have been a good alternative for utilization together with Caco-2 cells in drug absorption studies.

However, pig small intestinal mucus (PSIM) or pig gastric mucus is not suited for utilization together with the Caco-2 cells for various reasons. The main reason is poor compatibility between the cells and the mucus because the mucus disrupts the monolayer of Caco-2 cells (Bøgh et al., 2013) (Boegh et al., 2014). Also, it is challenging working with native mucus, as the samples are inhomogeneous and contains various amounts of contaminants expected to be found in the intestines, like undigested food, debris, luminal fluids, degradable enzymes etc. (Groo and Lagarce, 2014). Native mucus samples often show a lot of variation both in content and properties from different physiological sites, between individuals and between species. Furthermore, certain collection methods are known to e.g. stimulate water secretion, altering the mucus' properties (Girod et al., 1992) (Groo and Lagarce, 2014).

Researches at the University of Copenhagen have in connection with the EU-project, COMPACT, developed a biosimilar mucus with inspiration from Lahred et al. (Larhed et al., 1998). The biosimilar mucus was originally developed for cell compatibility with the CaCo-2

cells for "assessment of the effect of mucus on drug adsorption" (Bøgh et al., 2013). The viscoelastic properties have also been optimized for a comparable rheological profile with pig intestinal mucus (Bøgh et al., 2013) (Boegh et al., 2014). The main components of the biosimilar mucus are Sigma pig gastric mucins type II: crude, high molecular weight polyacrylic acid (PAA), lipids and bovine serum albumins (BSA) (Bøgh et al., 2013).

Besides the compatibility with Caco-2 cells, the biosimilar mucus has several advantages compared to native mucus. The artificial mucus mixture is homogenous and hence presents a more stable model system, avoiding the contaminations and variations found in native mucus. It is readily made in sufficient amounts in the laboratory; it does not require expensive or complicated equipment, and is made from relatively cheap commercially available chemicals.

1.2 Aim of the thesis

The aim of the thesis is to investigate how nanoparticles interact in and with mucus, by characterizing the adhesion and distribution of different sized and charged nanoparticles in and on pig small intestinal mucus (PSIM) and biosimilar mucus. The overall goal is to get an increased understanding of how nanoparticle drug delivery systems might be utilized in delivering biopharmaceuticals via the gastrointestinal tract, and evaluate the applicability of biosimilar mucus as a model for small intestinal mucus in nanoparticle drug delivery studies.

The main focus is to develop a new high throughput method of characterizing the adhesion of different sized and charged nanoparticles on PSIM and biosimilar mucus, where different variables can be incorporated to check how they affect the mucoadhesion of the particles. The method is an attempt to mimic the intestinal situation *in vivo*. The distribution of different nanoparticles on and in PSIM and biosimilar mucus will also be investigated for an increased understanding of the nanoparticles' encounter with mucus, and how mucus interacts with the nanoparticles as a function of charge and size.

Working with both PSIM and biosimilar mucus will give a better understanding of the differences and similarities between the two mucous model systems regarding the adhesion and distribution of nanoparticles. In this way the applicability of biosimilar mucus in that

particular area of absorption studies can be evaluated. Furthermore, the rheological profile of the biosimilar mucus is to be characterized and compared to the rheological profile of the PSIM. The biosimilar mucus has been developed to produce a comparable rheological profile to PSIM, but it is desirable to further investigate the similarities and differences of the rheological profiles of the two mucous systems by looking at other rheological parameters than what has previously been described (Bøgh et al., 2013). This will give a better basis for evaluation of biosimilar mucus.

The next section gives an introduction to the principles behind the scientific techniques utilized for the investigation of distribution and adhesion of nanoparticles on mucus and rheological measurements on mucus.

1.3 Technical introduction

1.3.1 Fluorescence and scientific methods utilizing fluorescence

The characterizing of how nanoparticles adheres to and distributes on and in mucus requires methods to image and detect the nanoparticles. Fluorescent nanoparticles are suitable for this task, as fluorescence has high sensitivity toward detection (Lakowicz, 2006), and can be utilized both for imaging by confocal microscopy (distribution studies) and fluorescence intensity measurements by a plate reader (adhesion studies).

1.3.1.1 Introduction to fluorescence

Luminescence is the phenomena of emission of light from a given material. This happens when "disturbing" energy is absorbed and causes the excitation of loosely held electrons. The excited electron is in an unstable state, and returns to the more stable ground state by emitting a photon, detected as luminescence. Dependent on the lifetime, luminescence is divided into two categories; phosphorescence and the more common fluorescence (Lakowicz, 2006) (Henderson et al., 2009). The lifetime of luminescence is defined as the average time between the excitation of an electron and the return to the ground state. The fluorescence lifetime is from 1 to 100 nanoseconds, and the lifetime of phosphorescence is typically from

milliseconds to seconds (Lakowicz, 2006) (Henderson et al., 2009). The concept of fluorescence is illustrated by a Jakobski energy diagram in Figure 1.2.
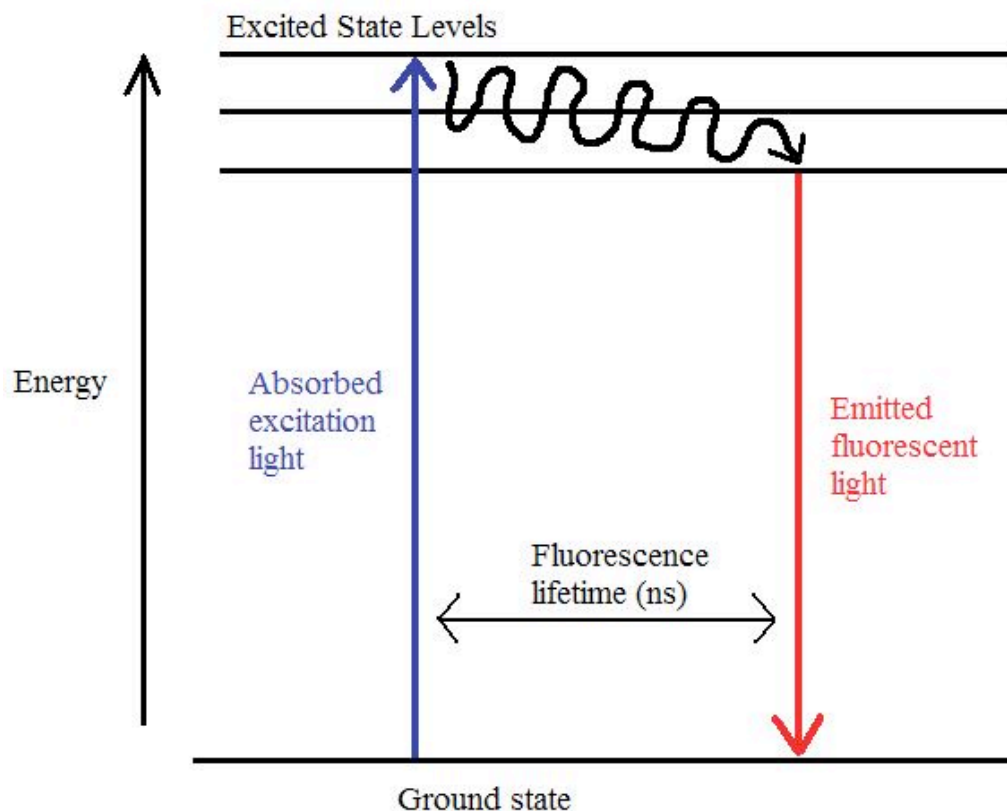
Figure 1.2 A Jakobski energy diagram, explaining the concept of fluorescence. Excitation light is absorbed by an electron, causing it to gain energy and jump to an excited, unstable state. During the short excitation period some energy is dissipated by molecular collisions or transferred to a nearby molecule. The remaining energy is emitted as a photon to relax the electron back to the stable ground state. Modified from (Snider, 2013).

Fluorescence is normally emitted from aromatic molecules, collectively termed fluorophores. The emission wavelengths are characteristic for the specific molecular conformation of each fluorophore. Emission data are usually presented by emission spectra where the intensity of the fluorescence is plotted against wavelength, so that the emission maxima can be found. Generally the same emission spectrum is obtained regardless of the excitation wavelength. The energy of the absorption is higher than the energy of the emission (called a Stokes shift), and is the reason a substance is excited by high-energy waves/radiation and emits photons of lower wavelengths (Lakowicz, 2006).

Fluorescence has high sensitivity towards detection, and the utilization of fluorescence technology has within the three last decades had a dramatic growth in many scientific disciplines. This includes methods and techniques like fluorescence spectroscopy, time-resolved fluorescence, flow cytometry, fluorescence imaging, genetic analysis, DNA sequencing etc. (Lakowicz, 2006).

1.3.1.2 Laser scanning fluorescence confocal microscopy

Laser scanning fluorescence confocal microscopy, short: confocal microscopy, is an imaging technique used to obtain sharp in focus images. Conventional fluorescence microscopes continuously illuminate the whole depth of the sample, and detect emitted light from the focal plane of interest in addition to all the out-of-focus light. Confocal microscopy differs from conventional fluorescence microscopes by its ability to focus all the light in one spot in a focal plane of interest, and filter away light that is not in focus using optical pinholes (Földes-Papp et al., 2003) (Furrer and Gurny, 2010).

During imaging a laser is filtered through a pinhole, and reflected off dichromatic mirrors through an objective. The objective focuses the light in a specific point in the plane of interest of the fluorescent sample and excites the fluorophores. The fluorescence light is emitted back through the lens, and filtered through a pinhole that is located in a conjugate plane right in front of a photomultiplier/detector. Only the light reflected from the focal plane is detected because the light coming from other planes in the sample cannot pass through the selective pinhole. The smaller the pinhole is, the less out-of-focus light reaches the detector. The pinhole eliminates out of focus objects or blur that will occur in an image from a conventional fluorescence microscope, and makes it possible to obtain sharp images from thicker samples. As all the light is focused into one spot, the entire sample has to be scanned in order to obtain a complete 2D or 3D image (Földes-Papp et al., 2003) (Furrer and Gurny, 2010). A schematic presentation of the principle behind confocal microscopy is presented in Figure 1.3.
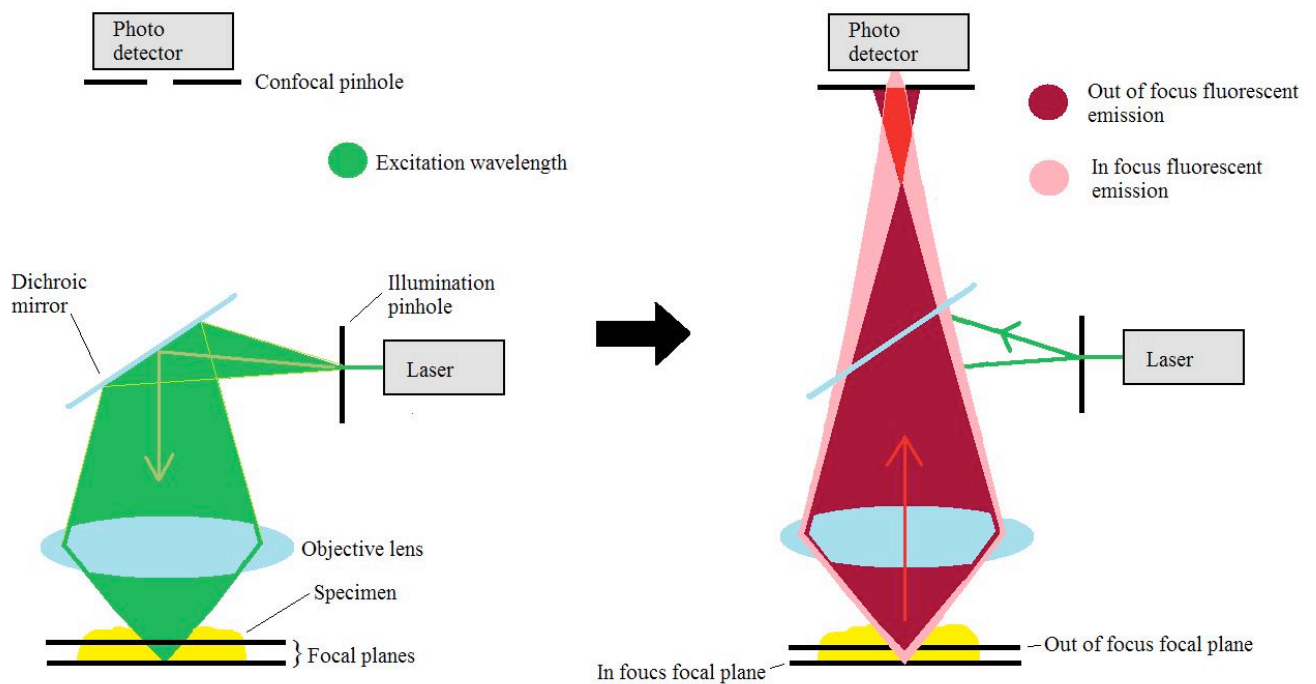
Figure 1.3 The principle behind a laser scanning fluorescence confocal microscopy. A laser is filtered through a pinhole, reflected off dichromatic mirrors (for convenience only one mirror is shown) and through an objective. The objective focuses the light in a specific point in the plane of interest of the fluorescent sample and excites the fluorophores (left). The emission light is reflected back through the lens, and filtered through a pinhole that is located in a conjugate plane right in front of a photodetector. This eliminates out of focus light and blur (right). Modified from (BIOimaging, 2008).

1.3.1.3 Plate reader

A plate reader is an instrument for performing high-throughput screening of multiple samples. Samples are distributed in wells of microtitrer plates, which commonly have 6, 24, 96, 348, or 1536 wells arranged in a rectangular matrix of ratio 2:3. Plate readers most commonly perform different kinds of fluorescence measurements, absorbance measurements, and some can also handle light scattering (Lakowicz, 2006) (Jameson and Ross, 2010).

During measurement the microtitrer plate with samples are put inside the reader. The light source of the emission light is commonly a xenon flash lamp. The light is directed through an excitation monochromator, selecting the desired excitation wavelength. One or more dichromatic mirrors reflect the excitation light through an objective and into the sample,

either from the top of the plate or the bottom of the plate (only for transparent plates). The objective adjusts the excitation light to the desired focal point of the sample, finding the correct z-position. The emission light from the excited sample is directed trough an emission monochromator and into the fluorescence detector system by the same mirror transmitting the excitation light. A simplified sketch of the optics of a plate reader is presented in Figure 1.4. The microtitrer plate is moved in the correct xy-position for measurement of the individual samples in the wells (Lakowicz, 2006) (Jameson and Ross, 2010).
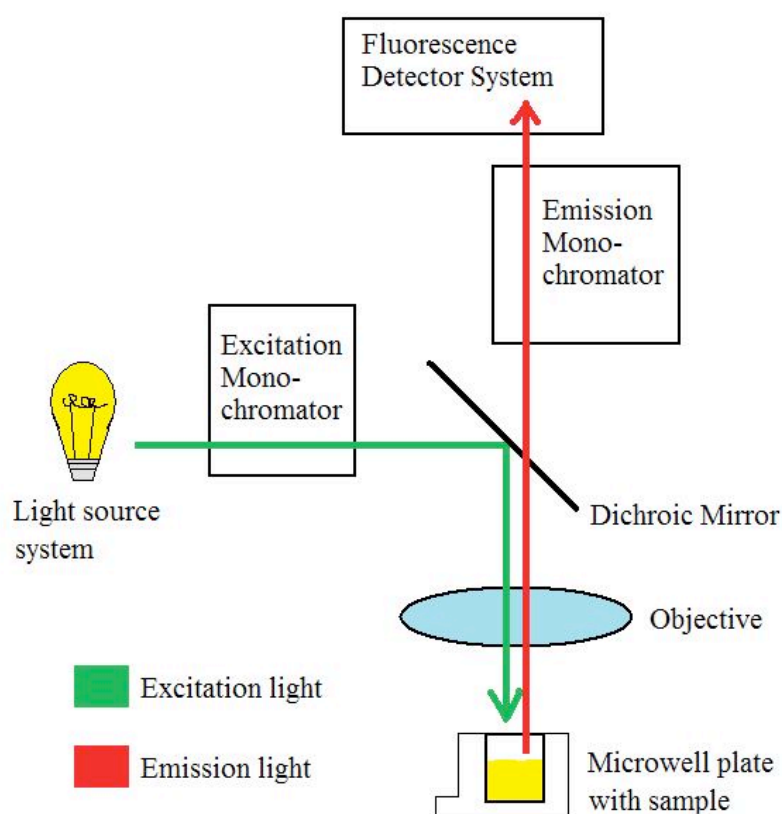
Figure 1.4 The optics behind a plate reader. A light source emits light going through an excitation monochromator, selecting the desired wavelength of the excitation light. The excitation light is reflected in dichromatic mirrors, directing the light through an objective adjusting the correct z-position and into the sample. From the excited sample the emission light is directed through the same dichromatic mirror, through and emission monochromator selecting the desired emission wavelengths and into the fluorescence detection system. Modified from (Jameson and Ross, 2010) (Tecan Austria GmbH, 2010).

1.3.2 Rheology

Rheology is the science of flow and deformation of materials (Picout and Ross-Murphy, 2003) (Wagner Jr et al., 2014). Rheological measurements quantify the elastic and viscous properties of a material, and thus give information about the materials' behaviour (Wyss et al., 2007). Viscous properties are connected to loss of energy. In response to an applied force a viscous material will flow and deform. When the force is removed, the material will keep its' new shape (Smidsrød and Moe, 2008). Elastic properties are linked to the storage of energy. In response to an applied force an elastic material will deform, and the energy will be stored in the material. When the force is removed the material will regains its' original shape. Viscoelastic materials show a combination of these two behaviours (Smidsrød and Moe, 2008).

Dependent on the time scale of the rheological experiment, all materials can behave either as solids or liquids (Picout and Ross-Murphy, 2003). At very long time scales solid materials, e.g. glass, can flow as liquids under a prolonged stress, and at very short time scales (or at very high frequencies) fluid materials behave as solids. The quantity of viscous to elastic behaviour in a material is thereby determined by the time scale of the experiment (Picout and Ross-Murphy, 2003). Viscoelastic properties of a material can be quantified by e.g. oscillatory rheological measurements (Wyss et al., 2007).

1.3.2.1 Oscillatory measurements and rheometer set-up

For biological liquids and gels, the cone and plate rheometer is most commonly used, in combination with oscillatory measurements (Lai et al., 2009b). Small deformation oscillatory measurements is non-destructive, and provide information about viscosity and elasticity of a material without changing the structure made up of non covalent bonds (Kočevar-Nared et al., 1997). The oscillating cycle corresponds to a sinusoidal curve, where the applied strain is the amplitude and the frequency is the wavelength (Zhong and Daubert, 2013). During a rheological measurement with cone and plate geometry, a sample is put on top of a plate and a shallow inverted cone is lowered on top of the sample (Lai et al., 2009b). The cone oscillates

at predetermined rates, and the plate is stationary while measuring the torque (Wagner Jr et al., 2014). Figure 1.5 illustrates the plate and cone set-up.
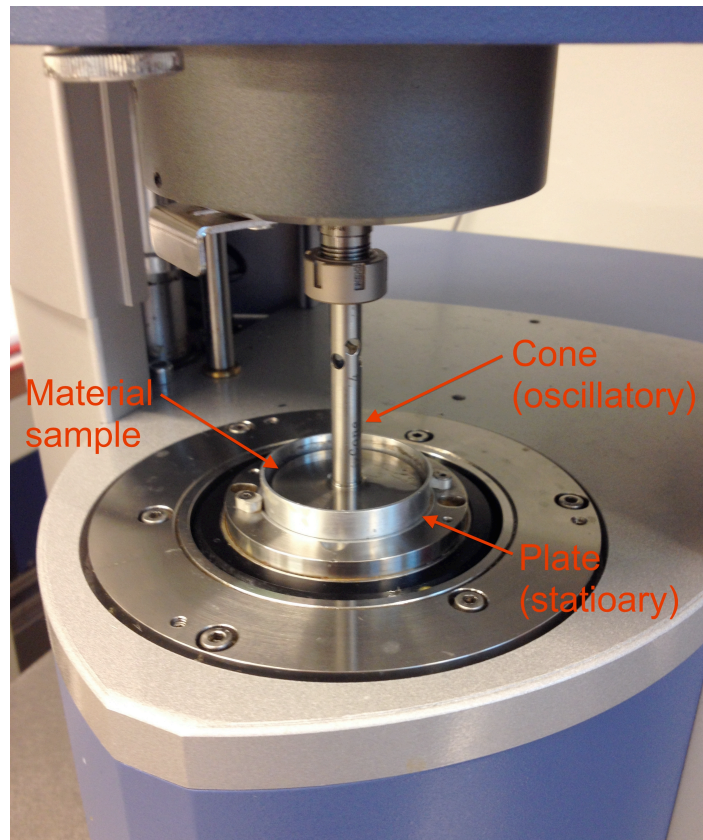
Figure 1.5 The set-up of a rheometer. The material sample is put on the plate and the cone is lowered on top of it before the measurements starts.

The strain/amplitude and frequency of the measurement is known, and the rheological measurement finds the relationship (phase lag) between stress and strain from the applied strain and the measured torque, see Figure 1.6. From this relationship rheological variables like phase angle, apparent viscosity, storage and loss moduli describing the viscoelastic behaviour of the sample is found (Lai et al., 2009b) (Zhong and Daubert, 2013).
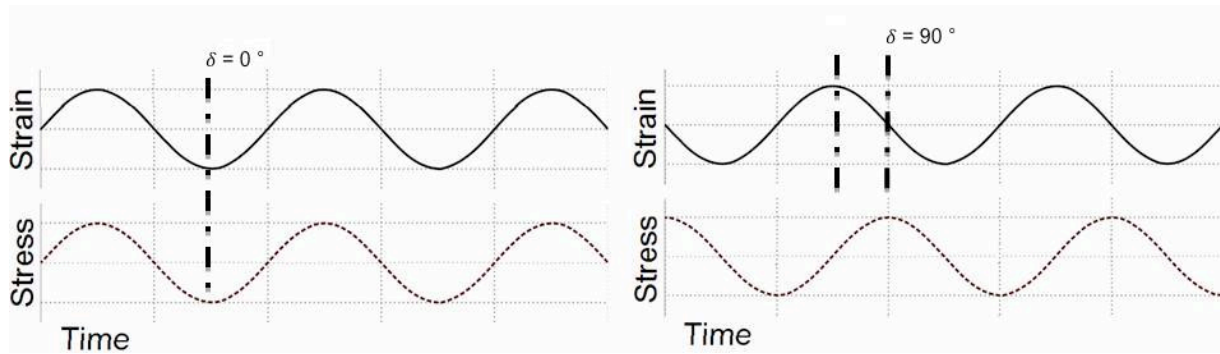
Figure 1.6 The phase lag between the stress and strain waves of a perfectly elastic material (left) and a perfectly viscous material (right). A perfectly elastic solid will immediately respond to the stress, and the phase angle between the two waves is 0 °. A perfectly viscous material will have a strain wave that is 90 ° out of phase with the stress wave. A viscoelastic material will behave in between these two extremes. Modified from (Society of Plastics Engineers, 2012).

The phase lag between the sinusoidal wave of the applied strain and the resultant stress wave, or vice versa, is quantified by the phase angle, δ, which gives the relationship between the storage modulus (G') and the loss modulus (G'') (Girod et al., 1992). A perfectly elastic material respond to the strain immediately, and the stress wave will be exactly in phase with the strain wave, giving a phase angle of 0° (Zhong and Daubert, 2013). For a perfectly viscous liquid the stress wave would be 90° out-of-phase with the strain wave (Picout and Ross-Murphy, 2003). For a viscoelastic material the phase angle will have values between 0° and 90°. If 0° < δ < 45° the storage modulus (G') has greater values than the loss modulus (G''), and the material will show a more solid like, than liquid like, behaviour. If 45° < δ < 90° the loss modulus (G'') has greater values than the storage modulus (G'), and the material will show a more liquid like behaviour (Smidsrød and Moe, 2008). However, this is frequency dependent, and different pre-set frequencies of the measurements may yield different behaviour of samples (Lai et al., 2009b).

The relationship between the phase angle (δ), storage modulus (G'), loss modulus (G'') and the complex shear modulus (G*) is explained by equation 1 and equation 2, and illustrated in Figure 1.7 (Picout and Ross-Murphy, 2003). The meaning of the different rheological parameters is explained in the next section.

16

$$\tan \delta = G''/G' \tag{1}$$

$$G^* = (G'^2 + G''^2)^{1/2} \tag{2}$$
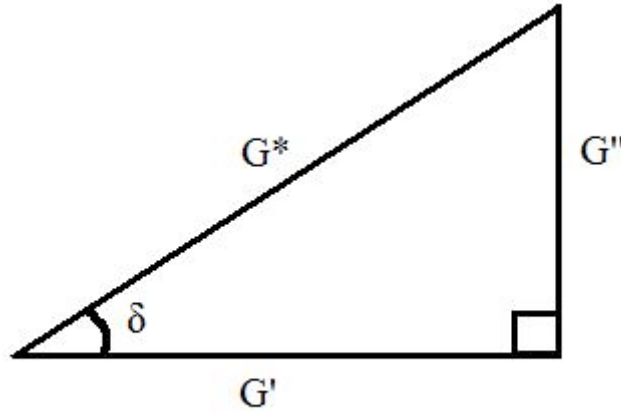
Figure 1.7. The relationship between the storage modulus (G'), the loss modulus (G''), the complex shear modulus (G*) and the phase angle (δ). Modified from (Chaplin, 2012).

1.3.2.3 Important rheological variables

Rheological measurements yield a lot of data of from various rheological variables. The following list explains in more detail the meaning behind the rheological variables considered most important for this thesis.

- Stress, τ, is defined as the force acting per area, and has the unit Pascal (Pa). Stress produces a deformation or strain (Picout and Ross-Murphy, 2003) (Zhong and Daubert, 2013).

- Strain, γ, is defined as the amount of deformation relative to the original dimensions. Stain in dimensionless (Picout and Ross-Murphy, 2003) (Zhong and Daubert, 2013).

- The loss modulus or viscous modulus, G'', is a measure of the viscous component of flow. It characterizes the fluid-like contributions to the measured stress response. The higher the value of G'' is, the more liquid-like is the behaviour of the material (Smidsrød and Moe, 2008) (Wagner Jr et al., 2014).

- The storage modulus or the elastic shear modulus, G', is a measure of the recoverable portion of the elastic deformation. It characterizes the solid-like contributions to the measured stress response. A high value of G' indicates high elastic properties of a material (Wyss et al., 2007) (Wagner Jr et al., 2014).

- The phase angle, δ, is a measure of the phase difference between the applied strain wave and the resultant stress wave, or vice versa, and gives the relationship between the loss modulus (G'') and the storage modulus (G') (Picout and Ross-Murphy, 2003).

- The complex shear modulus, G*, is the ratio of the stress amplitude to the imposed strain amplitude, or vice versa (Picout and Ross-Murphy, 2003).

1.3.2.3 Rheological measurements

1.3.2.3.1 Strain Sweeps

The stability of a material can be determined by running a strain sweep, where oscillating strains of increasing/decreasing values are applied to a material at a fixed frequency (Zhong and Daubert, 2013). The log-log plot where the rheological variables are plotted against the strain can be divided into two regions; (1) the linear viscoelastic region where the strain is not affecting the entanglements, interactions and bonds of the material and (2) a region where the imposed strains starts to disentangle and break interactions and bonds in the material (Zhong and Daubert, 2013). The linear viscoelastic region is recognized by a horizontal, or even slightly convex graph of the rheological parameters, and ends when the absolute values of the parameters start to decrease (Zhong and Daubert, 2013), see Figure 1.8. The information of which strains are within the linear viscoelastic region is utilized in a succeeding frequency sweep on the same sample, to ensure that the frequency sweep is run under non-destructive conditions.
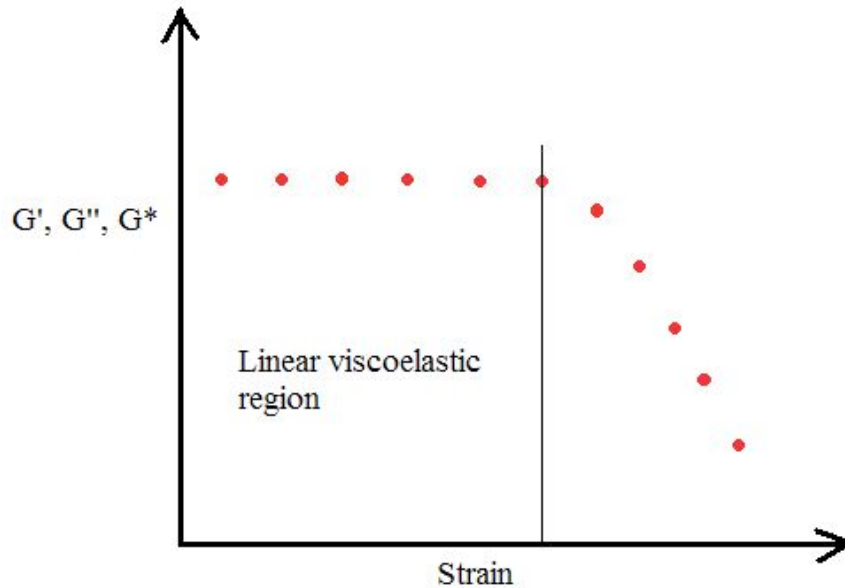
Figure 1.8 An illustration of the appearance of a strain sweep used to determine the linear viscoelastic region of a material. In the linear viscoelastic region the rheological variables are independent on the applied strain. Modified from (Zhong and Daubert, 2013).

1.3.2.3.2 Small deformation frequency sweeps

A frequency of an oscillation is the reciprocal of the time it takes for the cone to complete an oscillating cycle of the sinusoidal curve (Zhong and Daubert, 2013). Frequency sweeps gives information about the mechanical spectra of a material, which is the frequency dependency of the materials behaviour. In a frequency sweep the strain or stress is fixed at a value within the linear viscoelastic region, and the cone is set to oscillate at increasing frequencies (most commonly) (Zhong and Daubert, 2013). A change of frequency from low to high corresponds to a change in the wavelength of the sinusoidal curve from long to short. Since the changing variable of a frequency sweep is the frequency of the oscillation, the behaviour seen in a frequency sweep is due to time dependent effects of different types of entanglements, links and interactions in the material. In addition, the relationship between the storage modulus (G') and loss modulus (G'') can tell if the material should be classified as a gel, concentrated solution or diluted solution (Zhong and Daubert, 2013). For gels, like mucus, the absolute values of the storage modulus (G') is greater than the absolute values of the loss modulus (G'') (Zhong and Daubert, 2013).

2. Materials & Methods

2.1 Materials

2.1.1 Nanoparticles (FluoSpheres®)

Polystyrene based fluorescent nanoparticles (FluoSpheres®) from Invitrogen (Paisley, UK), provided in 2 % aqueous solutions, utilized in the distribution experiments are together with their properties summarized in Table 2.1 and Table 2.2. The nanoparticles utilized in the development of the plate method are together with their properties summarized in Table 2.3.

The PEGylated particles are carboxylate-modified 200 nm yellow-green FluoSpheres® coated with polyethylene glycol (PEG) by Morten Johnsen Dille. The particles have a calculated zeta-potential of -10.92 mV.

Table 2.1 The nanoparticles mixed into and put on top of PSIM and biosimilar mucus samples during the distribution experiments.

Surface (charge)	Size (diameter)	Colour	Excitation/emission maxima (nm)
Carboxylate-modified (-)	200 nm	yellow-green	505/515
Carboxylate-modified (-)	100 nm	yellow-green	505/515
Carboxylate-modified (-)	1 μm	yellow-green	505/515
Amine-modified (+)	200 nm	yellow-green	505/515
Amine-modified (+)	100 nm	yellow-green	505/515
PEGylated (-)	200 nm	yellow-green	505/515

Table 2.2 The nanoparticles mixed into Sigma mucin solutions and dissolved pig gastric mucin in the distribution experiments.

Surface (charge)	Size (diameter)	Colour	Excitation/emission maxima (nm)
Carboxylate-modified (-)	200 nm	yellow-green	505/515
Carboxylate-modified (-)	100 nm	yellow-green	505/515
Amine-modified (+)	200 nm	yellow-green	505/515

Table 2.3 The nanoparticles utilized in the development of the plate method.

Surface (charge)	Size (diameter)	Colour	Emission/excitation maxima (nm)
Carboxylate-modified (-)	200 nm	yellow-green	505/515
Carboxylate-modified (-)	200 nm	red	580/605

2.2.2 FluoroNunc™ microtitrer plates

The microtitrer plates utilized in the plate method were of the type FluoroNunc™ 96-well black plates, coated with MaxiSorp™ (Thermo Scientific, VWR International). The plates had a recommended working volume of 350 μL.

2.2.3 Glass chambers

The chambered coverglass utilized in the distribution experiments were of the type Lab-Tek® Chambered #1.0 Borosilicate Coverglass System (Thermo Fisher Scientific Inc., New York, USA). There were 8 chambers/wells on each slide with an area of 0.8 cm^2 and a recommended working volume of 0.2-0.4 mL.

2.2.4 Sample preparations

2.2.4.1 Pig small intestinal mucus

Pig small intestinal mucus (PSIM) was collected from pig intestines, delivered by Gilde slaughterhouse in Steinkjer, from newly slaughtered pigs. The intestines were cut open, and the mucus carefully scraped off with a spatula. The mucus was divided in aliquots, and stored in a -18 °C freezer. The mucus was thawed on the lab bench before utilization.

2.2.4.2 Biosimilar mucus

Biosimilar mucus was prepared according to a protocol optimized at the University of Copenhagen (Boegh et al 2013). A lipid mix were made by mixing linoleic acid (0.11 % (w/v)) (Sigma Aldrich co., St.Louis, USA), cholesterol (0.36 % (w/v) (Sigma Aldrich co., St.Louis, USA) and phosphatidylcholine (0.18 % (w/v)) (Sigma Aldrich co., St.Louis, USA) in an eppendorf tube and then adding polysorbate 80 (0.163 % (w/v) (Sigma Aldrich co., St.Louis, USA). An isotonic 10 mM HEPES buffer (Sigma Aldrich co., St.Louis, USA) containing 1.3 mM $CaCl_2$ (Merck KGaA, Darmstadt, Germany), 1.0 mM $MgSO_4$ (Merck, Darmstadt, Germany) and 137 mM NaCl (Merck KGaA, Darmstadt, Germany) were added and the mixture stirred with a magnetic mixer until homogeneity occurred. In another container high molecular polyascorbic acid (PAA) (0.9 % (w/v)) (Reckitt & Coleman Products, Kingston Upon Hull, UK) was dissolved in portions in 10 mM HEPES buffer containing 1.3 mM $CaCl_2$ and 1 mM $MgSO_4$ under magnetic stirring. Sigma porcine gastric mucin type II: crude (5 % (w/v)) (Sigma Chemical co., St.Louis, USA) were stirred into the polymer mixture in portions, and 15 µL of 5 mM NaOH were added for each mL mucus made to increase the pH. Under magnetic stirring, bovine albumin serum (3.1 % (w/v)) (Sigma Chemical co., St.Lous, USA) was added followed by the addition of the lipid mixture. The amount of lipid mixture to polymer solution was 1:9. The pH was adjusted to 7.4 using NaOH. Before utilization the biosimilar mucus were stored at 4 °C over night.

2.2.4.3 Pig gastric mucin

Purified pig gastric mucins were obtained from Professor J.P. Pearson at Institute for Cell and Molecular Biosciences, University of Newcastle upon Tyne. The purification protocol is listed in Appendix A.1.

Purified pig gastric mucins were dissolved in physiological NaCl water to a total concentration of 5 %. The mucins were mixed in by careful magnetic stirring at 4°C over night

2.2.4.4. Sigma mucin solutions

Two different Sigma mucin solutions were made. The first were prepared by adding Sigma mucin type II in portions to physiologic NaCl water under magnetic stirring, to a total concentration of 5 %. This solution was utilized in the distribution experiments.

The Sigma mucin solutions utilized in the rheological measurements were prepared by adding Sigma mucin type II in portions to 10 mM HEPES buffer containing 1.3 mM $CaCl_2$ and 1 mM $MgSO_4$ under magnetic stirring. Three solutions of different concentration were prepared, 5 % (w/v), 8 % (w/v) and 10 % (w/v). The solutions were stored at 4 °C over night, and stirred with a magnetic stirrer prior to measurements.

2.2.4.5. Agar gel

Dried agar (Becton Dickinson Company Sparks, USA) was dissolved in MQ water at 80 °C to a total concentration of 5 % (w/v). At 50 °C 0.10 g of the liquid agar were pipetted in a glass chamber with a cut of pipette tip, and was allowed to gel in the glass chamber.

2.2.4.6 Nanoparticle solutions

All the nanoparticle solutions utilized were made by diluting the 2 % (w/v) nanoparticle solutions in MQ-water. For each dilution step the solutions were thoroughly mixed by vortexing.

A complete list of all the chemicals utilized in the master thesis is enclosed in Appendix A.2.

2.2 Methods

2.2.1 Distribution of nanoparticles

2.2.1.1 Distribution of nanoparticles in mucus

2.2.1.1.1 Biosimilar mucus and PSIM

Mucus samples of 0.20 g were weighed up and put in an eppendorf tube by pipetting with a cut off pipette tip. Six different nanoparticle solutions were added (see Table 2.1), one in each tube, to an end concentration of 0.08 % (w/v). The nanoparticles were thoroughly mixed into the mucus with the aid of a spatula and vortexed, before the samples were distributed in different chambers of a glass slide with spatulas. The samples were allowed to settle overnight at 4 °C before the nanoparticles were images by laser scanning fluorescence confocal microscopy. This was performed with PSIM samples and biosimilar mucus samples.

2.2.1.1.2 Sigma mucin solutions

Three replicates of 200 µL Sigma mucin solutions were added in eppendorf tubes by pipetting, and three types of nanoparticle solutions (see Table 2.2) were added to an end concentration of 0.08 % (w/v), one solution in each of the tubes. The solutions were added in glass chambers and the nanoparticles imaged by laser scanning fluorescence confocal microscopy.

2.2.1.1.3 Pig gastric mucins

200 µL dissolved pig gastric mucins were added in eppendorf tubes, and three different types of nanoparticle solutions (see Table 2.2), were added to an end concentration of 0.08 % (w/v), one in each tube. Each mixture were added in glass chambers, and the samples were imaged by laser scanning fluorescence confocal microscopy.

2.2.1.2 Distribution of nanoparticles on top of mucus

2.2.1.2.1 Biosimilar mucus and PSIM

100 µL mucus were added in glass chamber wells by pipetting with a pipette with a cut off pipette tip. The glass slide was put on a weight prior to mucus addition to ensure the right amount was added in each well. Six different nanoparticle solutions (see Table 2.1) with a concentration of 0.1 % (w/v) were made. 100 µL of each nanoparticle solution were carefully pipetted on the top of the mucus samples, one nanoparticle solution in each chamber. The nanoparticles were imaged by laser scanning fluorescence confocal microscopy. This was performed with both PSIM and biosimilar mucus samples.

2.2.1.2.2 Pig gastric mucins

100 µL of dissolved pig gastric mucins were pipetted into a glass chamber. 0.1 % (w/v) 1 µm sized carboxylate-modified nanoparticles were carefully pipetted on top of the pig gastric mucin layer, and the nanoparticles were imaged by laser scanning fluorescence confocal microscopy.

2.2.1.2.3 Agar gel

A 5 % (w/v) agar gel was prepared, where 0.10 g was allowed to gel in a glass chamber. After gelation 0.1 % (w/v) 1 µm sized carboxylate-modified nanoparticles were put on top of the

agar layer, and the nanoparticles were imaged by laser scanning fluorescence confocal microscopy.

2.2.1.3 Imaging with laser scanning confocal microscopy

All samples were visualized and imaged in a laser scanning fluorescence confocal microscopy of the type Zeiss LSM 510 Meta (Carl Zeiss Microscopy, Jena, Germany) with serial number 2110000865.

The argon laser (488 nm) was utilized together with a water objective with 40 x magnification, a numeric aperture of 0.8 and a working distance of 1.7 mm. For all measurements the strength of the laser were set to 10.1 %, and the detector gain and amplifier offset were adjusted so that approximately the same fluorescence intensity would be detected in each of the samples. The images were analysed/investigated in LSM Image Browser.

2.2.2 The plate method

The development of the plate method is described in detail in section 3.2.

2.2.2.1 Fluorescence intensity measurements

All the fluorescence intensity measurements were carried out by a Tecan Infinite 200 PRO (Tecan Austria GmbH, Salzburg, Austria) plate reader with serial number 1111001422, in combination with the software Tecan iControll. Before each measurement the excitation maxima, emission maxima and z-position were set. The yellow-green and red nanoparticles had ex./em. maxima of 505/515 nm and 580/615 nm respectively. The excitation and emission maxima used as "standard" ex./em. wave-lengths were 495/353 nm for the yellow-green particles, and 580/615 nm for the red nanoparticles. This was due to a requirement of at least 35 nm between the set excitation maxima and the emission maxima to prevent the xenon-lamp from transmitting light directly into the fluorescence detector, which would yield false results. In all measurements at least one blank sample of MQ-water were included.

2.2.3 Rheological measurements

All rheological measurements were run on a Rheologica StressTech (Rheologica, Lund, Sweden) instrument with serial number 903-31111, with cone and plate geometry. The cone used in the measurements of the biosimilar mucus and PSIM had a diameter of 40 mm and an angle of 4 degrees. The cone used in the measurements of the Sigma mucin solutions had a diameter of 40 mm and an angle of 1 degree. Unless otherwise mentioned all measurements were run on 25 °C. Before measurements the cone was lowered to "zero gap", and an appropriate amount of sample was added to the plate. After lowering of the cone the samples of PSIM and biosimilar mucus were covered in silicone oil (Dow Corning ® 200/100S fluid (VNR International LTD, Butterworth, UK) to avoid evaporation of water from the samples during measurement. The software to register the measurements was Rheoexplorer. Microsoft Excel and SigmaPlot were utilized for further data analysis.

2.2.3.1 Rheological measurements of PSIM

Frequency sweeps kept within the linear viscoelastic region were run on different PSIM samples in the interval 0.001-10 Hertz. Ten minutes prior to each of the frequency sweeps, strain sweeps were run in the strain region $1*10^{-5}$-10 for determination of the linear viscoelastic region. Furthermore, up-down strain sweeps in the strain region $1*10^{-5}$-10 were run. All the strain sweeps were run with a fixed frequency of 1 Hertz, and on different samples.

2.2.3.2 Rheological measurements of biosimilar mucus

Frequency sweeps kept within the linear viscoelastic region were run on individual biosimilar mucus samples from two different batches in the region 0.001-10 Hertz. Prior to the frequency sweeps, strain sweeps on other samples in the strain range $1*10^{-5}$-10 were run for determination of the linear viscoelastic region. Up-down strain sweeps in the same strain region were also run. All the strain sweep measurements had a fixed frequency of 1 Hertz.

2.2.3.3 Rheological measurements of Sigma mucin solutions

For each of the Sigma mucin solutions of 5 % (w/v), 8 % (w/v) and 10 % (w/v) the following procedure were conducted;

Strain sweeps in the strain region $1*10^{-5}$-100 were conducted with a fixed frequency of 1 Hertz, instantly followed by a frequency sweep with a fixed strain of 0.05 in the frequency region 0.001 – 10 Hertz. This was repeated three times on the same sample, at 15 °C, 25 °C and 37 °C.

3. Results & Discussion

3.1 Distribution studies of nanoparticles in and on mucus

Absorption studies of nanoparticles is an important part of breaking the code to how nanoparticle drug delivery systems can be utilized in oral delivery of pharmaceuticals. For a successful delivery of the drug load at the target cell/tissue/organ, the nanoparticle drug delivery system has to be transported or diffuse through the mucus matrix, and be absorbed by the epithelial cells of the intestines (Ensign et al., 2012). This can be studied by Caco-2 cells in combination with biosimilar mucus. The biosimilar mucus was originally developed for compatibility with the Caco-2 cells. However, compatibility with the cells does not mean that biosimialr mucus is an applicable mucus model system in nanoparticle drug delivery studies if the mucus affects the nanoparticles in different ways than what native mucus might do.

By studying the distribution of nanoparticles mixed into biosimilar mucus and PSIM, the cells' ability to internalize the given particles after it has diffused through the mucous systems is investigated. Nanoparticles of different size and charge will most likely have different distribution patterns when mixed into mucus, and the pattern might not be similar when the same particle is mixed into different mucous systems. The nanoparticles can distribute in a uniform manner or form aggregates. Aggregate formation might prevent or complicate the absorption of nanoparticles by the epithelial cells, if the aggregates become too large.

Investigation of how different nanoparticles distributes on top of mucus gives cues to how the first encounter of the particles in the intestines might be affected by the particles' charge and/or size. These variables might influence if the ability of the nanoparticles to penetrate the mucus mesh, and if the nanoparticles are able to diffuse through the mucus layer at all and reach the epithelial cell for internalization. By investigating this in both PSIM and biosimilar mucus, a comparison can be made and the applicability of biosimilar mucus in drug absorption studies evaluated.

3.1.1 Distribution of nanoparticles mixed into mucus

When looking at the distribution of nanoparticles in a confocal microscopy the fluorescent nanoparticles are the only thing that will be detected and visualized. This can thus reveal how the nanoparticles distribute in mucus; from a complete uniform distribution in the entire sample to formation of large aggregates.

An aggregate is a general structure formed by the cohesion between two or more particles (Mørk, 1999). The charged nanoparticles will not form aggregates by themselves as they repulse each other; hence there must be interactions with components of the mucus matrix that induces aggregation formation. It is not straightforward to stipulate the mechanism behind the aggregation of nanoparticles in the mucous systems, but it might be due to bridging flocculation, in which the components of the mucus acts as polymer flocculants. The nanoparticles might interact with different components of the mucus matrix, creating a layer of molecules on the nanoparticle surface called the corona. The corona layer might shield the repulsive forces of the nanoparticles, and introduce electrostatic interactions, van der Waals forces, ionic interactions and/or hydrogen bonds, which enable the particles to aggregate (Mørk, 1999).

3.1.1.1 XY images of the distribution of nanoparticles in PSIM and biosimilar mucus

Six types of fluorescent nanoparticles of different size and surface charge were mixed into PSIM and biosimilar mucus with an end concentration of 0.08 % (w/v). Furthermore, the distribution of three of the nanoparticle types was investigated in two supplement model mucous systems; pig gastric mucins (5 % (w/v)) and Sigma mucin type II solution (5 % (w/v)). The confocal images of the distribution of nanoparticles captured in the XY direction are collected in Figure 3.1.

	PSIM	Biosimilar mucus	Pig gastric mucins	5 % (w/v) Sigma mucin
100 nm A				
100 nm C				
200 nm A				
200 nm C				
200 nm P				
1 µm C				
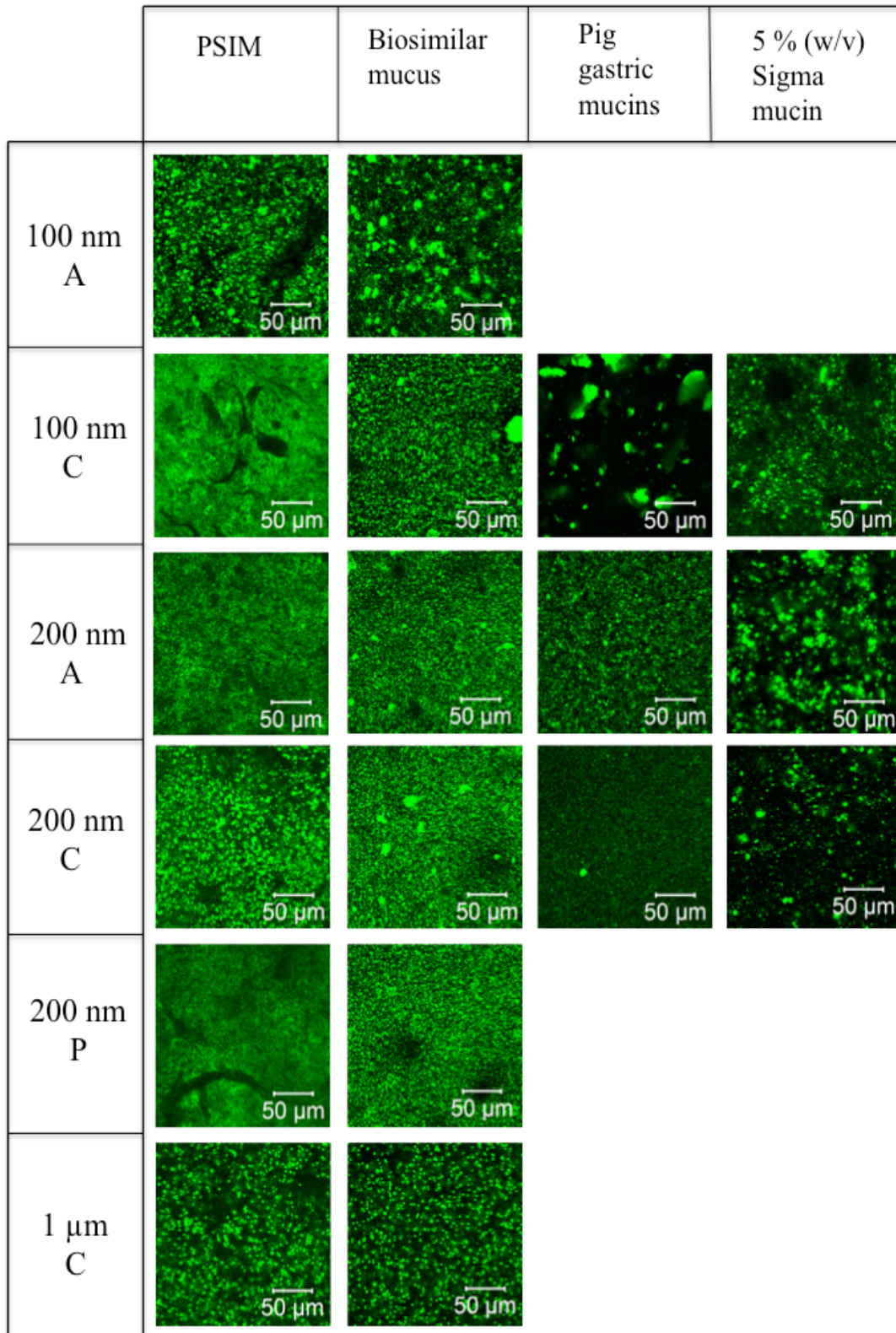
Figure 3.1 XY confocal images captured of various types of fluorescent nanoparticles mixed into different mucous systems. The size and charge of the nanoparticles are indicated in the column to the left, were A = amine modified (+), C = carboxylate modified (-) and P = PEGylated (-).

The images in Figure 3.1 present the distribution of the different nanoparticles in the XY-direction in the four mucous systems, and reveals that the different nanoparticles distribute in different manners in the four systems. This implies that the distribution of nanoparticles in the four mucous systems tested is dependent on the size and surface charge of the particles, and the matrix of the mucous system.

Some special considerations regarding the PSIM matrix have to be taken into account when studying the nanoparticle distribution resented in Figure 3.1. Black fields are visible in the images of the PSIM. This is an artefact observed due to inhomogeneities like debris from the intestines, pockets of air etc., which prevents the nanoparticles from distributing in these areas of the mucus. This artefact is an expected observation, as the PSIM was extracted from the intestines and is a naturally inhomogeneous material (Groo and Lagarce, 2014). Figure 3.2 presents the distribution of the 200 nm PEGylated particles in the PSIM, which emphasises this artefact. Some small black areas can also be seen in some of images of the biosimilar mucus (200 nm carboxylate-modified and 200 nm PEGylated nanoparticles), which is likely due to air bubbles. No inhomogeneities are expected in this matrix, as it is produced in the laboratory by homogenously mixing the ingredients together.
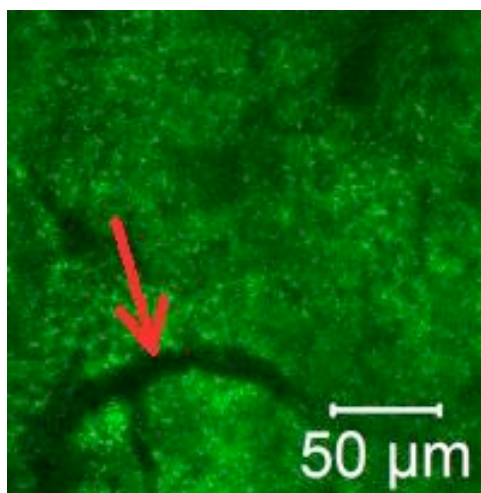
Figure 3.2 The distribution of 200 nm PEGylated nanoparticles in PSIM. The arrow points to debris in the PSIM matrix.

Upon comparison of the images of the PSIM and biosimilar mucus, the 200 nm PEGylated nanoparticles has the most even distribution in both the mucous systems. PEGylation of particles are known to modify the biodistribution of particles and enhance their solubility

(Veronese, 2001). Also, PEGylation of particles has been used to improve mobility of the particles in mucus and reduce the mucoadhesion of the particles (Lai et al., 2009a). This is expected to lead to a more even distribution of the particles, therefore was not a surprising to see that the PEGylated particles had the most uniform distribution. The most uneven distribution is of the 100 nm amine-modified and 1 μm carboxylate-modified particles. The uneven distribution of the 1 μm sized particles might be due to the large size, which could restrict the particles to distribute in "pockets" of the gel matrix where they can fit. Small aggregates of nanoparticles are observed in both the PSIM and biosimilar mucus, but are somewhat more prominent in the biosimilar mucus. This means that some of the components of the biosimilar mucus interact with the nanoparticles and induce larger aggregates than when the same nanoparticles interact with components of the PSIM. The largest aggregates are in general found in the mucus samples containing negatively charged particles, but aggregate formation is also seen in the samples were positively charged particles are mixed in. A trend toward larger aggregates of negatively charged nanoparticles might indicate that (i) components of the mucous systems are better at shielding the repulsive forces between the negatively charged nanoparticles than between the positively charged nanoparticles, and/or (ii) that when components interact with the negatively charged particles more aggregation forming interactions are introduced than when components of the mucus interact with positively charged particles (Mørk, 1999).

The pig gastric mucins (PGM) and Sigma pig gastric mucins are as their names implies, both extracted from pig stomachs, and thus of the same origin. One might expect the nanoparticles to distribute in the same manner in these mucin systems, but this is not the case, as seen in Figure 3.1. The nanoparticles have a diametrically opposite distribution in the PGM and Sigma mucin solutions. The reason for the differences in nanoparticle distribution observed between PGM and Sigma mucin is most likely that they have been exposed to different purification processes. During a purification process the non-mucin components of the mucus are removed, which might free binding sites in the mucin molecules. The Sigma mucins are not purified to the same level as PGM, and contains non-mucin proteins and lipids. The difference in the accessibility of binding sites on the mucin molecules of Sigma mucin and PGM, means they have different interaction potentials, leading to dissimilar aggregation of nanoparticles (Mørk, 1999). This is evident when comparing the Sigma solution and PGM where the 100 nm carboxylate-modified nanoparticles are mixed in. In PGM the nanoparticles

form very large aggregates, which are not observed in the Sigma mucin solution. The intense aggregation of the 100 nm carboxylate-modified particles in the PGM is hence an artefact of the purification process, which might have given access to new binding sites where the nanoparticles of 100 nm size and negative charge can interact. The reason this artefact is not observed for any of the 200 nm sized nanoparticles might be that they do not have access to the revealed binding sites due the larger size. The observed aggregation of nanoparticles is hence dependent on the purification process of the mucins.

Despite the sol-like consistency of the Sigma mucin solutions, all the particles aggregate to some degree in the solutions. This indicates that it is not a gel network in itself that prevents nanoparticles from distributing in a uniform manner in mucus, but that the Sigma mucins interact with the nanoparticles and induce aggregation. Most likely are the mucins partially shielding the repulsive forces between the nanoparticles, and introducing electrostatic, ionic and or H-bonding interactions that makes the nanoparticles aggregate (Mørk, 1999).

In contrast to the Sigma mucin solutions, the biosimilar mucus does not induce the same degree of aggregation, despite also containing Sigma mucins at the same concentration. This means that there likely are non-mucin components of the biosimilar mucus that prevents formation of larger aggregates by interacting with the nanoparticles, changing their coronas, which do not induce the same degree of aggregation. The Sigma mucin solutions cannot be directly compared to the PSIM in the same manner as there is no Sigma mucins in the PSIM, but the small aggregates observed in the PSIM confirms that native components of the PSIM creates structures which do not induce aggregation formation in the same manner as observed in the biosimilar mucus.

The differences observed in the distribution of nanoparticles in PSIM, biosimilar mucus, Sigma mucin solutions and dissolved PGM highlights the intricacy of working with complex molecules like mucins and mucous systems, which is not always straightforward.

3.1.1.2 XZ images of the distribution of nanoparticles in PSIM and biosimilar mucus

The six types of nanoparticles (0.08 % (w/v)) mixed into the PSIM and biosimilar mucus were also imaged in the XZ-direction. What is important to keep in mind when investigating the confocal images of the XZ-direction, is the lower resolution of these images compared to the XY-images, which will not reproduce the same details and accuracy of the XY-images. The confocal images captured in the XZ-plane are presented in Figure 3.3.

	Native porcine small intestinal mucus	Biosimilar mucus
100 nm A		
100 nm C		
200 nm A		
200 nm C		
200 nm P		
1 μm C		
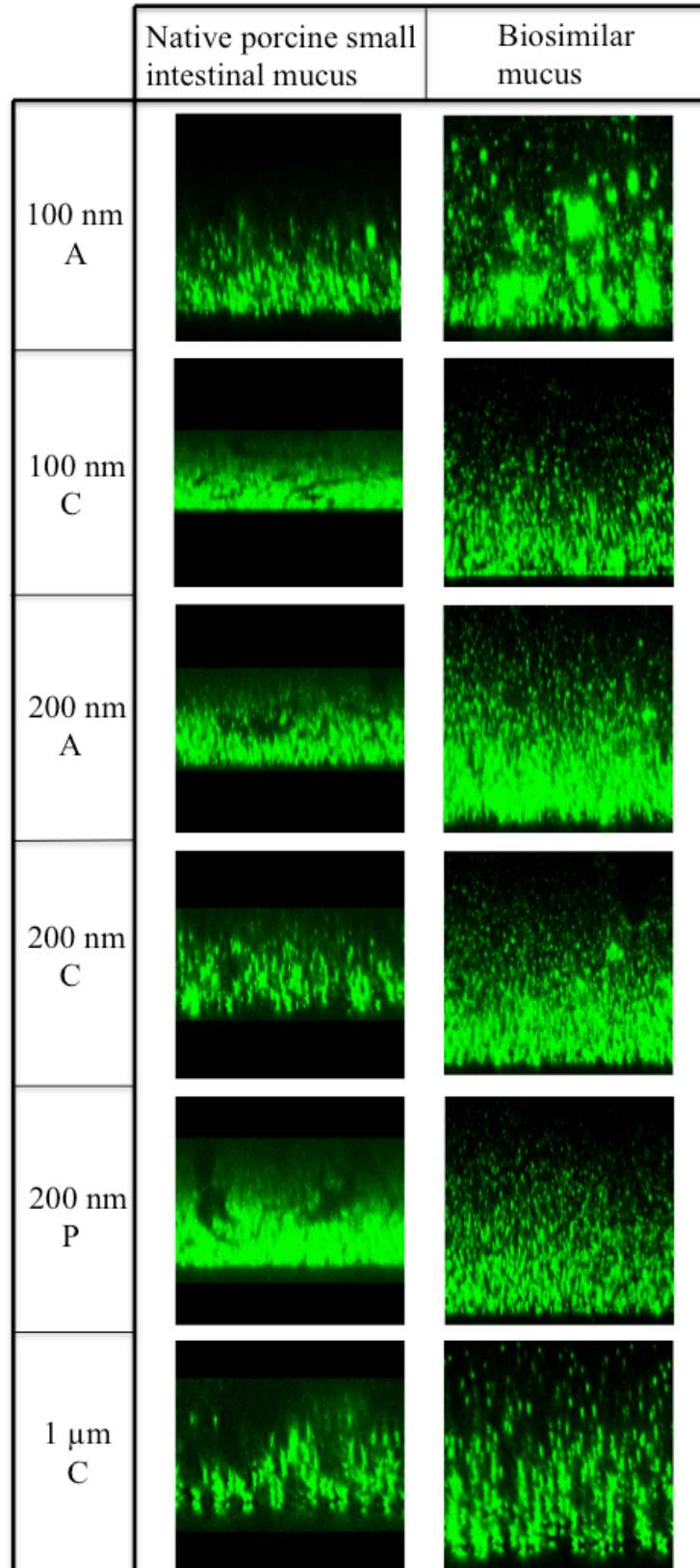
Figure 3.3 The confocal images captured in the XZ direction of different nanoparticles mixed into PSIM and biosimilar mucus. The charge and size of the nanoparticles are indicated in the column to the left, were C = carboxylate-modified (-), A = amine-modified (+) and P = PEGylated (-). The horizontal plane is the X-plane, and the vertical plane is the Z-plane.

36

From the images in Figure 3.3 it is evident that the laser beam of the confocal microscope has problems penetrating the entire height of the mucus and nanoparticle mixtures in the glass chambers. This is in particular prominent in the images of the PSIM, where the image program automatically inserts black fields in the top and bottom of the image if the width of the image (x) is not matched by the height (z) and does not produce a quadratic image.

The reason the confocal laser beam is unable to penetrate the PSIM in particular might be a combination of several things. First of all the PSIM has a darker colour and is denser than the biosimilar mucus. Second of all, the nanoparticles generally distributes in the PSIM in a more uniform manner than in the biosimilar mucus, which will further inhibit the penetration of the laser beam. Less of the excitation light is penetrated through the dense PSIM with an even distribution of nanoparticles; hence fewer signals will be detected in the mucus layers further from the laser.

The image program did not allow for scale bars to be put in the XZ images. However they are shown at the same scale and the absolute height in the z-direction of the images is summarized in Table 3.1.

Table 3.1 A table with the distance in the z-direction of the XZ confocal images in Figure 3.3. The charge and size of the nanoparticles are indicated in the column to the left, were C = carboxylate-modified (-), A = amine-modified (+) and P = PEGylated (-).

	PSIM	**Biosimilar mucus**
100 nm A	180 μm	290 μm
100 nm C	83 μm	243 μm
200 nm A	102 μm	282 μm
200 nm C	111 μm	250 μm
200 nm P	143 μm	249 μm
1 μm C	152 μm	289 μm

The 200 nm PEGylated particles distribute in the most uniform manner, both in the PSIM matrix and the biosimilar mucus matrix, which was also seen in the XY images. Overall there

is no characteristic trends observed in the distribution of the positively charge particles versus the negatively charged particles, despite the overall negative charge of the mucins. This means that the mucins and the other components in the mucus must hold an array of different types of interactions of attractive and repulsive nature, enabling the interaction of both positively and negatively charged particles. This is supported by the knowledge that in a mucin gel network several types of interactions contribute to keeping the network together, like transient "flickering" bonds such as hydrophobic bonds, electrostatic and ionic interactions, H-bonds and van der Waals interactions (Kočevar-Nared et al., 1997) (Taylor et al., 2003). With the exception of the somewhat uneven distribution of the 1 μm sized carboxylate-modified particles, the size of the nanoparticles seemingly does not affect the distribution pattern of the nanoparticles. This implies that the mesh spacing of the gel network of the two mucous systems might be large enough to allow for a similar distribution of both the 100 nm sized and 200 nm sized nanoparticles. Differences in the mesh spacing of the biosimilar mucus and the PSIM might be a contributing factor for the differences seen in nanoparticle distribution between the two systems. The more even distribution of nanoparticles in the PSIM might indicate that the gel structure of the PSIM is more ordered, compared to a less ordered structure in the biosimilar mucus. This might lead to more evenly distributed nanoparticles in the PSIM, and less even distributed particles in the biosimilar mucu. Considering that the PSIM is of native origin and the biosimilar mucus is an artificial mucous system created in the laboratory, this is not unlikely. There is no clear correlation between the size of the aggregates in the two mucous systems and the surface charge and/or size of the nanoparticles.

As there are no overall trends in the distribution of nanoparticles relating to size or charge, it will not be possible to predict the distribution pattern of other nanoparticles based on these data.

3.1.1.3 Control measurements

3.1.1.3.1 Correcting for dissimilar amounts of nanoparticles

In the distribution experiments were nanoparticles were mixed into mucus and visualized by confocal microscopy, the end concentration of all the different nanoparticles were set to be 0.08 % (w/v). When different sized nanoparticles have the same concentration, the amount of

nanoparticles will differ between the nanoparticle solutions of different sized particles. In order to make sure that the differences seen in the distribution patterns of nanoparticles are not to some degree affected by differences in amounts of nanoparticles in the mucous systems, a control experiment were conducted.

Two nanoparticle solutions of the 100 nm carboxylate-modified nanoparticles were prepared and mixed into PSIM. The first solution had a concentration of 0.08 % (w/v) and the total amount of particles was calculated to be $2.91*10^{11}$ particles. The amount of particles of a 0.08 % (w/v) 200 nm nanoparticle solution was calculated to be $3.62*10^{10}$. Hence, the second 100 nm solution was made with $3.62*10^{10}$ nanoparticles, to a total concentration of 0.01 % (w/v). Calculations are found in Appendix B.1. The results after visualizing the nanoparticles by confocal microscopy are presented in Figure 3.4.
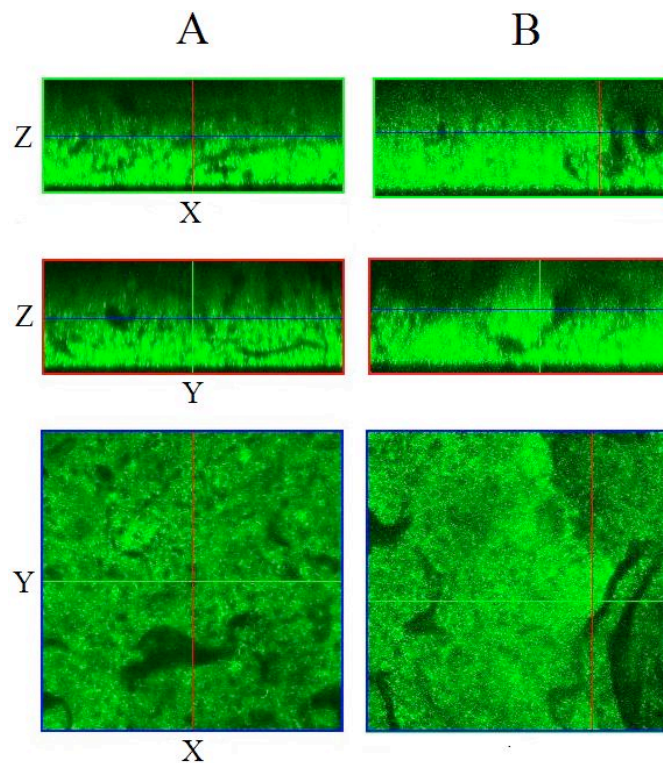
Figure 3.4 The confocal images of 100 nm sized carboxylate-modified fluorescent nanoparticles mixed into PSIM. The images of column *A* represent the sample were the concentration of nanoparticles in the mucus is 0.08 % (w/v), and the amount of particles is calculated to be $2.91*10^{11}$. The images of column *B* represents the sample were the concentration of nanoparticles in the mucus is 0.01 % (w/v), and the amount of particles is calculated to be $3.62*10^{10}$. Letters next to the samples of column *A* indicates the XYZ-planes of the images in the corresponding rows.

The images in Figure 3.4 reveal no substantial qualitative differences between the two samples of PSIM containing nanoparticles of different amounts. This lead to the conclusion that the differing amounts of nanoparticles in the mucous systems have not influenced the distribution patterns within the nanoparticle concentration regime utilized.

3.1.1.3.2 Different mixing procedures

The mixing procedure of the nanoparticles and mucus of the distribution experiments consisted of adding nanoparticles to the mucus sample, mixing with a small spatula and vortexing until a homogenous mixture was obtained. To find out if the mixing procedure might have had some impact on the distribution patterns of nanoparticles observed, 200 nm carboxylate-modified and 200 nm PEGylated nanoparticles were mixed into an aliquot each of biosimilar mucus in the making, to an end concentration of 0.08 % (w/v). The nanoparticles were mixed into the mucus previous to the step of adjusting the pH to 7.4, which thickens the biosimilar mucus mixture to gel consistency. The nanoparticles of the two samples were visualized by confocal microscopy, and the results presented together with images of the same nanoparticles mixed into biosimilar mucus after it was made, in Figure 3.5.
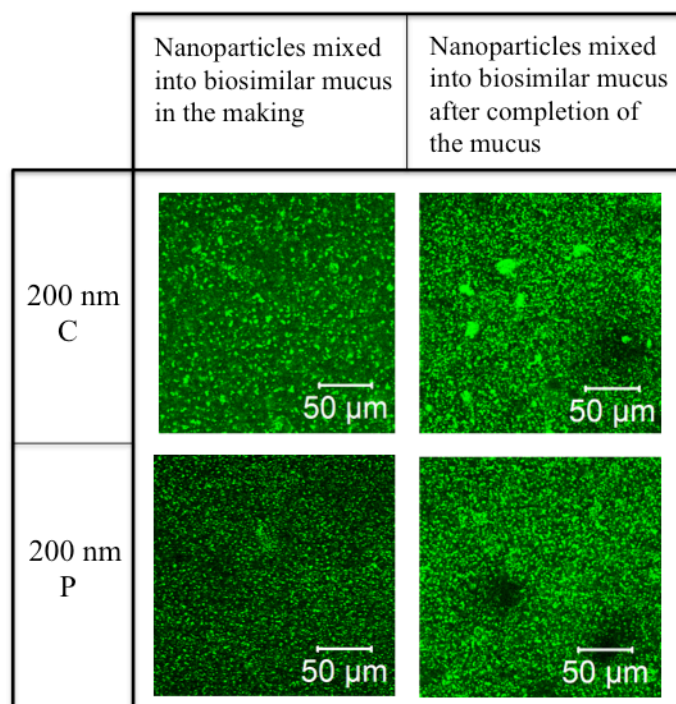
Figure 3.5 Confocal images in the XY direction of 200 nm sized carboxylate-modified (C) and PEGylated (P) nanoparticles mixed in biosimilar mucus. In the images of the first column, the nanoparticles are added in biosimilar mucus in the making, and in the images of the second column the nanoparticles are added to biosimilar mucus already made.

The confocal images of Figure 3.5 reveal a quite similar distribution pattern of the nanoparticles, independent of how they are mixed into the biosimilar mucus. The 200 nm carboxylate-modified particles forms small aggregates in both samples, although some larger aggregates are seen in the samples were the particles are added after the biosimilar mucus were made. This might be explained by two theories.

First of all the difference might be explained by the difference in pH between the two mucus samples when the nanoparticles were mixed in. When the nanoparticles were mixed into the biosimilar mucus mixture prior to pH adjustment to 7.4, the PAA of the mixture had not yet dissolved and had an overall neutral charge. When the nanoparticles were mixed into the biosimilar mucus after completion of the mucus the PAA was dissolved, and hence introduced more negative charges to the mixture. These two different conditions might have affected the corona layer of the 200 nm carboxylate-modified nanoparticles. Both the nanoparticles and the PAA have an overall negative charge, and the nanoparticles and dissolved PAA have to compete for the same things like lipids and bovine serum albumin to interact with. Different corona layers of the nanoparticles before and after pH adjustment might affect the interactions

inducing aggregation. This might be the reason for the bigger aggregates seen in the sample where the 200 nm carboxylate-modified nanoparticles are mixed into the mucus after the biosimilar mucus were completed.

The second theory that might explain the difference in aggregate size seen between the two samples of 200 nm carboxylate-modified nanoparticles, might be the introduction of a gel structure in the completed biosimilar mucus. When mixing the nanoparticles into the biosimilar mucus gel, particles might accumulate in pockets in the gel structure, which gives the impression of aggregate formation when imaged by confocal microscopy.

The nanoparticle distribution of the 200 nm PEGylated nanoparticles have a much more similar pattern, where small aggregates can be seen in both of the samples, and are only slightly more prominent in the sample were the particles are mixed into the biosimilar mucus after the completion of the mucus. This is support for the theory of variation in corona layers being the cause of the differences in the distribution patterns of the 200 nm carboxylate-modified particles. If there was only an effect of the gel structure, the same aggregation patterns should have been seen in both types of nanoparticles, which they are not.

There is a small difference in the intensity of the images of the 200 nm PEGylated particles, which is due to small differences in the setting of the detector gain and amplifier offset of the measurement.

3.1.2 Distribution of nanoparticles on top of mucus

The distribution of nanoparticles on top of PSIM and biosimilar mucus was investigated to get an idea of how the size and charge of nanoparticles affected the distribution and absorption of nanoparticles on the mucus surface. An illustration of the concept is presented in Figure 3.6 where 1 μm carboxylate-modified nanoparticles settles on the surface of an agar gel. Due to the large size of the nanoparticles it was expected to see a migration front of nanoparticles, which would accumulates on the gel surface without being absorbed.
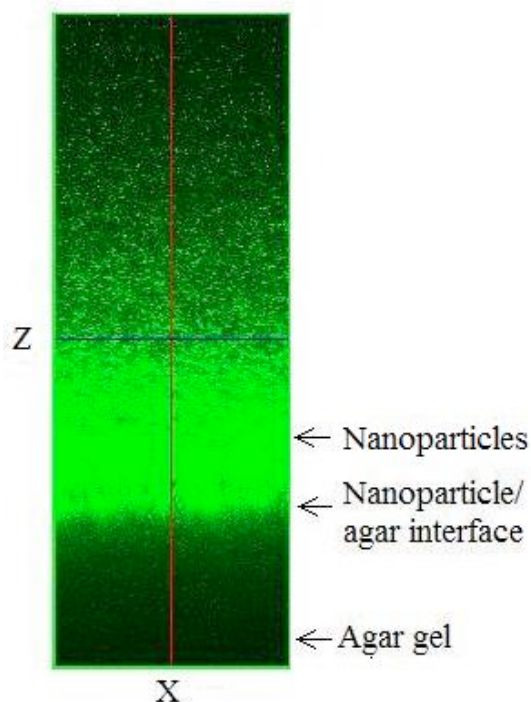
Figure 3.6 XZ confocal image of the distribution of 0.1% 1 µm carboxylate-modified nanoparticles on top of a 5 % (w/v) agar gel. A gradient of the nanoparticles is clearly seen, where the nanoparticles accumulate on the agar surface, unable to penetrate the agar gel.

The average mesh spacing of mucus has been suggested to be 10-200 nm, but properly coated particles up to 500 nm has been reported to diffuse rapidly through mucus (Lai et al., 2007). Therefore it was expected to see some penetration/adsorption of the 100 nm sized and 200 nm sized nanoparticles on top of the mucus layers.

Biosimilar mucus and PSIM were added in glass chambers, nanoparticles applied on top, and the distribution of the nanoparticles on top of and into the mucus visualized by confocal microscopy.

3.1.2.1 Mucus displacement

The experimental set-up was early on challenged by instant displacement of the mucus layer upon addition of the nanoparticle solution, in particular for the biosimilar mucus. Different methods like putting the pipette tip against the glass chamber wall, pipetting very carefully and using the 5-50 µL pipette to make the droplets smaller were attempted, but independent

of the way the nanoparticle solution were added, the drops moved the 1.25 mm thick mucus layer into the corners of the glass chamber, as illustrated in Figure 3.7.
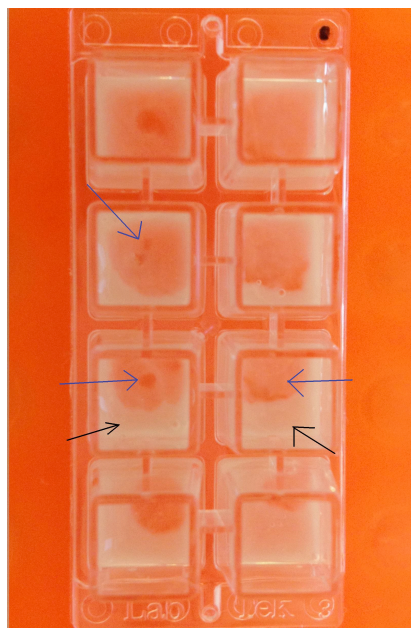
Figure 3.7 An eight chambered glass slide filled with 0.10 grams of biosimilar mucus in each chamber. For illustration, 100 µL MQ-water has been carefully pipetted into each of the chambers in various ways. The mucus layer is displaced by the addition of water, marked by blue arrows. The yellow arrows mark areas where the mucus layer is still intact.

Putting the glass chambers in the freezer after addition of mucus solved the displacement problem. The nanoparticles were instantly added to the frozen mucus after retrieving the glass chambers from the freezer. Mucus in chambers with newly added nanoparticle solutions is depicted in Figure 3.8.

Figure 3.8 Side view of glass chambers containing different 0.1% (w/v) nanoparticle solutions on top of 0.1 g biosimilar mucus (left) and 0.1 g PSIM (right). The pictures were captured straight after addition of nanoparticles.

3.1.2.2 Finding the nanoparticles in top of the mucus

The mucus layer was calculated to be ~1.25 mm thick (see Appendix B.2). The chosen objective of the confocal microscopy was a water objective with magnification 40 x, and a numeric aperture of 0.8. This objective had the greatest working distance of the objectives available with this magnification, 1.7 mm, and was able to visualize the whole height/z-direction of the mucus sample and ~ half of the nanoparticle solution on top of it. However, nanoparticles on top of the mucus were not found because the laser had problems penetrating the mucus layers. As already indicated by the distribution experiments of nanoparticles *in* mucus, both the biosimilar mucus, and particularly the PSIM, were hard to penetrate for the laser light. The XZ images of the nanoparticles mixed into the two mucous systems (Figure 3.3) clearly displayed a light gradient from the bottom of the glass chambers to the top, where the laser could not reach the nanoparticles of the higher mucus layers. Increasing the strength of the laser, enabling it to penetrate further through the mucus layers, was not an option, because both the mucous systems spread the laser light to a great extent, which resulted in a lot of unwanted noise in the confocal images.

Some experiments with thinner mucus layers were conducted, but minor perturbations caused the mucus layers to be displaced by the nanoparticle solutions. Thinner mucus layers were rejected as a possible option because they were not robust enough for the experimental conditions.

During experiments it was observed that the nanoparticle solutions slowly started to dissolve the mucus, making it swell from the top, see Figure 3.9.
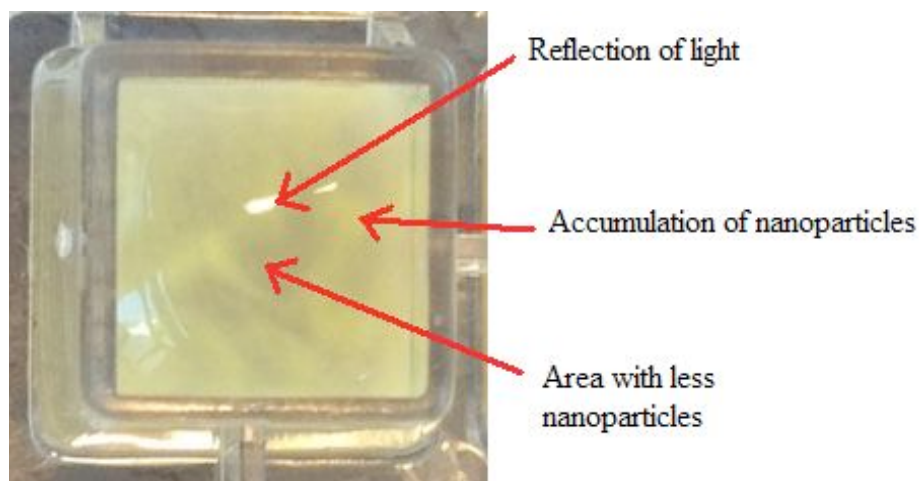
Figure 3.9 Top view of a glass chamber containing 100 µL 1 % 200 nm carboxylate-modified nanoparticles on top of 0.10 g biosimilar mucus. The picture is captured a couple of hours after the nanoparticle solution was added to the mucus, when the nanoparticle solution had started to dissolved the mucus and displace it, making the nanoparticles distribute in a random manner in the mucus.

This was in particular prominent in the biosimilar mucus. The driving force behind this phenomenon may be difference in the strength of the ions between the mucus matrix and the nanoparticle solutions. A small experiment where performed to confirm how the ion concentration of water is affecting the distribution of water on top of mucus. 0.10 g of biosimilar mucus and PSIM were put in four glass chambers each, and MQ-water and NaCl-water of differing concentrations (150 mM, 250 mM, 350 mM) was put on top. The glass slide was left for 24 hours and checked for any gradients in the water. The wells with PSIM in the bottom had the same appearance; no differences could be seen between the four wells. The wells with biosimilar mucus in the bottom had a very weak gradient of more dissolved mucus in the well with highest NaCl concentration contra the MQ-water. This means that it is probably not the difference in the ion concentration that is the driving force behind the dissolution of the mucus by the nanoparticle solutions because the nanoparticle solutions do not have a very high ion concentration compared to the biosimilar mucus which contains 10 mM HEPES buffer with 1.3 mM $CaCl_2$, 1 mM $MgSO_4$ and 137 mM NaCl. The dissolution of biosimilar mucus by the nanoparticle solution is probably due to other mechanisms than a difference in ion concentration.

After addition of nanoparticles, the mucus layer became more sensitive towards small perturbations with time, which was very inconvenient with the experimental conditions. The

nanoparticle solution would eventually displace the mucus layer and/or dissolve the top layers of the mucus, which made the nanoparticles distribute in a random manner in the mucus, see Figure 3.9 and Figure 3.10. Without a stabile mucus layer below the nanoparticles it was impossible to study how the nanoparticles distributed on top of, and down in the mucus.

Figure 3.10 Bottom view of a glass chamber containing different nanoparticles (1 % (w/v)) on top of 0.10 g PSIM (top row) and 0.1 g biosimilar mucus (bottom row). The picture is captured after experiments, ~3 hours after addition of nanoparticles. The picture illustrates the problems of the nanoparticle solutions dissolving and displacing the mucus layer of each well, making the nanoparticles distribute in a random manner in the mucus. This was seen to a greater extent in the biosimilar mucus than the PSIM.

During the confocal microscopy sessions, nanoparticles were found in the bottom part of the mucus, and these images do not represent what was expected to be found, see Figure 3.6. Two of the images presented in Figure 3.11 illustrate the appearance of the nanoparticles visualized by the laser.
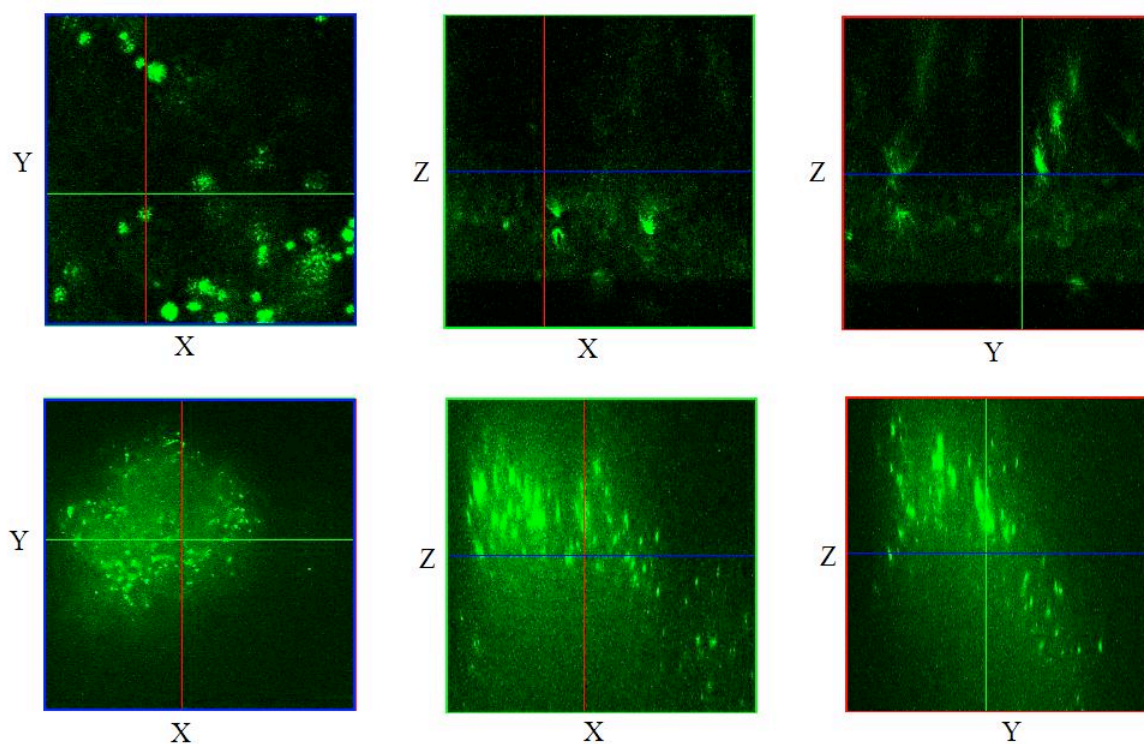
Figure 3.11 Confocal images in the XY, XZ and YZ direction of 0.1 g PSIM (top row) and 0.1 g biosimilar mucus (bottom row), were 100 µL 0.1 % (w/v) 1 µm carboxylate-modified nanoparticles were applied to the top of the mucus layers.

3.1.2.3 Control measurements

In order to test if the method works better with another mucous matrix, purified pig gastric mucins were dissolved in physiological NaCl water to concentration of 5 % (w/v), and 0.10 g of the gel was added to a glass chamber prior to freezing. 1 µm carboxylate-modified nanoparticles (0.1% (w/v)) were gently placed on top and visualized by confocal microscopy. It was expected to find the nanoparticles on top of the gel layer, as the large size prevents them from being absorbed. Also the gel was close to transparent, which the confocal laser were penetrate with ease. The results are presented in Figure 3.12.
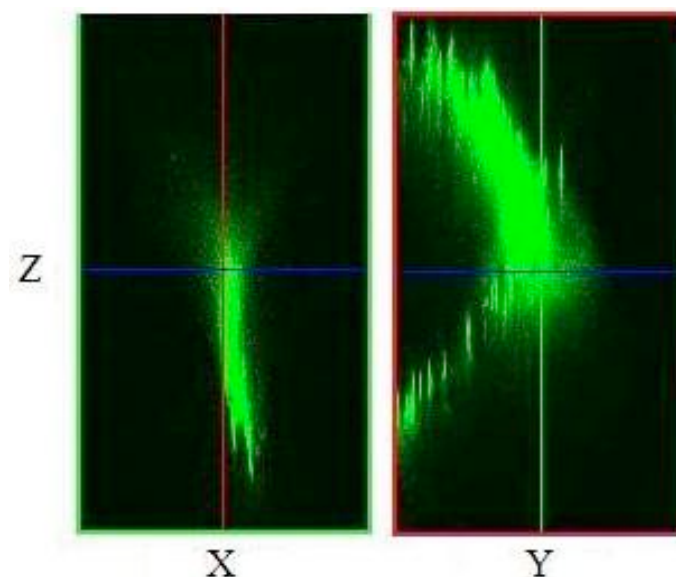
Figure 3.12 XZ and YZ confocal images of 100 µL 0.1 % 1 µm carboxylate-modified nanoparticles put on top of 0.10 g 5 % (W/V) pig gastric mucin matrix. The nanoparticles were found in channels and holes in the matrix near the bottom of the glass chamber.

As expected were the pig gastric mucin matrix easily penetrated by the laser because of the transparent gel. However, as soon as the frozen sample was thawed, the nanoparticle solution started to dissolve the pig gastric mucin gel. When visualizing the nanoparticles by confocal microscopy, the nanoparticles were found at the bottom of the glass chamber. The PGM matrix, just like biosimilar mucus and PSIM, were not robust enough for the experimental conditions, but was easily penetrated by the laser.

3.1.3 Conclusive remarks on the distribution experiments

The results of the distribution experiments were the nanoparticles were mixed into PSIM and biosimilar mucus, showed no characteristic trends in the distribution patterns of nanoparticles, which could be related to the size and/or charge of the nanoparticles. The negatively charged particles formed somewhat larger aggregates than the positively charged particles, but aggregate formation was seen for all the particles. Based on these data it will not be possible to predict the distribution pattern of other nanoparticles. The distribution patterns of the nanoparticles in biosimilar mucus were quite similar to the distribution patterns observed in PSIM; no large aggregates, which would make it impossible for cells to absorb the

nanoparticles, were formed. This is good news for the utilization of biosimilar mucus in drug absorption studies in combination with Caco-2 cells.

The method of adding nanoparticles on the top of mucus and visualizing the distribution with confocal microscopy is valid, proven by the 1 µm carboxylate-modified nanoparticles put on top of agar (Figure 3.6). The PSIM and biosimilar mucus was not suitable for this type of experiments mainly due to two things; the laser of the confocal microscopy had problems penetrating the mucus matrixes, the PSIM in particular. Neither of the matrices was robust enough for the experimental conditions, which resulted in a random distribution of the nanoparticles in the XYZ plane of the mucus. This was especially prominent in the biosimilar mucus. It can be argued that in a nanoparticle drug delivery study the biosimilar mucus will be more stable when put on top of Caco-2 cells, compared to the stability seen in the glass chambers. The Caco-2 cells have a glycocalyx (Lochner et.al, 2003), which interacts with the mucus and may stabilize it. This would create a more stable mucus surface, and give better mucus attachment to the surface. However, this does not mean that similar artefacts as observed in the distribution experiments might not be observed if biosimilar mucus is utilized in nanoparticle drug absorption studies. If so, it would probably be a source of false results, and researchers working with biosimilar mucus in absorption studies should be aware of this.

What is important to have in mind when investigating confocal images like the ones presented in this section is that the discussion and conclusions are based on qualitative data. The images in the figures are a representative selection, but might not reveal all the details regarding nanoparticle distribution, and one should be careful to make generalized conclusions based on these data.

3.2 Development of the plate method

The majority of nanoparticles entering the small intestines undergo direct transit and elimination through the faeces. In order to avoid direct elimination of nanoparticle drug delivery systems (NDDS), the nanoparticles has to interact at the mucus surface, which would result in a prolonged residence time at the site of adsorption and/or increase the drug concentration gradient over the mucus layer. An interaction of NDDS at the mucus surface requires that the particles have mucoadhesive properties. It is also crucial for the NDDS not to adhere too well to the mucus, which might restrict the absorption of the nanoparticles (Lai et al., 2009a) (Ponchel and Irache, 1998).

More knowledge and information regarding mucoadhesion is still needed for effective delivery of NDDS over the mucus barrier in the intestines. The objective of developing the plate method was to find a high throughput method of characterizing the adhesion of nanoparticles in mucus and how different variables might affect the mucoadhesion of various nanoparticles. The method is an attempt to mimic the *in vivo* situation.

3.2.1 The plate method

The basic idea behind the plate method is to coat the wells of microtiter plates with mucus by adding an appropriate amount of mucus and letting it partially dry. Fresh mucus is not stable enough for the subsequent steps of the method, but will stabilize sufficiently when it dries to a certain amount. Fluorescent nanoparticles are added, and within a given time frame removed. The last step of the method is to gently wash off particles that have not attached to the mucus, followed by fluorescence intensity measurements of the adhered particles. The fluorescence should then be directly correlated to the adhesion of nanoparticles on the mucus. The main steps of the method are illustrated in Figure 3.13. Furthermore, the effect of variations in variables like pH and osmolality, addition of bile sales, intestinal fluid etc. would be able to be tested on the mucoadhesion of nanoparticles.

A plate-based system gives a high throughput screening, and can simultaneously test many different nanoparticles and variables that might influence the adhesion of the nanoparticles. The system would also be able to handle several replicates at the same time, making the test system very efficient.
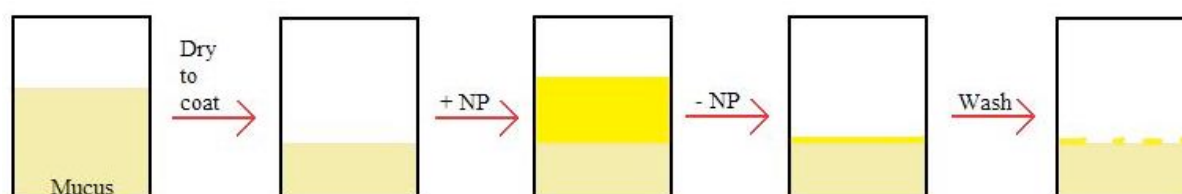
Figure 3.13 The main steps of the plate method for characterizing the adhesion of nanoparticles to mucus. Mucus is added to a microtirer well and left to dry to coat the bottom of the well. A nanoparticle solution of fluorescent nanoparticles are added, and removed within a given time frame. An additional washing procedure makes sure that the particles that have not adhered to the mucus are removed. Fluorescence intensity measurements of the adhered nanoparticles would then directly correlate to the amount of nanoparticles that adhered to the mucus surface.

The process of developing the new plate method can be divided in two distinct phases; (i) the optimization phase, which includes experimentation and optimization of different conditions regarding the applicability of the method, and (ii) the test phase, with fluorescence measurements of nanoparticle mucoadhesion under varying conditions and variables.

3.2.2 The Optimization process

It was determined to start the optimization process using biosimilar mucus, and later include the PSIM into the experiments. The biosimilar mucus was preferred to the PSIM, as it is a more homogenous system, and can easily be produced in the laboratory.

The first challenge was the amount of mucus each well should contain, and how long and by which method the drying should be done. Especially three criteria had to be met in order to optimize these variables; (i) the drying time and method should leave the mucus surface looking even and moist without any cracks, (ii) the mucus should be homogenously dried,

without pellicle formation, and (iii) after drying the mucus has to be stable enough to enable the nanoparticle solution to be lightly knocked out of the microtitrer plate wells without mucus also becoming dislodged.

3.2.2.1 Determining the time of drying and the correct drying method

Prior to, and after addition of mucus in the wells, the microtitrer plates were weighed so that the total amount of mucus added and percentage mucus to be evaporated could be determined. The mucus was added in each well by pipetting with a cut off pipette tip, since the narrow tip complicated the aspiration of the viscous mucus into the pipette tip. Because pipetting a viscous gel like biosimilar mucus with a shortened tip is not a very appropriate approach, the mucus applied in each well were weighed out, with the assumption that the weight of 100 μL of mucus were 0.10 g.

The approach to determine how long the mucus should dry was to add a given amount of mucus in 8 wells of a microtitrer plate and leave it to dry on the lab bench in a humidity and temperature regulated laboratory. When the mucus had dried an appropriate amount of time so that the surface was moist and even without any cracks, the stability of the mucus was tested. First the plate were turned 90 ° and movement of the mucus were observed. If the mucus allowed for it, the plate were turned 180 ° and given some gentle knocks to see if the mucus were dislodged onto a sheet of paper or was dry enough to stick to the well walls without exposing the well bottom. Dislodged mucus on a sheet of paper is illustrated in Figure 3.14 (left). If the mucus had dried enough to stand this "stability testing", the stability with addition of water were tested. 100 μL MQ-water were added to one well at the time, where the water of the first well were allowed to stay in the well for 1 minute before it was gently knocked out, onto a sheet of paper. The sheet of paper was then examined for traces of mucus. No mucus traces on the sheet of paper were positive results. This technique were repeated with the remaining mucus coated wells, where the water was allowed to stay in the well for 2 minutes, 3 minutes, 5 minutes, 10 minutes, 15 minutes, 20 minutes and 30 minutes. Figure 3.14 (right) illustrates the appearance of the sheet of paper after the stability testing with water. In addition to testing the stability of the mucus, this method also indicated how long the nanoparticle solutions could reside on top of the mucus before it would be completely absorbed by the dried mucus, which was not desirable.

Figure 3.14 To the left a picture of the dislodging of mucus (red ring) from the wells of the microtitrer plates, before the addition of water. To the right an example of how the sheet of paper might appear after the stability testing. The initial wet spots from the water are traced with a blue pen. The wet spots were checked for traces of mucus.

The method of drying and stability testing the mucus were repeated with various amounts of mucus and time frames. As the 96 well microtitrer plates utilized had wells where the recommended working volume were 350 µL (VWR International, 2014) mucus volumes of 400 µL, 200 µL and 100 µL were looked at as possible appropriate volumes with the fact that the volume of the mucus would shrink during drying, in mind. The drying times tested ranged from 5 hours up to 70 hours, and the time and initial amount of mucus in the wells were optimized.

After several experiments with 100 µL, 200 µL or 400 µL mucus in each microtitrer plate well, the optimal amount was found to be 200 µL. When using 400 µL mucus in each well, the time to dry the mucus was very long, and a lot of mucus ended up stuck to the well walls and sometimes cracked, see Figure 3.15. This was not ideal upon addition of water, where the dried mucus on the walls would very easily absorb the water and slide down the walls and on top of the dried mucus surface. When using 100 µL of mucus in each well the drying time was the lowest, but the meniscus the mucus created was in general quite steep, and with this small amount of mucus in the well, the bottom layer of the mucus ended up being very thin and dry compared to the mucus comprising the meniscus. With 200 µL in each well, the "wall effect" were minimized and the cracked up mucus seen in the wall wells with 400 µL were also markedly reduced, see Figure 3.16.
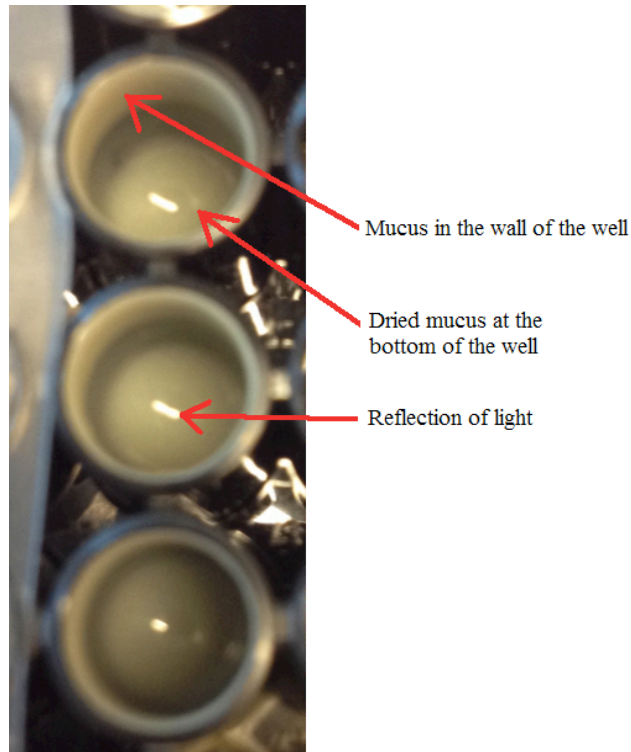
Figure 3.15 The appearance of mucus after drying on the lab bench, when applying 400 µL biosimilar mucus in each well. The arrows point to the mucus that are left in the walls of the wells, the dried mucus in the bottom of the wells, and highlights an artefact seen; light reflection in the mucus.
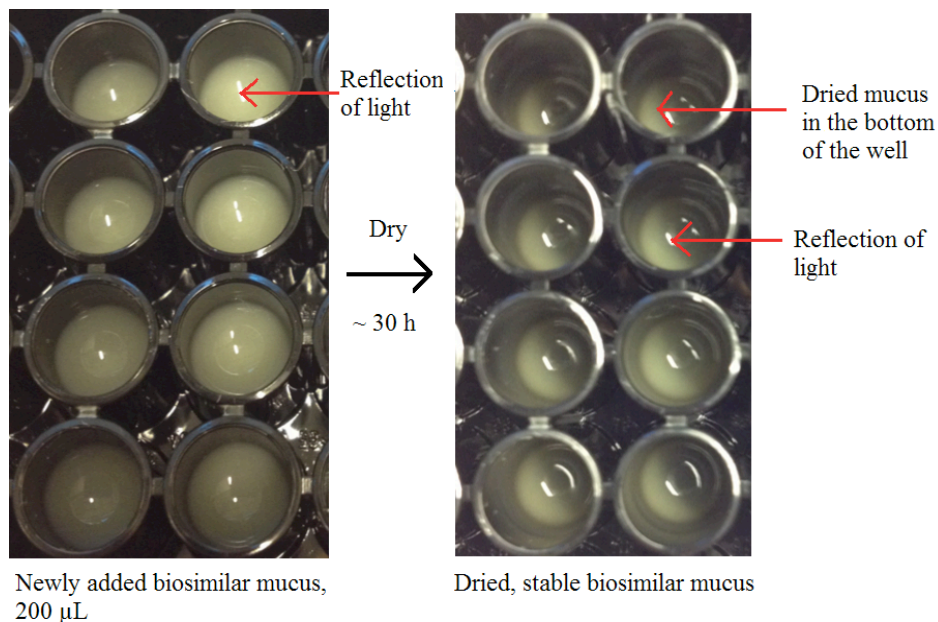
Figure 3.16 The appearance of 200 µL newly added biosimilar mucus to wells (left) and the appearance of the same mucus after drying on the lab bench in a temperature and humidity regulated laboratory for ~30 hours. The "white spots" in each well is a light reflection artefact.

55

When drying the mucus on the lab bench, the optimized time was found to be ~30 hours for the wells containing 200 µL biosimilar mucus. After replicate experiments, the weight to evaporate from the mucus was found to be 65-70 %, so that only 30-35 % of the start weight of mucus remained in the wells (calculations in Appendix C.1). At this point the mucus surface was smooth and moist (see Figure 3.16), and the mucus "passed" the stability tests.

As mentioned, the stability testing of mucus with water also gave indications of how long the nanoparticle solution can reside on top of the mucus surface without affecting it. The dried mucus was expected to absorb water, but if all the water of the nanoparticle solutions were absorbed, the nanoparticles would not be able to be removed from the mucus surface. There was a clear distinction in appearance of the mucus surface and especially the mucus near and on the walls after water had been added in the wells for 5 minutes and 10 minutes. After the water had been on the mucus surface for 10 minutes the driest mucus on the walls had absorbed a lot of water, and started to slide down the wall wells. This trend became more pronounced the longer the water resided in the wells. After 5 minutes or less this trend could not be seen, which lead to the assumption that the nanoparticles were to be added and removed from the mucus surface within five minutes during the actual fluorescence measurements. This trend could also be seen on the paper sheet the water was knocked onto. The amount of water to end up on the sheet was considerably greater after the water had resided on the dried mucus for 5 minutes, than 10 minutes or longer, indicating more water absorption at 10 minutes than 5 minutes.

As an attempt to find an alternate and more time efficient drying method, different amounts of mucus were attempted to be dried in a heating cabinet holding 50 °C. The mucus surface was examined and the mucus stability tested. The drying cabinet method resulted in an inhomogeneous drying of the mucus with pellicle formation, and this technique was rejected in favour of the drying of mucus on the lab bench, which gave homogeneous drying results. These results indicated that the drying of the mucus should not take place too quickly.

3.2.2.2 Determining the amount and concentration of nanoparticles

After determining the optimal amount of mucus, the best drying method and time, optimization regarding the nanoparticles was carried out.

The first thing looked at was the volume of nanoparticles that should be added in each well. The nanoparticle volume should with ease coat the entire mucus layer. By pipetting MQ-water in the amounts 25 µL, 50 µL, 60 µL, 75 µL and 100 µL into empty wells, the ability of the water to cover the bottom of the well was evaluated. This was replicated with wells containing dried mucus, because of different surface properties of the empty wells and the dried mucus. The water spread with more ease in the wells with mucus coating the bottom, and the determined required amount of liquid to coat the mucus were $\geqq$ 75 µL. It was assumed that the nanoparticle solutions would spread in approximately the same manner as the water, i.e. have contact angles not far from the MQ-water.

Dilution series of nanoparticles with minimum concentration 0.0000001 % (w/v) and a maximum concentration of 0.01 % (w/v) of the fluorescent nanoparticles FluoSpheres® 200 nm carboxylate-modified yellow-green and 200 nm carboxylate-modified red were made, and a standard curve of the fluorescence intensity of each of the dilution series were plotted, see Figure 3.17. The standard curve could then later be interpolated to calculate the amount of particles that still adhered to the mucus after the particle removal and washing step of the plate method. The fluorescence of the nanoparticle dilution series was measured in microtitrer plates with no mucus coating in the bottom of the wells.
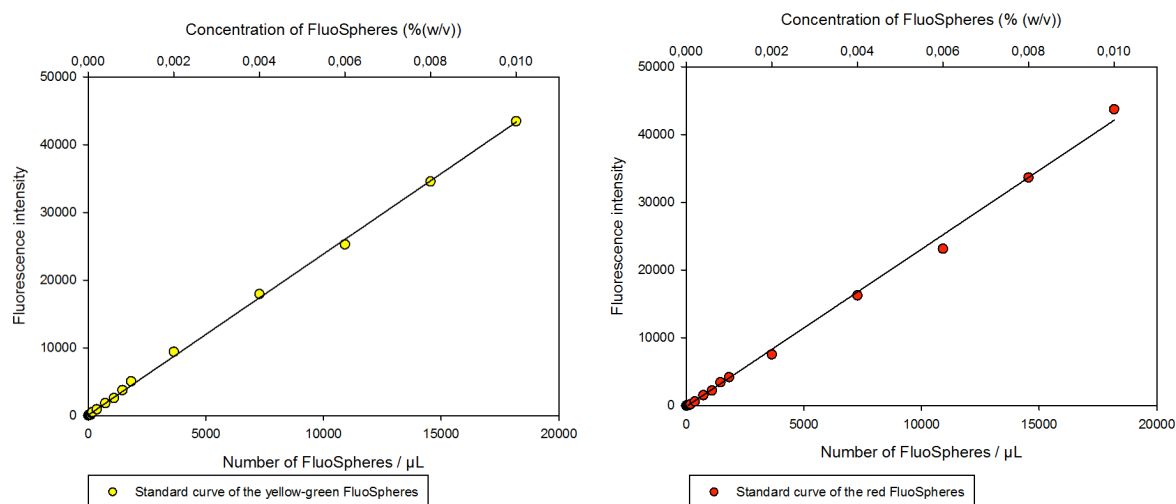
Figure 3.17 Standard curves of the FluoSpheres® yellow-green (left) and red (right), made with average values of three replicates. The ex./em. wave-lengths of the measurements were 495/535 nm for the yellow-green particles, and 580/615 nm for the red particles. The volume of nanoparticle solution in each well was 100 µL.

The fluorescence measurements of the dilution series of yellow-green and red FluoSpheres® (Figure 3.17) revealed that the lowest concentration of nanoparticles detected by the plate reader were 0.000002 % (w/v). When the highest concentration of the nanoparticle dilutions was 0.01 %, the standard curves were still within the linear region.

To investigate if the plate reader measures the fluorescence based on the amount of particles in a solution or the concentration of nanoparticles, two dilution series of yellow-green FluoSpheres® were made. The amount of nanoparticles of sample one of dilution series number one was calculated to be the same as sample one of the second dilution series etc., but with differing concentrations. The volume of the solutions in dilution series one was 100 µL, and the volume of the solutions in the second dilution series was 200 µL. The dilution series are given in Table 3.2, and the results of the fluorescence intensity measurements are presented in Figure 3.18.

58

Table 3.2 The dilution series of yellow-green FluoSpheres® used to determine if the plate reader measures the fluorescence intensity based on the amount of nanoparticles in a solution or the concentration of nanoparticles in a solution. The two solutions of each row, contains the same amount of nanoparticles.

Dilution series #1: 100 µL nanoparticle solutions with concentration (% (w/v))	Dilution series #2: 200 µL nanoparticle solutions with concentration (% (w/v))
0.0001	0.00005
0.00004	0.00002
0.00001	0.000005
0.000004	0.000002
0.000001	0.000005
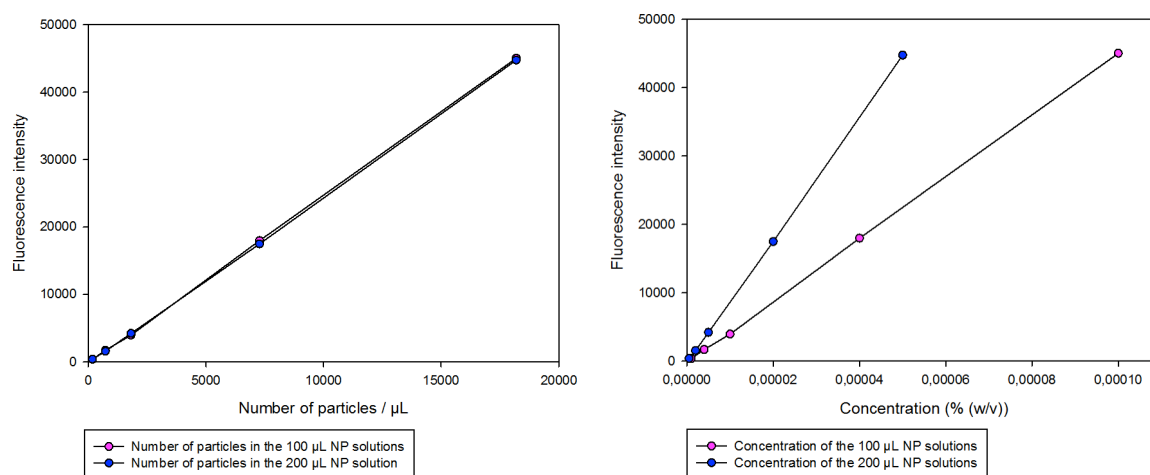
Figure 3.18 Two dilution series of nanoparticles were the number of nanoparticles of the solutions in dilution series one, matches the number of nanoparticles in dilution series two, but has differing concentrations. In the plot to the left the measured fluorescence intensity is plotted against the number of particles in the 100 µL solutions and the 200 µL solutions. In the plot to the right the fluorescence intensity is plotted against the concentration of the 100 µL solutions and the 200 µL solutions.

From Figure 3.18 it is seen that the graphs plotting the amount of nanoparticles of each solution in the two dilution series overlap, and that the graphs plotting the concentration of the two dilution series do not overlap. This shows that the plate reader measures the fluorescence

based on the amount of fluorescent particles in the solution, not the concentration of the solution.

3.2.3 Background fluorescence

Early experiments of fluorescence intensity measurements of nanoparticles on top of dried biosimilar mucus gave high fluorescence (data not included for early measurements), leading to the examination of the background fluorescence of biosimilar mucus. Fluorescence intensity measurements were conducted on eight replicates of fresh biosimilar mucus, dried bioismilar mucus and dried biosimilar mucus with 100 µL MQ-water on top. The results of the measurements are presented in Figure 3.19 and can be found as a table in Appendix C.2.
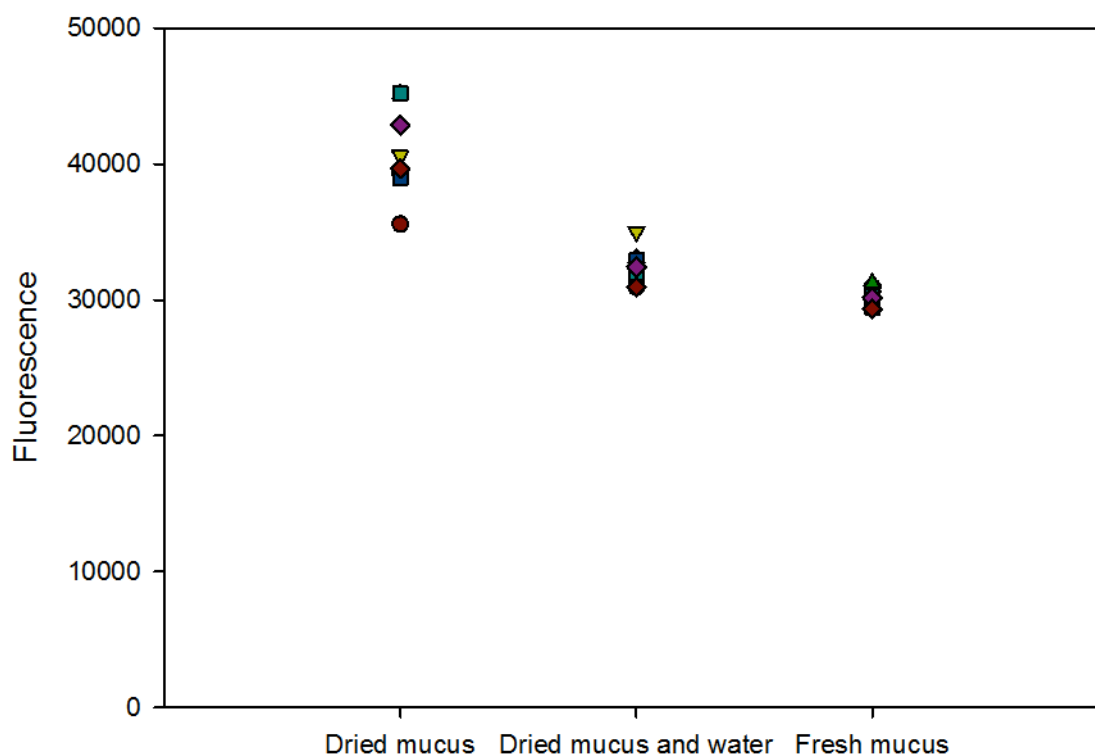
**Figure 3.19** Background fluorescence intensity measurements of different conditions of biosimilar mucus; 200 µL mucus dried for ~30 hours, 200 µL mucus dried for ~30 hours then added 100 µL MQ-water and 200 µL fresh mucus. For each of the mucus conditions, eight replicates were measured. The ex./em. wavelengths of the plate reader were set to the wavelength used to measure the yellow-green FluoSpheres®; 495/535 nm.

From the results presented in Figure 3.19 it was obvious that the biosimilar mucus gave high background fluorescence, which was dependent on the condition of the mucus; whether it was dried or not. It was considered to drop the utilization of biosimilar mucus, and continue the development of the method with PSIM, but it would have to be verified that PSIM did not give any background fluorescence first.

Little or no background fluorescence were seen in the distribution experiments (see Figure 3.3), which gave no reason to believe that biosimilar mucus or PSIM would give off any background fluorescence. However, it was also seen that both the PSIM and biosimilar mucus spread the laser light of the confocal microscopy to a great extent. It could not be ruled out that the plate reader might have detected some form of wavelengths, which not necessarily were fluorescence. Therefore a more thorough investigation of the background fluorescence of both PSIM and biosimilar mucus was performed.

New control background fluorescence measurement were performed on eight replicates of fresh biosimilar mucus, fresh PSIM, 5 % (w/v) Sigma mucin solution, 0.00001 % (w/v) yellow-green FluoSpheres®, 0.00001 % (w/v) red FluoSpheres®, MQ-water and empty wells. All the volumes were 200 µL. The fluorescence of 5 % (w/v) Sigma mucin solution was measured to check whether the Sigma mucin was responsible for the high background fluorescence of the biosimilar mucus. The MQ-water and empty wells were zero controls. The choice of the low concentration of the FluoSpheres® were made with the assumption that it would mimic the amounts of nanoparticles to be found on the mucus surface after the nanoparticle removal and washing step of the plate method. The fluorescence intensity measurements were performed twice; with the ex./em. wavelengths corresponding to excitation of the yellow-green FluoSpheres® - 495/535 nm, from now on referred to as yellow-green wavelengths - and the ex./em. wavelengths corresponding to the excitation of the red FluoSpheres® – 580/615 nm, from now on referred to as red wavelengths. The results of the background fluorescence measurements are presented in Figure 3.20. The same results are presented in Table 3.3 and Table 3.4 for a more precise illustration.
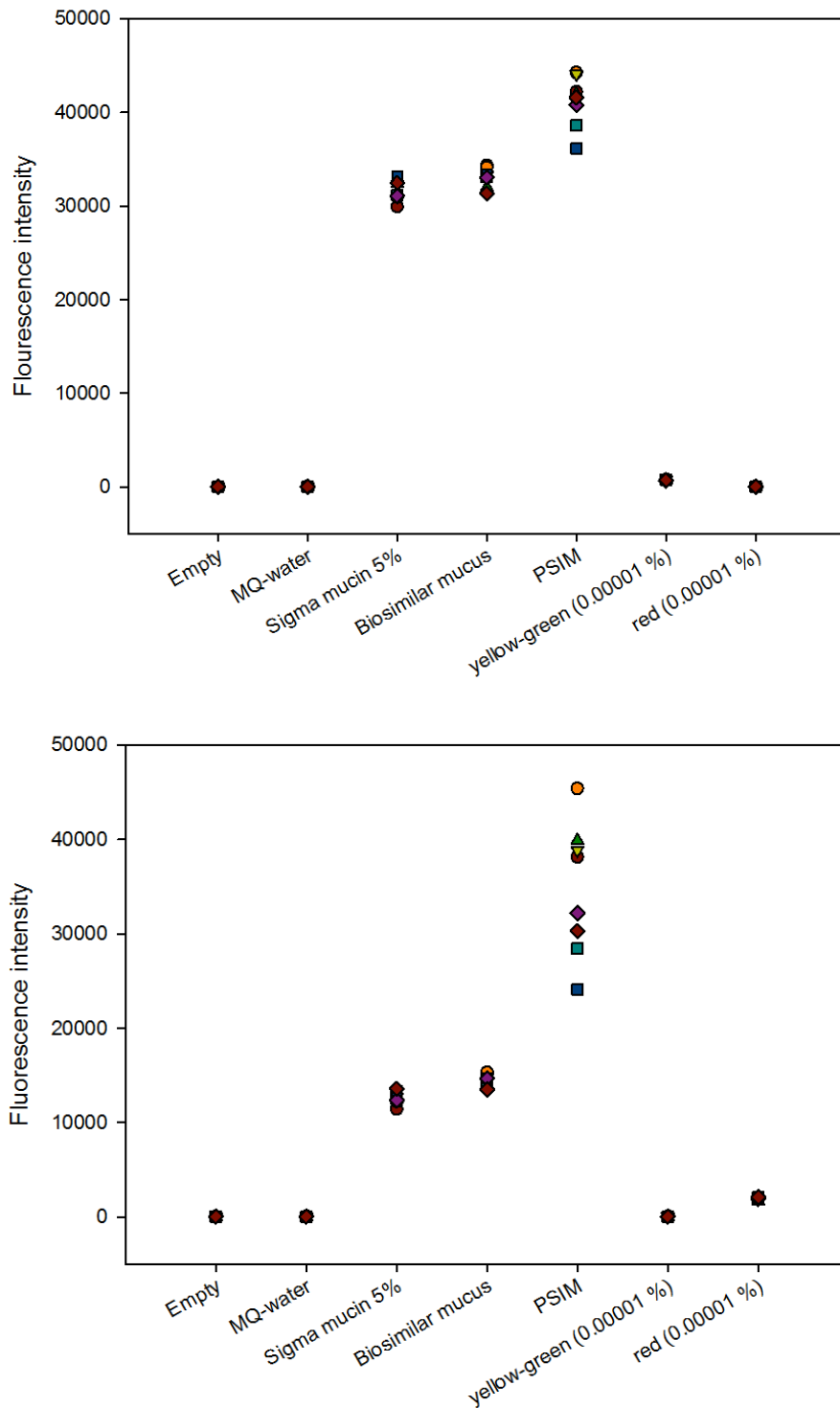
Figure 3.20 Fluorescence intensity measurements of eight replicates of fresh biosimilar mucus, fresh PSIM, 5% (w/v) Sigma solution, yellow-green FluoSpheres® (0.00001% (w/v)), red FluoSpheres® (0.00001% (w/v), MQ-water and empty wells. The upper plot is fluorescence measurements performed with ex./em. wave-lengths of the yellow-green FluoSpheres® (495/535 nm) and the lower plot is performed with ex./em. wave-lengths of the red FluoSpheres® (580-615 nm). The volume of sample in each well was 200 µL.

Table 3.3 Fluorescence intensity measurements of eight replicates of fresh biosimilar mucus, fresh PSIM, 5% (w/v) Sigma solution, yellow-green FluoSpheres® (0.00001% (w/v)), red FluoSpheres® (0.00001% (w/v)), MQ-water and empty wells. The fluorescence measurements are performed with ex./em. wave-lengths of the yellow-green FluoSpheres® (495/535 nm), and with 200 µL sample in each well. The values of the bottom row are average values of the eight replicate measurements.

Empty	MQ-water	Sigma mucin 5%	Biosimilar mucus	PSIM	yellow-green (0.00001 %)	red (0.00001 %)
19	23	29931	34341	42203	720	30
20	35	30925	34130	44247	772	35
17	25	32316	33301	44072	744	27
14	20	32351	32002	41968	753	25
28	28	31176	33071	38598	788	25
19	26	33160	33362	36118	754	33
18	28	31106	33055	40798	661	21
26	25	32470	31349	41599	741	30
20.13	**26.25**	**31679.38**	**33076.38**	**41200.38**	**741.63**	**28.25**

Table 3.4 Fluorescence intensity measurements of eight replicates of fresh biosimilar mucus, fresh PSIM, 5% (w/v) Sigma solution, yellow-green FluoSpheres® (0.00001% (w/v)) , red FluoSpheres® (0.00001% (w/v)), MQ-water and empty wells. The fluorescence measurements are performed with ex./em. wave-lengths of the red FluoSpheres® (580-615 nm), and with 200 µL sample in each well. The values of the bottom row are average values of the eight replicate measurements.

Empty	MQ-water	Sigma mucin 5%	Biosimilar mucus	PSIM	yellow-green (0.00001 %)	red (0.00001 %)
43	53	11416	15200	38147	60	1958
24	55	12227	15320	45391	40	1889
28	45	12640	14751	38857	47	1923
20	45	12493	13900	39883	46	1693
63	51	12734	14082	28449	24	1956
28	36	13277	14713	24116	51	2104
46	45	12385	14682	32205	43	1929
58	33	13581	13492	30300	55	2090
38.75	**45.38**	**12594.13**	**14517.50**	**34668.50**	**47.75**	**1942.80**

The results presented in Figure 3.20 , Table 3.3 and Table 3.4 show that the biosimilar mucus, 5 % (w/v) Sigma mucin solution and the PSIM have high average background fluorescence values compared to the FluoSpheres®.

The highest fluorescence intensity was quite unexpectedly detected in the PSIM samples. Auto fluorescence does occur in nature, but is most common in bacteria, algae, some insects, moths and aquatic invertebrates. Native mucus form pig intestines is not expected to exhibit much auto fluorescence (Heredia et al., 2008). However, the detection of high background fluorescence might be connected to the great light scattering of the confocal laser seen in the nanoparticle distribution experiments. A plausible explanation for the high background fluorescence in the PSIM, biosimilar mucus and the Sigma mucin 5% (w/v) solution might be that the detector of the plate reader has detected Raman scattering. When a light beam interacts with a material, part of the light is reflected, part of it is transmitted and part of it scattered. When the scattered light has different wavelengths than the incoming light, the

scattered light is called Raman scattering, and is a sort of inelastic scattering (Washington University in St.Louis Department of Earth and Planetary Sciences, 2014). This type of scattering can be detected by the detectors of plate readers and other scientific instruments, and would in this case give the impression of high background fluorescence of the PSIM, biosimilar mucus and Sigma mucin. Another plausible reason for the detection of high background fluorescence in the PSIM might be that the pig was feed food that contained fluorescent components or had fluorescent bacteria in the intestines, contaminating the samples. The mucus of the intestines was not rinsed after extraction from the intestines, and debris was visible. However, the most plausible explanation is the occurrence of Raman scattering, supported by the fact that the laser light of the confocal microscopy was spread to a great extent.

The average values of the fluorescence intensity of all the systems tested were higher when exposed to the green wavelengths than the red wavelengths, which indicates that whatever is causing the detected fluorescence, it is sensitive to the ex./em. wavelength settings of the measurement. With the exception of the yellow-green FluoSpheres®, this was not expected. As no particular background fluorescence was detected in the distribution studies, it was not expected to see any background fluorescence in the PSIM and biosimilar mucus when excited by the xenon lamp of the plate reader in the first place. There was no reason to believe that the fluorescence intensity measured in the mucus samples were true fluorescence, and that it would be sensitive to the ex./em. wavelengths of the measurement. The trend was also seen in the zero controls, which is particularly hard to explain. The FluoroNunc plates utilized are specially designed for fluorescence measurements, and it is not clear why the trend is observed in the controls also.

The fluorescence intensity measured in the biosimilar mucus and the Sigma mucin 5 % (w/v) solution was quite similar, with the biosimilar mucus having fairly higher values in both the measurements. This confirmed the Sigma mucin to considerably contribute to the fluorescence intensity detected in the biosimilar mucus.

One of the most important results of the background fluorescence measurements were that the variation in fluorescence intensity between biosimilar mucus replicates are greater than the fluorescence measured in the nanoparticle solutions. This renders it impossible to solve the

65

background fluorescence problem by subtracting the background fluorescence of dried mucus from the actual measurements of adsorbed nanoparticles on dried mucus. It might be argued that the concentration of the nanoparticles should have been raised, but a very high concentration of nanoparticles would most likely not have represented the amount of particles expected to adhere to the surface of the mucus after the removal of the nanoparticles and the washing step of the plate method.

3.2.3.1 Control background fluorescence measurements

For a more thorough examination of the background fluorescence of the various mucous systems, additional and some replicative fluorescence measurements were conducted, see Figure 3.21 and Appendix C.2.2.
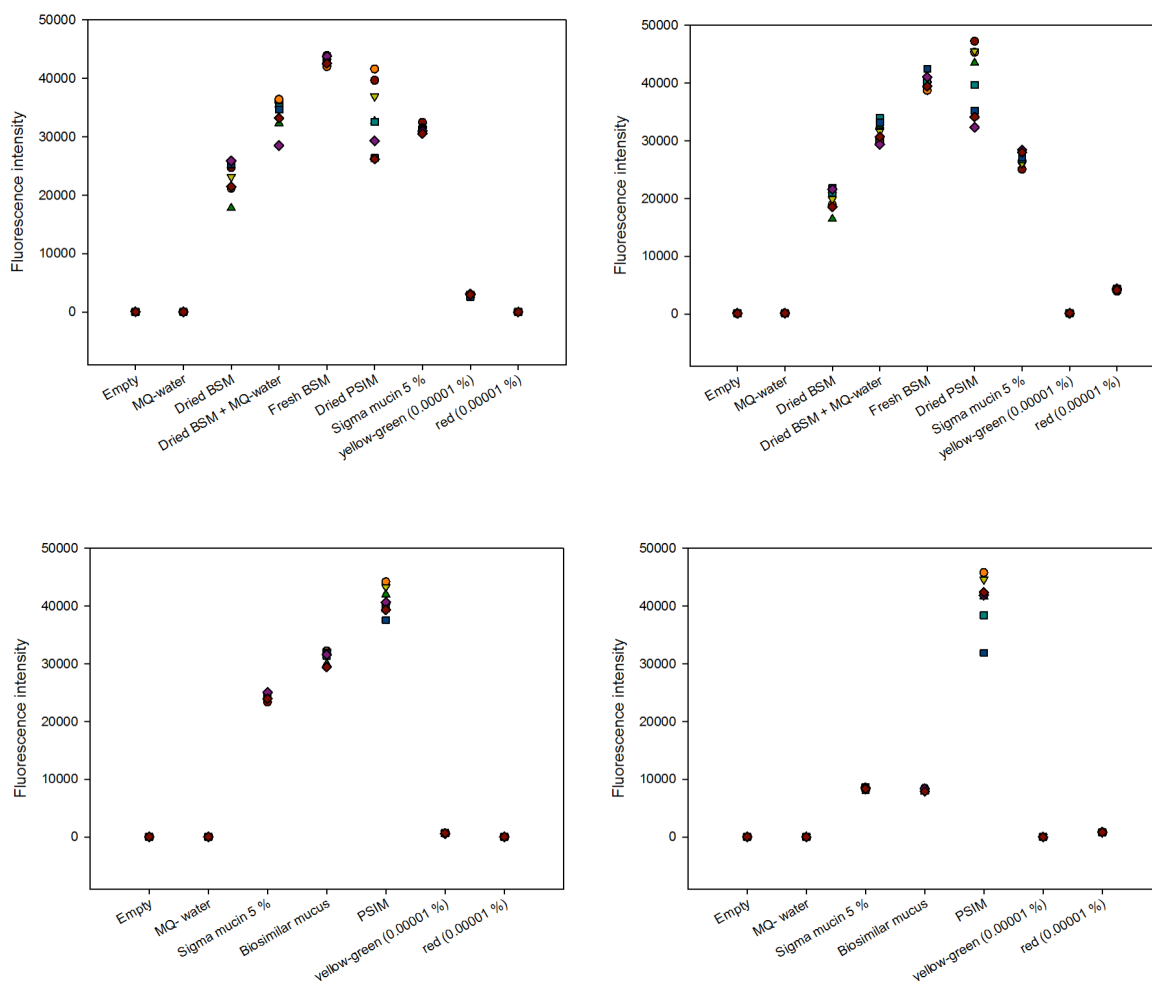
Figure 3.21 Additional background fluorescence intensity measurements. The upper row presents measurements of empty wells, MQ-water, dried biosimilar mucus (BSM), dried biosimilar mucus with MQ-water on top, fresh biosimilar mucus, dried PSIM, 5 % (w/v) Sigma mucin solution, yellow-green FluoSpheres® (0.00001% (w/v)) and red Fluospheres® (0.00001% (w/v)). The upper row results are measured with ex./em. wavelengths of 495/535 nm (left) and 580/615 nm (right). The lower row presents fluorescence intensity measurements of empty wells, MQ-water, 5 % (w/v) Sigma mucin solutions, fresh biosimilar mucus, fresh native small intestinal mucus, yellow-green FluoSpheres® (0.00001 % (w/v)) and red Fluospheres® (0.00001 % (w/v)). The results in the lower row are measured with ex./em. wavelengths of 505/545 nm (left) and 580/625 nm (right). All volumes were 200 µL.

From the additional background fluorescence measurements presented in Figure 3.21 it was verified that the PSIM, biosimilar mucus and Sigma mucin 5 % (w/v) solutions has differing amounts of fluorescence intensity dependent on the ex./em. wavelengths of the measurements.

67

This was verified when getting slightly different fluorescence intensity results after replicating the measurement presented in Figure 3.20 with somewhat different ex./em. wavelengths than the yellow-green and red wavelength of the earlier measurements (lower row of Figure 3.21). The new measurements of dried biosimilar mucus, dried biosimilar mucus with MQ-water and fresh biosimilar mucus (upper row of Figure 3.21) showed the opposite trends as the previous measurement (Figure 3.19), with the highest fluorescence intensity detected in the fresh biosimilar mucus. However, the values are still very high. Although there was seen some variation in the fluorescence intensity when comparing the additional measurements to the first ones, the trends were concurrent with a very high fluorescence intensity detected in both the PSIM and biosimilar mucus samples, both fresh and dry.

3.2.3.2 Sigma mucin gradient experiment

The fluorescence intensity of Sigma mucin was tested for concentration dependency to verify that the fluorescence detected was a real effect of the Sigma mucin. A dilution series of Sigma mucin solved in MQ-water were made, with concentrations 0.05 % (w/v), 0.1 % (w/v), 0.5 % (w/v), 1 % (w/v) and 5 % (w/v). The fluorescence intensity of 200 µL of each dilution was measured with yellow-green wavelengths and red wavelengths. The results from the measurements with the yellow-green wavelengths are presented in Figure 3.22, the remainder of the data is to be found in Appendix C.2.3.
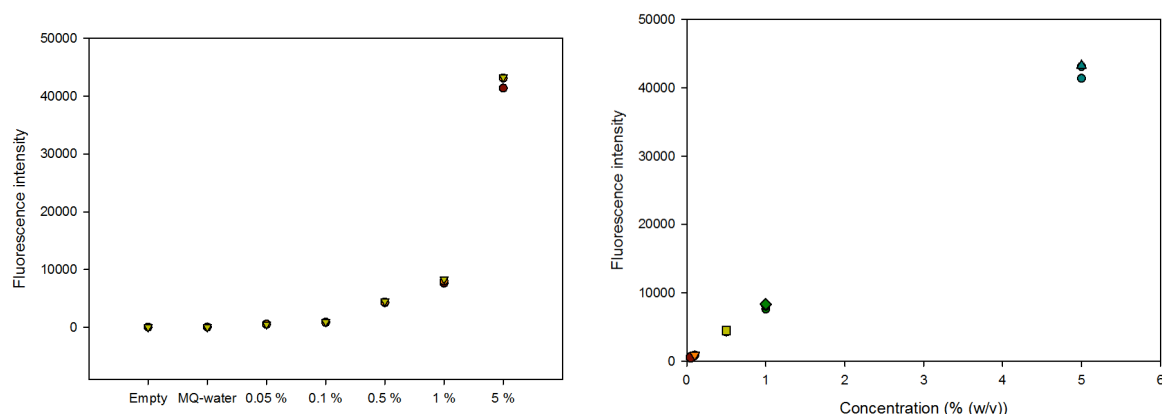
Figure 3.22 Fluorescent intensity measurements of three replicates of different concentrations of Sigma mucin solutions. The ex./em. wave-length of the measurements were 495/535 nm. The volume of the solutions was 200 µL. In the left plot: The percentages represent the concentration % (w/v) of the different solutions. Empty wells and MQ-water filled wells were also measured as control.

As seen in the results of Figure 3.22 there is a clear correlation between the concentration of Sigma mucin and the intensity of the fluorescence measured. It is a linear dose response relationship between the concentration of the Sigma mucin solutions and the fluorescence intensity.

3.2.3.3 Measuring the fluorescence of differing amounts of biosimilar mucus and PSIM

The fluorescence intensity of 100 µL and 200 µL fresh biosimilar mucus and fresh PSIM was measured to investigate the correlation between the amount of mucus and the intensity of the fluorescence. The measurements were conducted twice, with yellow-green and red ex./em. wavelengths. The results from the measurements of yellow-green wavelengths are presented in Figure 3.23 and the remaining measurements can be found in Appendix C.2.4.
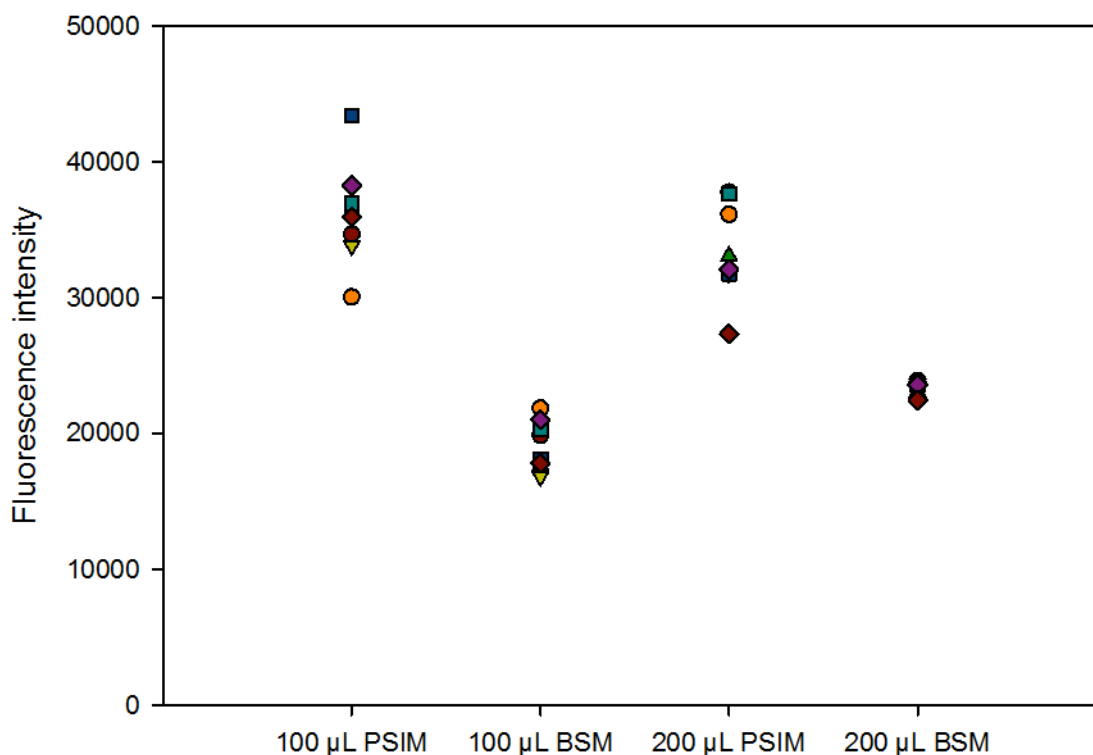
Figure 3.23 Fluorescence intensity measurements of different amounts of biosimilar mucus (BSM) and PSIM. The ex./em. wavelength in the measurement were 495/535 nm, and there were eight replicates of each amount of mucus.

Quite unexpected, the fluorescence intensity detected in 100 μL PSIM have almost the same values as the fluorescence intensity detected in 200 μL PSIM. It was expected to see a doubling of the fluorescence intensity in the 200 μL mucus samples to the 100 μL samples. The average values of fluorescence intensity of the 100 μL PSIM samples are actually somewhat higher than the average values of the 200 μL PSIM (see Appendix C.2.4). The biosimilar mucus measurements show a somewhat more expected trend, as the fluorescence of 100 μL biosimilar mucus show lower or the same amount of fluorescence intensity as the 200 μL wells, although not twice as high.

These results might suggest that the amount of fluorescence detected in 100 μL mucus "saturates" the fluorescence intensity possible to detect, so that higher amounts of mucus will give off approximately the same values. However, these results might rather indicate that there is some sort of surface effect in the mucus. From Figure 3.18 it was determined that the plate reader measures the amount of nanoparticles in a solution, and not the concentration of

the nanoparticles. In these measurements the xenon lamp of the plate reader had no problems reading off the correct fluorescence when there were only nanoparticles in the wells. For the measurements presented in Figure 3.23 it might be that the plate reader is not measuring the amount of "fluorescent" matter, because of poor penetration of the mucus. This is supported by the previous findings of poor laser penetration of the mucus by the confocal microscope (see section 3.1.1.2). Due to the xenon lamps' poor penetration of the mucus, the plate reader measures only the "fluorescence" in the surface of the mucus. Hence will the plate reader detect broadly the same fluorescence intensity from mucus samples of both 100 μL and 200 μL.

3.2.4 Conclusive remarks on the plate method

Some of the variation seen in the fluorescent measurements between replicates of the PSIM and between replicates of the biosimilar mucus, might be due to the method of weighing the correct amount of mucus into each well. This method is not very accurate, but due to the high viscosity of the mucus, pipetting of mucus was not possible. However, the experiment that measured the fluorescence intensity of 100 μL and 200 μL biosimilar and PSIM samples gave results that refute this theory, when it seemingly was no big difference in the fluorescence intensity measured between the two amounts of mucus.

As the measurements were wavelength dependent, it might have been possible to find wavelengths were the high fluorescence intensity of the biosimilar mucus and PSIM was not detected. However, the ex./em. maxima of the yellowgreen (505/515 nm) and red (580/605 nn) FluoSpheres® restricted the wavelengths of the measurements to these approximate regions of the light spectra.

Even though there was seen some variation in the fluorescence intensity between replicate experiments, all the fluorescence intensity measurements of the PSIM and biosimilar mucus were concurrently high. The high and varying amount of background fluorescence of the mucous systems was not feasible with the further development of the plate method. It shall not be ruled out that there might be a solution to the problem, but the restricted time of the master thesis was also a contributory factor to the decision to terminate the experiment series.

All in all the plate method looked promising up until it was detected a high background fluorescence intensity in the biosimilar mucus and the PSIM, which most likely is attributed to Raman scattering. The Sigma mucin is to a high extent responsible for the fluorescence intensity detected in the biosimilar mucus. With the exception of the red FluoSpheres® all the other variables tested gave off higher fluorescence intensity values when exposed to the yellow-green ex./em. wavelengths than the red ex./em. wavelengths, hence showing wavelength dependency. It was decided to terminate the series of experiments, as the results were not feasible with the further development of the plate method.

3.3 Rheological profiling of biosimilar mucus and PSIM

3.3.1 Rheological measurements

Oscillatory rheological measurements were performed on PSIM, biosimilar mucus and solutions of Sigma mucin type II. The measurements on biosimilar mucus and PSIM were performed to determine that the biosimilar mucus gives a comparable rheological profile and viscoelastic properties to the PSIM. The viscoelastic properties of mucus are predominantly a function of the mucin matrix (Lai et al., 2009b). The biosimilar mucus contains components like lipids, PAA and bovine serum albumin. To verify the necessity of these non-mucin components of the biosimilar mucus, control measurements were run on Sigma mucin type II dispersed in a 10 mM HEPES buffer containing 1 mM $MgSO_4$ and 1.3 mM $CaCl_2$. Three different concentrations of the mucin solutions were prepared and measured, 5 % (w/v) - which is the same concentration as in biosimilar mucus, 8 % (w/v) and 10 % (w/v).

Small deformation oscillatory frequency sweeps were chosen, as these measurements are run at non-destructive conditions and "best reflects mucus rheology in the native, unperturbed way" (Lai et al., 2009b). Also large deformation oscillatory strain sweeps were run in order to investigate the rheological reversibility of PSIM and biosimilar mucus.

3.3.2 Rheological measurements of PSIM

3.3.2.1 Frequency sweeps

Three replicates of strain controlled frequency sweeps in the range 0.001-10 Hertz were run on different PSIM samples. Ten minutes prior to the frequency sweeps, strain sweeps were run in the stain range $1*10^{-5}$-10 to determine the linear viscoelastic region where the rheological values are independent of the imposed strain. The time lag allowed for the rheological recovery of the mucus gel. Results from the three replicate frequency sweeps are presented in Figure 3.24.
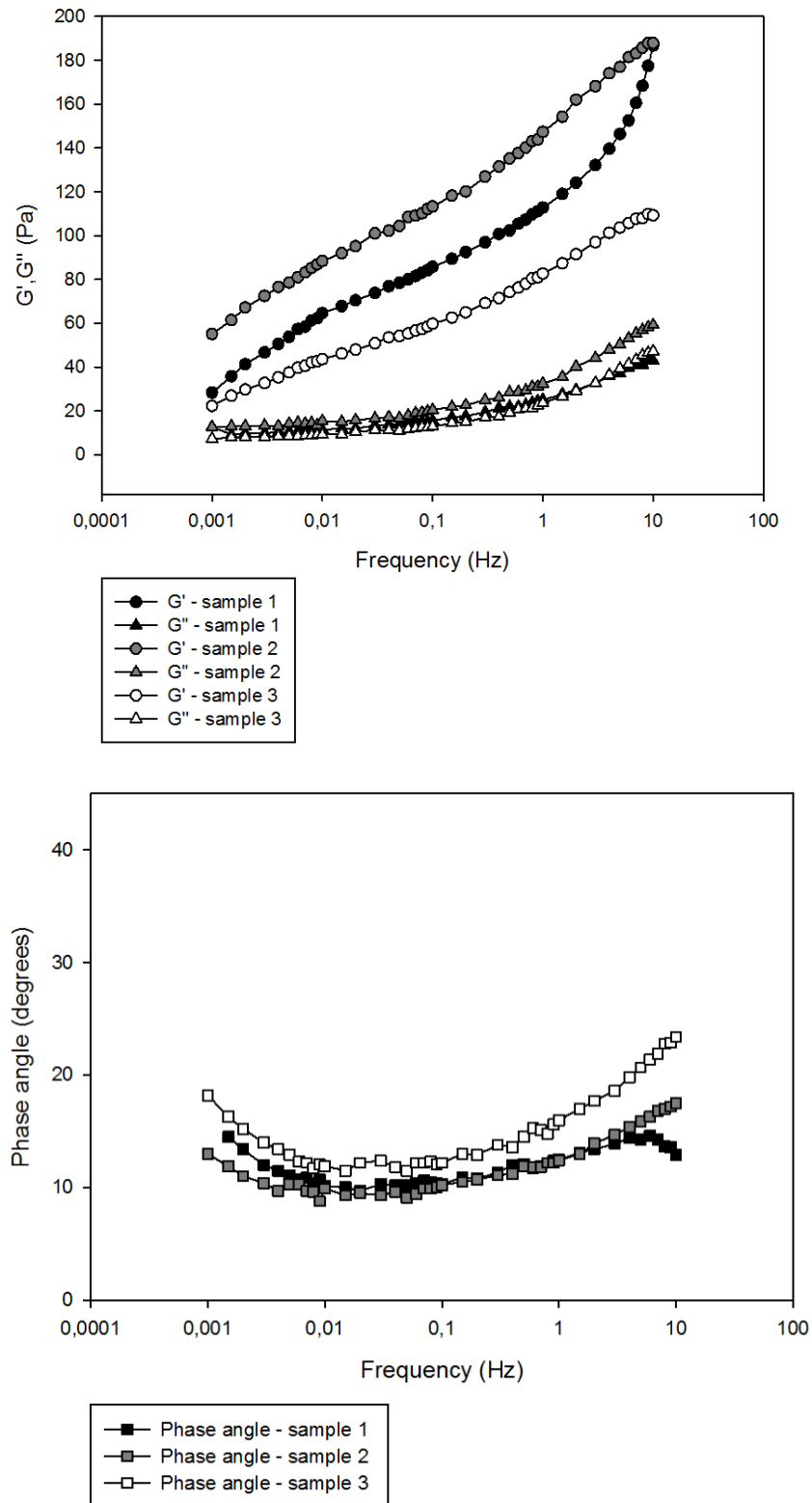
Figure 3.24 Frequency sweeps of PSIM in the frequency range 0.001-10 Hertz. The storage (G') and loss moduli (G'') are presented in the upper plot and the corresponding phase angles are presented in the bottom plot. All strains were fixed within the linear viscoelastic region, and run with a constant temperature of 25 °C.

74

The three frequency sweeps presented in Figure 3.24 generally display the same trends, with a dominant elastic-like behaviour of all the samples over the whole frequency interval. The absolute values of the storage moduli (G') are high compared to the absolute values of the loss moduli (G''). The variation in the absolute storage modulus (G') values probably reflects the natural variation expected to be found between samples of untreated *ex vivo* PSIM, as native mucus is an inhomogeneous material that consists of different amounts of mucins, water, ions, lipids, proteins, cell debris, nucleic acids, debris from food etc., that will affect the viscoelastic properties of mucus (Girod et al., 1992) (Smart, 2005).

The plots in Figure 3.24 display frequency dependency of the rheological variables as would be expected from un treated *ex vivo* PSIM (Zhong and Daubert, 2013). The different transient and non-transient intermolecular interactions that maintain the mucus gel matrix, like electrostatic, hydrophobic and H-bonding interactions, have differing lifetimes and relaxation times. When the frequency increase there will be less and less time for the rearrangement of the transient interactions (Taylor Nordgård and Draget, 2011), which restricts the flow of the mucus, and renders it to become more elastic in its' behaviour as the frequency increase. This is reflected as a steep increase in the storage modulus (G') values seen in the frequency sweep of Figure 3.24, and the low values of the phase angles in the bottom plot of Figure 3.24. The slight U-shape of the phase angles reflects both the behaviour of the storage moduli (G'), and the loss moduli (G''). With a dominant elastic behaviour, the PSIM is able to constitute a barrier in the intestines that protects the underlying epithelial surfaces from mechanical stress and hydrates the epithelial cells (Atuma et al., 2001) (Bansil and Turner, 2006).

3.3.2.2 Strain Sweeps

Several replicates of strain sweeps with strain range of $1*10^{-5}$-10 were run on different PSIM samples. Overall the trends are similar, with small shifts in the values of the moduli and phase angles. The most representative strain sweeps is presented in Figure 3.25.
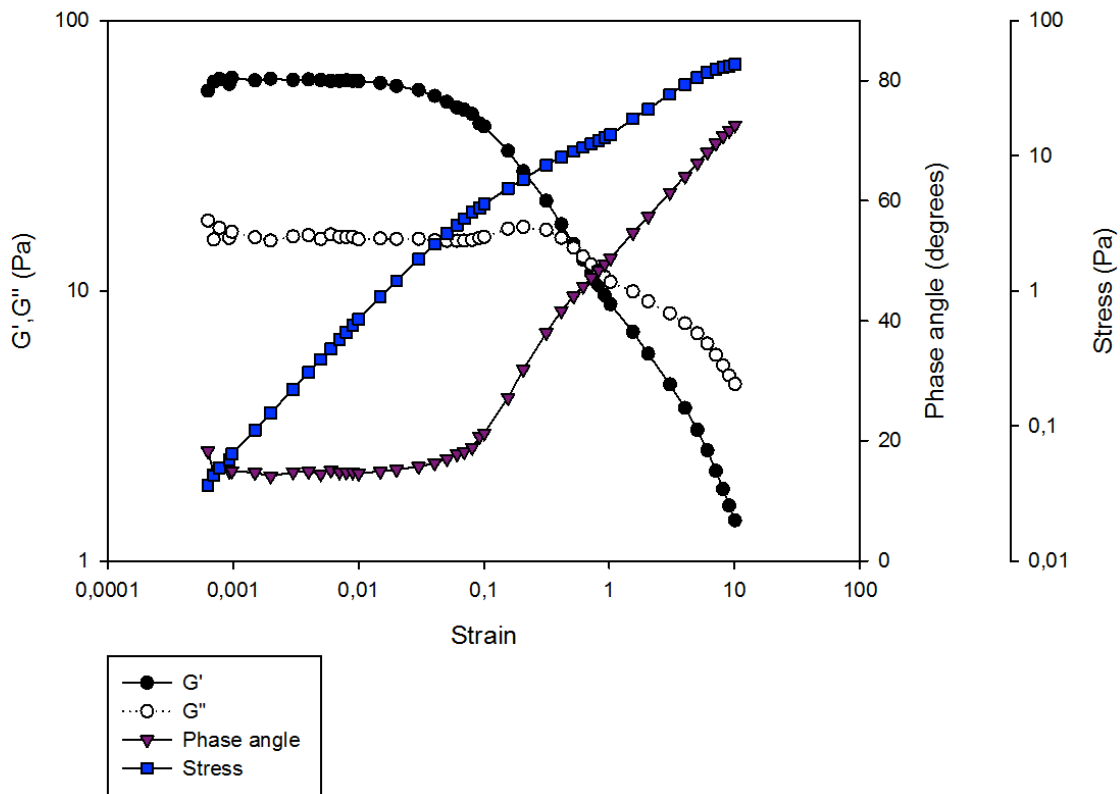
Figure 3.25 Strain sweep of PSIM with increasing strain in the range $1*10^{-5}$-10. Run at a frequency of 1 hertz and a temperature of 25 °C.

The increasing strain sweep of PSIM presented in Figure 3.25 indicates a smooth transition from an elastic-like behaviour of the mucus at lower strains, to a more viscous-like behaviour when the imposed strains reach 0.8 and increase. Data points at strains 0.00001-0.0007 were omitted because of noise in the data. There is a clear viscoelastic region at strains 0.0007 – 0.05, where the storage modulus values (G'), loss modulus values (G'') and hence the phase angle values are kept at the same level, and are independent of the strain (Zhong and Daubert, 2013). The loss modulus (G'') values exceed the values of the storage modulus (G') at strain 0.8, when the phase angle reaches 45 degrees. The stress curve shows how much stress is needed to induce the strain. The stress increases broadly linearly with increased strain. As the mucus becomes less able to resist deformation, the gradient of the stress curve changes, and less stress is needed to induce the same strain (Taylor et al., 2005a).

The gradual weakening of the gel, indicated by the rheological parameters, might on the molecular level in part be attributed to the "dangling chain ends" of the mucins (Taylor et al., 2003). As the imposed strain increase some bonds are broken, and some bonds are formed. The weakening of the gel occurs when the rate at which the bonds break are higher than the

76

rate at which new bonds form (Bøgh et al., 2013). When the strain is removed, the broken bonds of the gel reform (Taylor et al., 2003). Rheological reversibility is important for PSIM as it enables the mucus to be reused, as discussed below.

To illustrate the variation in the strain sweep results between the PSIM samples, the two samples yielding the highest and lowest values of the rheological variables are presented in Figure 3.26.
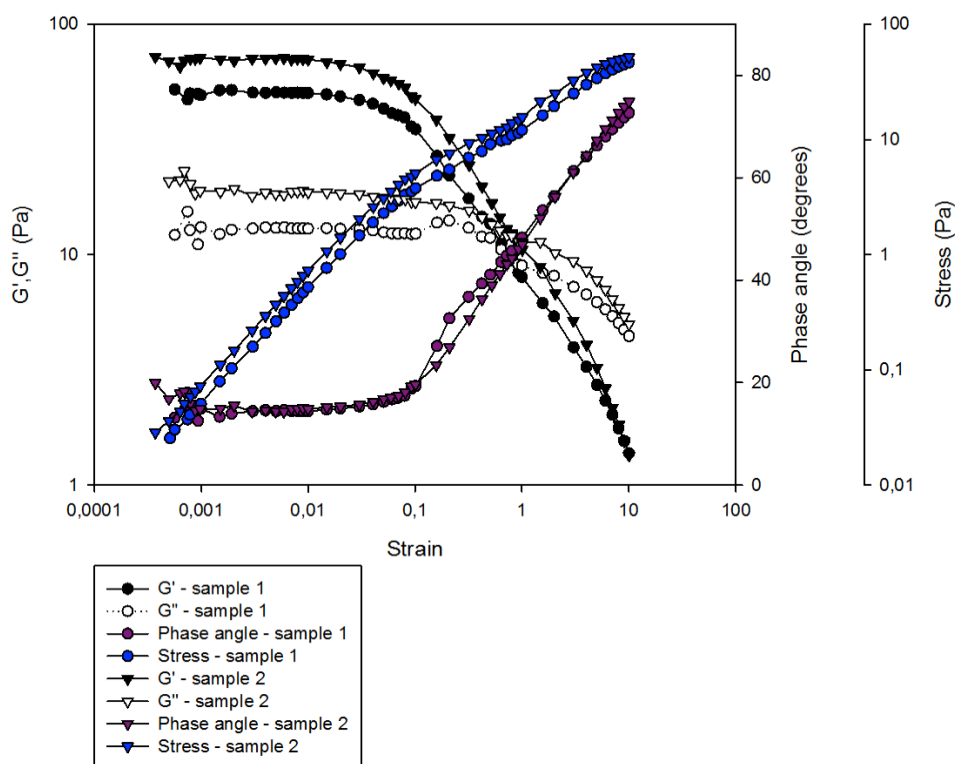
Figure 3.26 Strain sweeps of PSIM of two different samples, sample 1 represented by circles and sample 2 represented by triangles. The sweeps were run in the strain range $1*10^{-5}$-10, a frequency of 1 Hertz and a temperature of 25 °C.

The plots in Figure 3.26 reflect the differences in the general trends of the strain sweeps of PSIM, which are relatively small. The largest variations are found in the absolute values of the storage (G') and loss moduli (G''), but the near identical phase angles and the identical slopes of the stress curves confirm a similar behaviour in the PSIM samples when they are exposed to increasing strains. Similar phase angles implies that the relationship between the storage modulus (G') and loss modulus (G'') from one sample to the next is the same (Picout and Ross-Murphy, 2003).

3.3.2.3 Investigation of thixotropic effects of PSIM

The thixotropic effects of PSIM were investigated by running two up-down strain sweeps on two different samples in the strain range $1*10^{-5}$-10. Thixotropic effects would be reflected in an up-down strain sweep when the rheological variables do not follow the same path at increasing and decreasing strains. The two up-down strain sweeps run yielded similar results. One of them is presented in Figure 3.27.
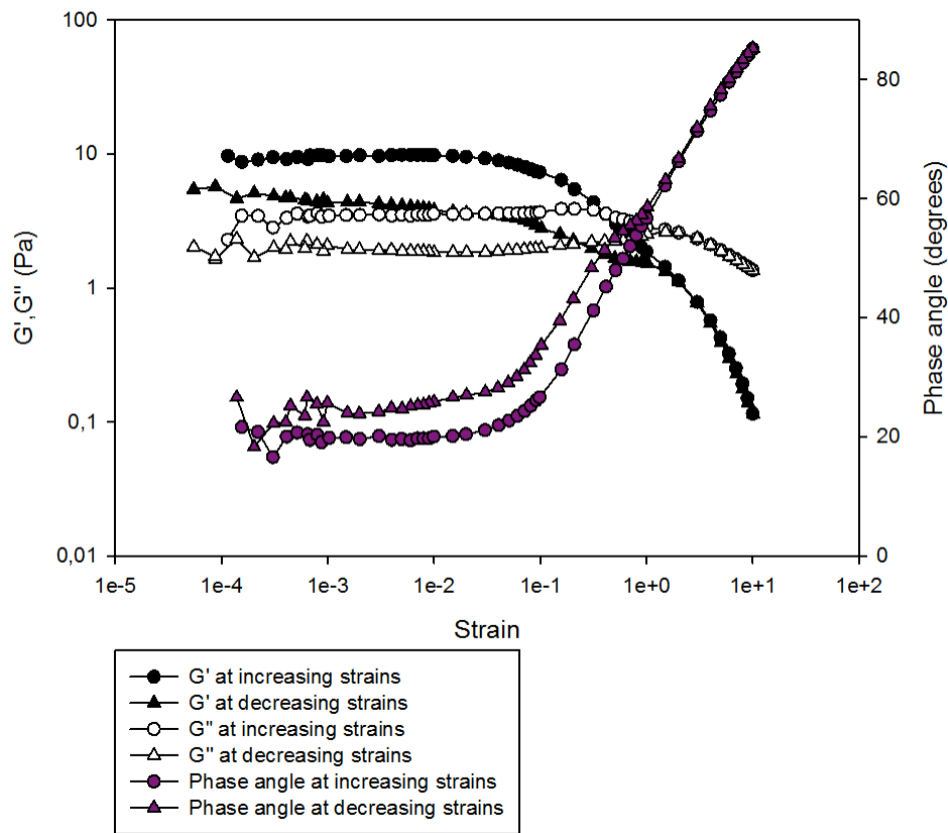
Figure 3.27 Up-down strain sweep of PSIM, where the circles represent values at increasing strains and the triangles represent values at decreasing strains. The sweep was run at a frequency of 1 Hertz and at 25 °C.

The up-down strain sweep in Figure 3.27 shows that the rheological variables do not follow the same path with increasing and decreasing strains. Data at strains 0.0001-0.001 was omitted because of noise. The moduli values are similar in the strain range ~1-10, where the PSIM show a viscous-like behaviour. Within this region the mucus has a completely shear thinning behaviour (Lai et al., 2009b). As the strains starts to decrease from 10 and reach the point where the transition from a viscous-like behaviour to a more elastic-like behaviour

78

occurs, the path of the rheological variables starts to deviate from the path seen as the strains increased. This occurs because the bonds and interactions in the matrix are not able to rebuild themselves in the given time scale of the experiment. The rheological reversibility of the mucus is in this region not only dependent on the imposed strain, but also on time (Moller et al., 2006).

Rheological reversibility includes both shear thinning, which is dependent on strain/shear, and thixotropy, which is dependent on strain/shear and time (Picout and Ross-Murphy, 2003) (Moller et al., 2006). The gradual weakening of the PSIM in Figure 3.25 & Figure 3.26 indicated shear thinning properties of the PSIM, and both shear thinning and thixotropic behaviour were observed in the up-down strain sweep of Figure 3.27, as discussed above.

As already mentioned, rheological reversibility is an expected and crucial property of PSIM as it enables the reuse of mucus (Taylor et al., 2005a). Of the 10 litres of mucus that are secreted in the human GI tract every day, 9.8 litres of it is reused (Cone, 2009). If the mucus did not have the ability to rebuild disrupted bonds, interactions and entanglements, the mucus gel would maintain its' liquid properties after strain/shear induced flow, and could not be reused. A loss of the mucus' viscoelastic properties would have rendered it non-functional as a lubricant or assisting in locomotion (Taylor et al., 2005a), and it would have been eliminated with the faeces, making the body spend great amounts of energy continuously generating new mucus (Cone, 2009).

The results from the rheological measurements of PSIM shows that there are some variations between replicate experiments on different PSIM samples, especially in the absolute values of the storage moduli. However, the phase angle of these replicate experiments is quite similar, reflecting the same behaviour of the PSIM samples. The variation observed are most likely due to natural variation, which is expected between mucus extracted from different places in the intestine or between different individuals (Girod et al., 1992).

3.3.3 Rheological measurements of biosimilar mucus

Frequency sweeps and strain sweeps were performed on biosimilar mucus samples for verification of viscoelastic behaviour and properties, and comparison with the PSIM.

3.3.3.1 Frequency sweeps

Three replicate frequency sweeps were run on different biosimilar mucus samples from the same batch, in the frequency range 0.01-10 Hertz and with a fixed strain within the linear viscoelastic region. The linear viscoelastic region was found prior to the frequency sweeps by running strain sweeps in the strain range $1*10^{-5}$-10 on different biosimilar mucus samples. A frequency sweep was also run on a fourth biosimilar mucus sample, from a second biosimilar mucus batch. On several samples of biosimilar mucus from the second batch stress controlled frequency sweeps were run in the frequency range 0.1-10 Hertz. The four replicates of the strain controlled frequency sweeps are plotted together in Figure 3.28.
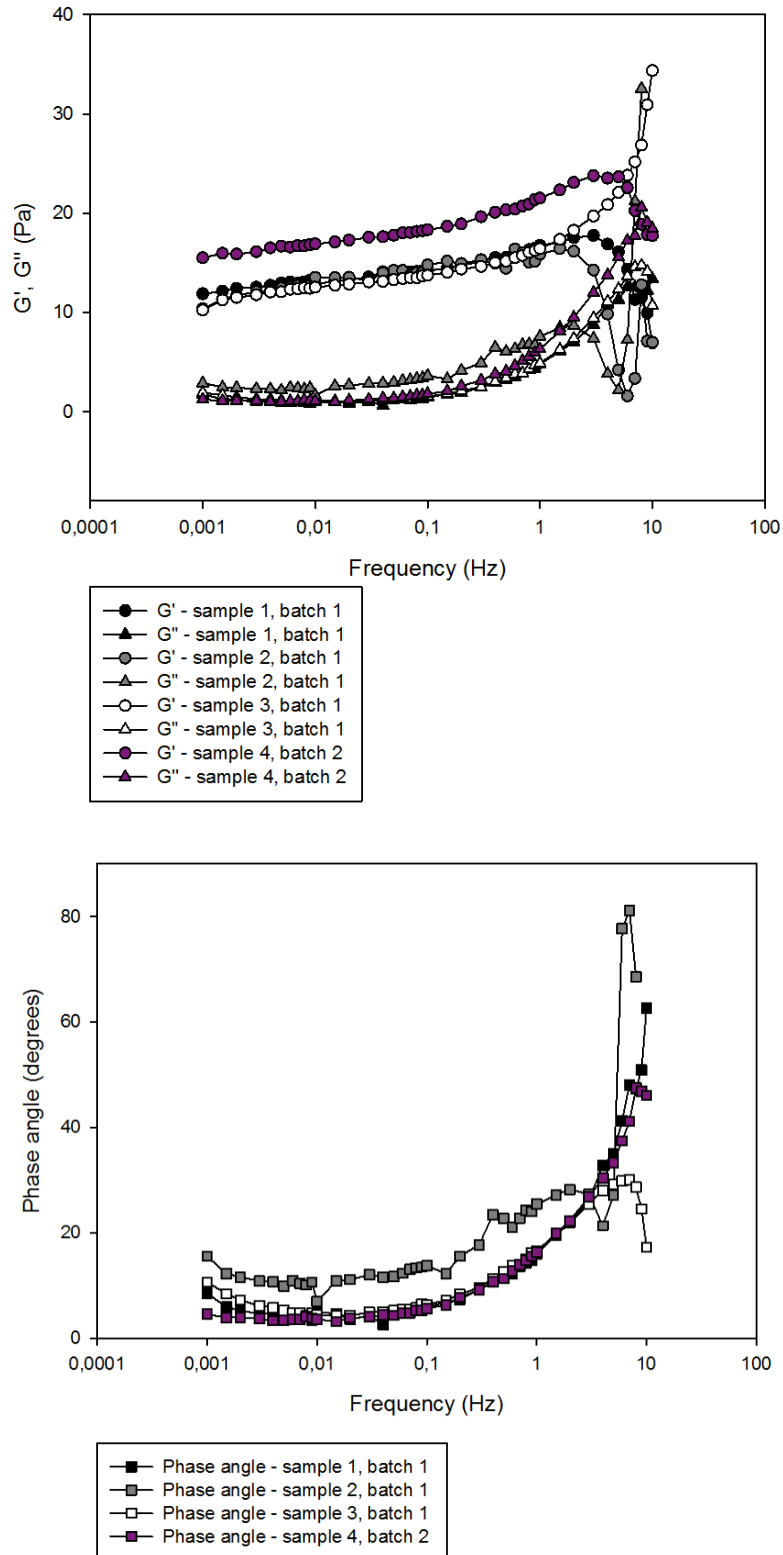
Figure 3.28 Four replicate strain controlled frequency sweeps of different biosimilar mucus samples, in the frequency range 0.001-10 Hertz. The fixed strain for all the measurements was within the linear viscoelastic region, and the temperature was 25 °C. The moduli values are presented in the upper plot, and the phase angle values are presented in the lower plot.

The four replicate frequency sweeps presented in Figure 3.28 shows that biosimilar mucus has an elastic-like dominant behaviour at strains 0.001-7 Hertz. The loss moduli values of the biosimilar mucus have a steep unexpected increase at frequencies 0.1-10 Hertz, which renders the behaviour of the biosimilar mucus more viscous-like in this frequency range. This is also reflected in the phase angles, which increase at the highest strains and reach well beyond 45 degrees. These trends are observed in three out of four samples. Similar to the PSIM discussed above, the biosimilar mucus was expected to show a dominant elastic behaviour through the whole frequency sweep, as the increased frequency is expected to inhibit rearrangement of the bonds and interactions in the gel matrix of the biosimilar mucus, so that an increased elastic-like behaviour is seen through the whole frequency range.

The unexpected behaviour at the highest frequencies, where the loss modulus (G'') values are higher than the storage modulus values (G'), implies that the bonds and interactions of the mucus have time to rearrange in this high frequency range. This is contradictory to theory (Zhong and Daubert, 2013), but might be explained by an occurrence of phase transition of the mucin molecules of the biosimilar mucus. Sigma mucin type III, which are partially purified mucins from pig stomachs, have previously been proven to enter a fluid liquid crystalline phase at temperatures above 24.8 °C, but only at concentrations 24-28 % (w/w) (Davies and Viney, 1998). However, this does not exclude the possibility of a phase transition in the Sigma mucin type II molecules of the biosimilar mucus. For the Sigma mucin type III in the studies of Davies and Viney, the interdigitation of the sugar side chains of the mucin molecules was though to be responsible for the phase transition (Davies and Viney, 1998). It is not unreasonable to think that this might have occurred in the Sigma mucins type II of the biosimilar mucus as well. The dense sugar side chains of the mucin molecules are the areas best protected from protease cleavage by the non-mucin proteins that are not purified from the mucins. The sugar side chains have probably kept most of the original structure found in the pig stomach in both Sigma mucin type II and type III.

The cause of the unexpected behaviour observed, might also be differences in the gel network in the biosimilar mucus, compared to the gel network of native mucus, like PSIM. The gel network of the biosimilar mucus comprise of Sigma mucin type II, supported by the scaffolding properties of PAA. This gel network is not built the in the same manner as the gel network of native mucus, which is mainly held by mucins alone (Lai et al., 2009b), and might

therefore also behave differently. Nevertheless, the biosimilar mucus was developed for cell compatibility with Caco-2 cells for drug absorption studies, and it is not likely that experiments as such introduce conditions corresponding to frequencies 7-10 Hertz.

Even though small batch variations can be observed in the frequency sweeps, all the samples follow the same trends in the frequency range 0.001- 2 Hertz. Above this frequency there are some differences in the moduli values, but in three out of four samples the values of the storage modulus hits a peak value and then decreases at the highest frequencies. In three out of the four samples the loss modulus keeps increasing until the frequency reach 10 Hertz. These results might indicate that the rheological behaviour of the biosimilar mucus is most stable at frequencies below 2 Hertz.

In the linear viscoelastic region the stress and strain is independent of the frequency (Picout and Ross-Murphy, 2003). To make sure that the stress did not increase when the strain was fixed and thereby could have had an effect reflected in the high loss modulus (G''), the results from a stress controlled frequency sweep were compared to two of the results from the strain controlled frequency sweeps, presented in Figure 3.29. The results from the stress controlled frequency sweeps were close to identical (not included).
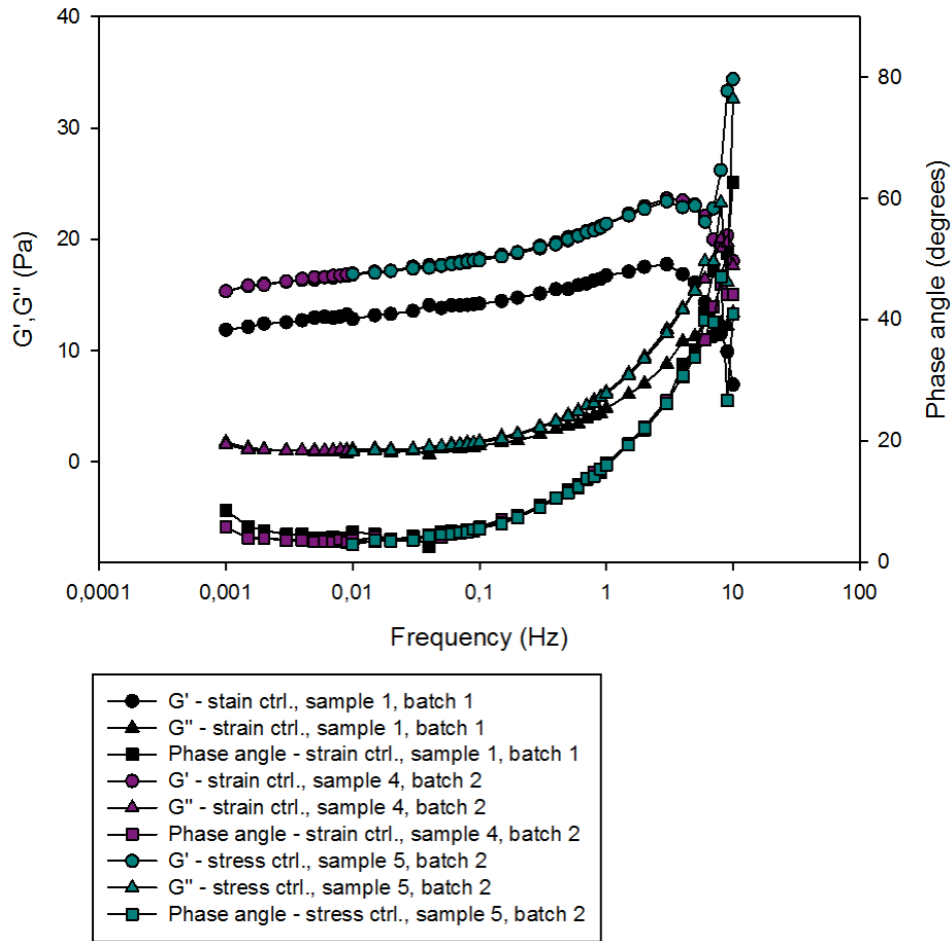
Figure 3.29 Frequency sweeps of biosimilar mucus with increasing frequencies, where two of the samples are strain controlled and one of the samples are stress controlled. The stress/strain were kept within the linear viscoelastic region, and all the measurements run at 25 °C.

As seen in Figure 3.29 the curves of the moduli and phase angle of the stress controlled frequency sweep of sample 5 follow almost the exact same curves as the corresponding variables of the strain controlled frequency sweep of sample 4. This indicates that the high values of the loss moduli in the frequency range of 0.1-10 Hertz is not an effect of increasing stress during the strain controlled frequency sweeps, since the exact same behaviour is observed in a stress controlled frequency sweep and a strain controlled frequency sweep. Sample 4 and sample 5 were from the second mucus batch, while sample 1 was from the first mucus batch. This again demonstrates some batch variations for the biosimilar mucus.

3.3.3.2 Strain Sweeps

Several strain sweeps in the strain region $1*10^{-5}$ - 10 were run on different biosimilar mucus samples, both from batch number one and batch number two. In general, the trends in the strain sweeps are similar, with some variation in the absolute values of the moduli. The most representative strain sweep is presented in Figure 3.30.
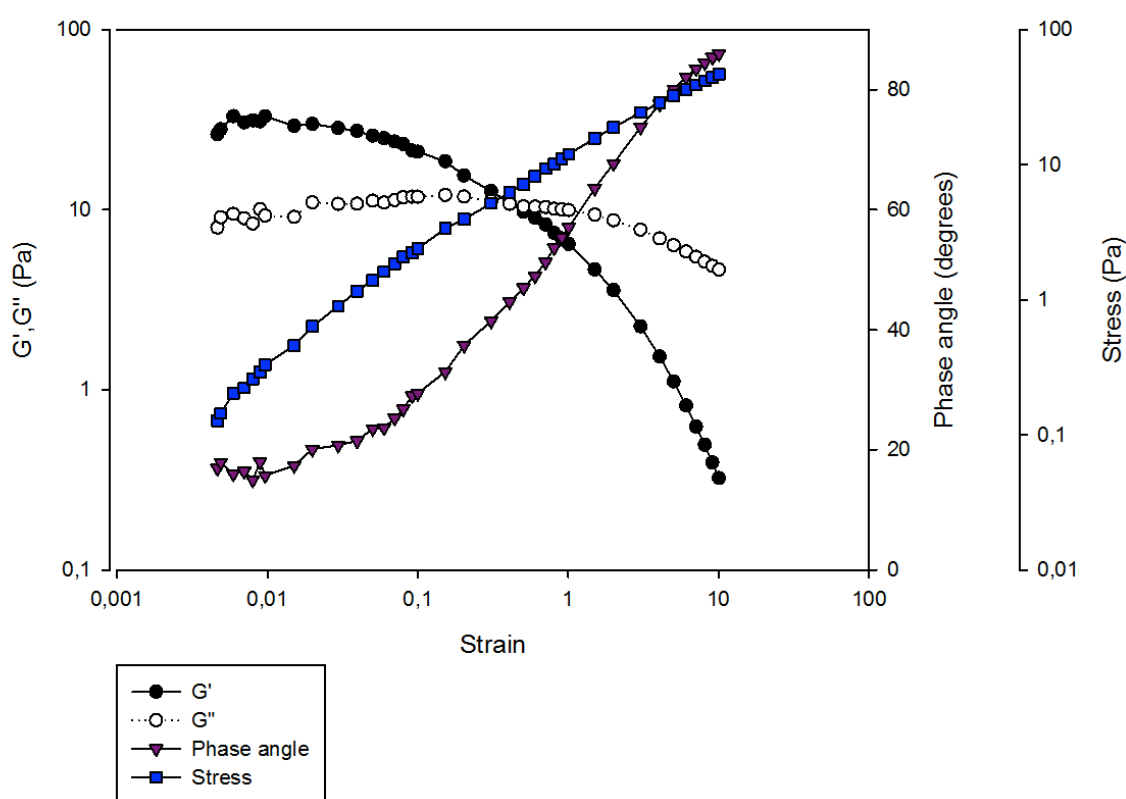
Figure 3.30 Strain sweep of biosimilar mucus with increasing strains, run at a fixed frequency of 1 Hertz and a temperature of 25 °C.

The increasing strain sweep of biosimilar mucus presented in Figure 3.30 shows that no catastrophic failure occurs. Data points at strains $0.00001 - 0.004$ have been omitted because of noise. A smooth transition from an elastic-like behaviour at low strains, to a viscous-like behaviour at high strains is observed. The behavioural transition occurs at strain 0.4, when the phase angle reaches 45 degrees. Just like the PSIM, the interactions and bonds of the gel network in the biosimilar mucus starts to break at a faster rate than new interactions are

formed as the imposed strain is increased (Bøgh et al., 2013), and a weakening of the gel occurs. The majority of the behavioural change is due to the decrease of the elastic-like behaviour rather than a big change in the viscous-like behaviour, seen as a steep decrease of the graph of the storage modulus (G') compared to a minor decrease of the graph of the loss modulus (G'') with increasing strains. The stress curve gradually levels off in the entire strain range, and indicates that less and less stress is needed to induce the strain, which fits well with a gradual weakening of the gel.

The same trends are observed in all the strain sweeps of biosimilar mucus, with some variation in the absolute values of the moduli. The sweeps of highest and lowest rheological variables are presented in Figure 3.31 to illustrate the variation between the mucus samples.
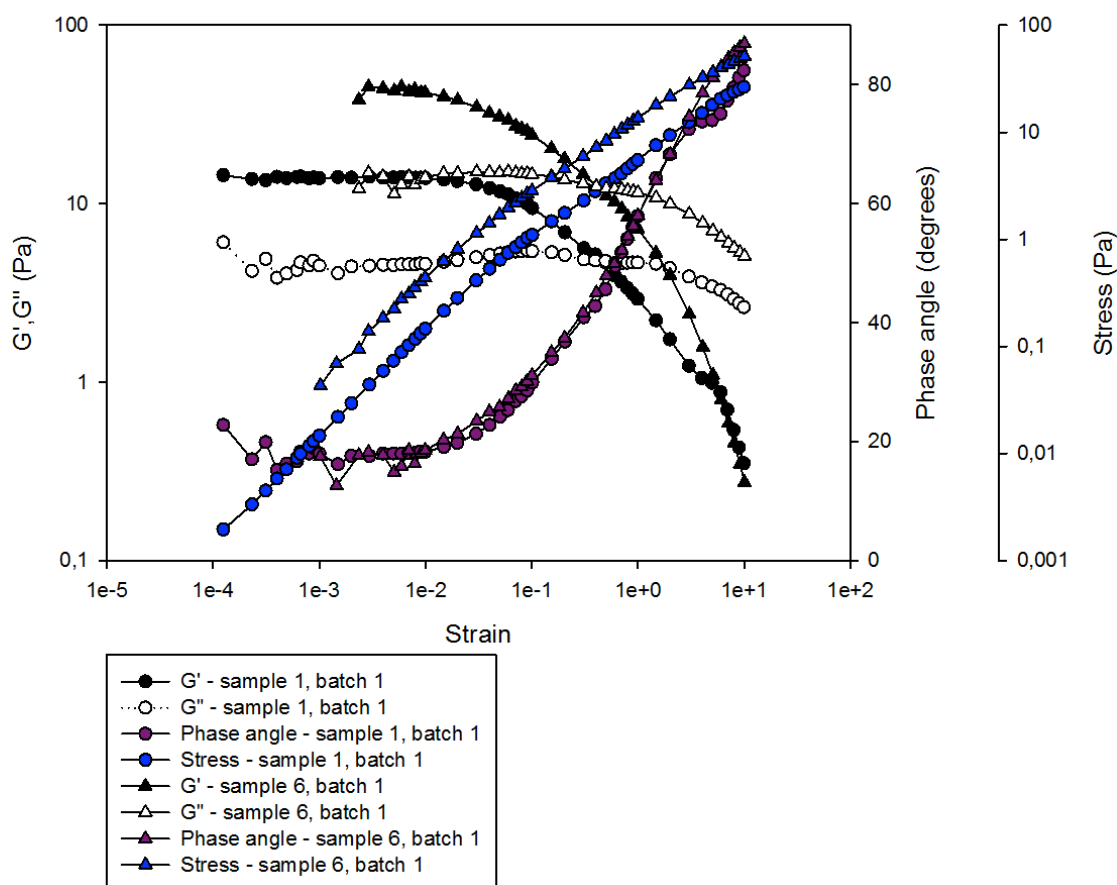
Figure 3.31 Strain sweeps of increasing strains run on two different biosimilar mucus samples taken from mucus batch number one. Circles represent sample 1 and triangles represent sample 6. The fixed frequency of the sweeps were 1 Hertz, and the temperature 25 °C.

The two strain sweeps of Figure 3.31 illustrates the variation in the rheological variables between the biosimilar mucus samples. Even thought it might seem like a substantial variation in the absolute values of the moduli and the stress curves, the phase angles of the two measurements are almost identical, which indicates the same rheological behaviour of the samples (Picout and Ross-Murphy, 2003). (For sample 1 data points in the strain region 0.00001 – 0.0001 are omitted because of noise, and for sample 6 data points in the strain region 0.00001- 0.002 are omitted because of noise.) No specific batch variation was observed between the samples of batch one and batch two. The shear thinning properties of biosimilar mucus is desired, as shear thinning properties was also observed in the PSIM. The biosimilar mucus should mimic the rheological properties of PSIM as close as possible, for it to be as good an intestinal mucus model system as it can be, in rheological terms.

3.3.3.3 Investigation of the thixotropic effects of biosimilar mucus

The thixotropic effects of the biosimilar mucus were investigated by running two up-down strain sweeps in the strain range $1*10^{-5}$-10. Time dependent thixotropic effects are verified if the plots of the rheological variables do not follow the same path when the strain is increasing and when the strain is decreasing. The two up-down sweeps yielded very similar results. One of the sweeps is plotted in Figure 3.32.
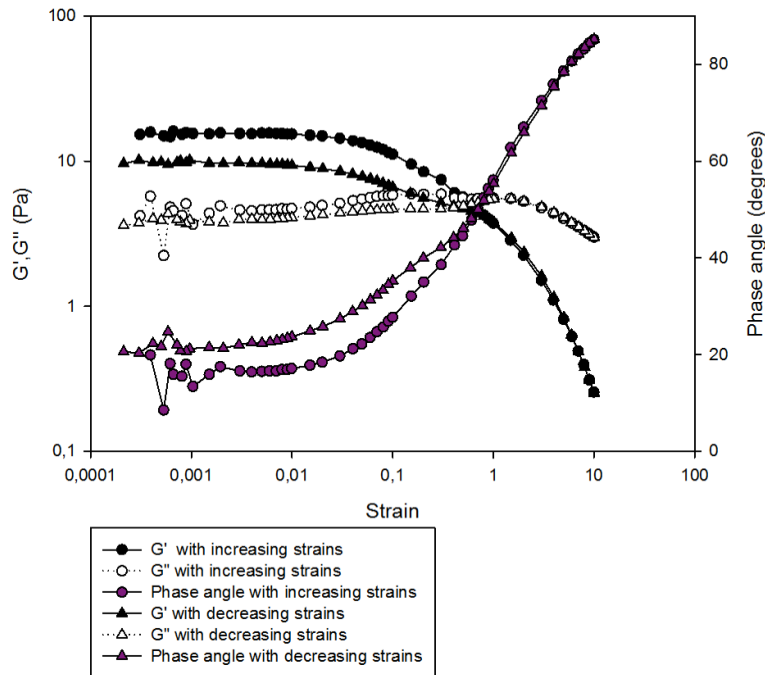
Figure 3.32 Up-down strain sweep of biosimilar mucus, in the range $1*10^{-5}$-10. The circles represent the moduli and phase angle values with increasing strains, and the triangles represent the moduli and phase angle with decreasing strains. The fixed frequency of the strain sweep was 1 Hertz, and the temperature 25 °C.

As shown in Figure 3.32, the rheological variables do not follow the same path with increasing and decreasing strains in the strain range 0.001-08. (Strain values in the range 0.00001-0.0002 are omitted because of noise in the data). The variables follow the same path at strains higher than 0.8, and behaves in a completely shear thinning manner, being viscous-like. At the point where the behavioural transition occurs (phase angle of 45 degrees) the paths of the rheological variables of increasing and decreasing strains starts to deviate. This occurs because the interactions broken as the strain increased are not able to rebuild themselves in the given time scale of the measurement when the strain decrease. Just like the PSIM, the biosimilar mucus holds thixotropic properties, which are dependent on the strain and the time frame of the experiment (Moller et al., 2006).

The rheological reversibility by shear thinning and thixotropy observed in the strain sweeps of biosimilar mucus are positive results for the applicability of the biosimilar mucus as a intestinal mucus model system, since native intestinal mucus is dependent on these properties, which enable reuse of the mucus in the intestines (Taylor et al., 2003).

Batch variations were observed only in the frequency sweeps, while strain sweep measurements did not produce these differences. This might indicate that there were some variation between the batches that affected the time frame of the rearrangement of the different bonds and interactions of the biosimilar mucus gel, while it did not affect the shear thinning properties of the gel.

When comparing the rheological measurements of the biosimilar mucus of this master thesis to the results of Bøgh et al (Bøgh et al., 2013) (data not shown), the results are broadly similar, revealing the same trends. Obtaining desired rheological behaviour from the biosimilar mucus was expected, because the biosimilar mucus has been optimized to mimic the rheological properties of PSIM.

3.3.4 Comparison of rheological measurements of PSIM and biosimilar mucus

The rheological measurements have revealed that the biosimilar mucus holds desirable rheological properties, similar to the properties observed in PSIM. The rheological profiles of the two mucous systems were directly compared to increase the understanding of the similarities and differences of the rheological profiles, and enable a more accurate evaluation of the applicability of the biosimilar mucus as a small intestinal mucus model system.

3.3.4.1 Frequency sweeps

Results from frequency sweeps of sample 1 of the PSIM and sample 1 from batch one of the biosimilar mucus were chosen to illustrate the results of the frequency sweeps of each mucous systems, as these were the most representative results from each mucous system. The moduli values are plotted together in the upper plot, and the phase angles are plotted in the lower plot in Figure 3.33.
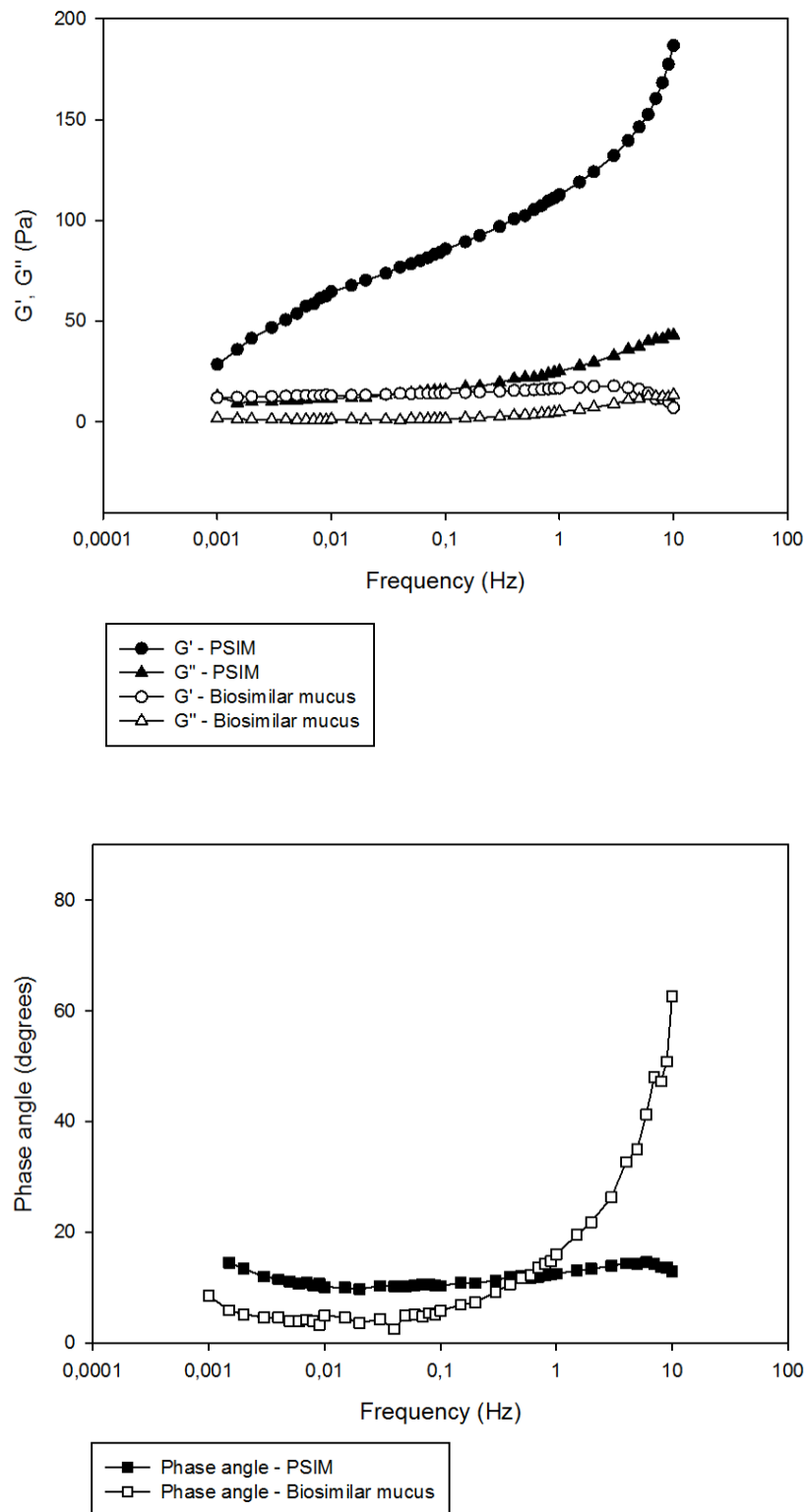
Figure 3.33 Frequency sweeps in the frequency range 0.001-10 Hertz of PSIM (black graphs) and biosimilar mucus (white graphs). The strain was fixed within the linear viscoelastic region. The temperature of both the measurements was 25 °C. The moduli values are presented in the upper plot, and the phase angle values are presented in the lower plot.

Upon comparison of the frequency sweeps of the PSIM and biosimilar mucus in Figure 3.33 it is evident that there are some dissimilarities in the behaviour of the two systems when exposed to increasing frequencies.

The most obvious difference is the absolute values of the storage moduli (G'). The PSIM has storage modulus (G') values up to ten times higher than the corresponding values found in the biosimilar mucus measurements. The slope of the storage modulus (G') of the PSIM is also much steeper than the slope of the storage modulus (G') of the biosimilar mucus. The absolute values of the loss moduli (G'') are more similar, and the slopes only deviate from each other in the frequency range 5-10 Hz, where the two graphs eventually intersect. The increase of the loss modulus (G'') of the biosimilar mucus, is due to the unexpected behaviour discussed earlier.

The phase angle is the more descriptive variable for the behaviour of the two systems (Picout and Ross-Murphy, 2003) (Taylor et al., 2004) (Taylor et al., 2005b). Broadly speaking the phase angles follow the same trends in the frequency range 0.001- 0.03 Hertz, with a low phase angle reflecting the dominant elastic-like behaviour of both the mucous systems. At frequencies >0.03, the phase angles of the PSIM and biosimilar mucus are dissimilar, which are mainly due to the unexpected behaviour of the biosimilar mucus at high frequencies.

3.3.4.2 Strain Sweeps

The most representative strain sweeps of each mucous system were plotted together in Figure 3.34 for comparison. The conditions of both sweeps were similar, with a fixed frequency of 1 Hertz and a temperature of 25 °C.
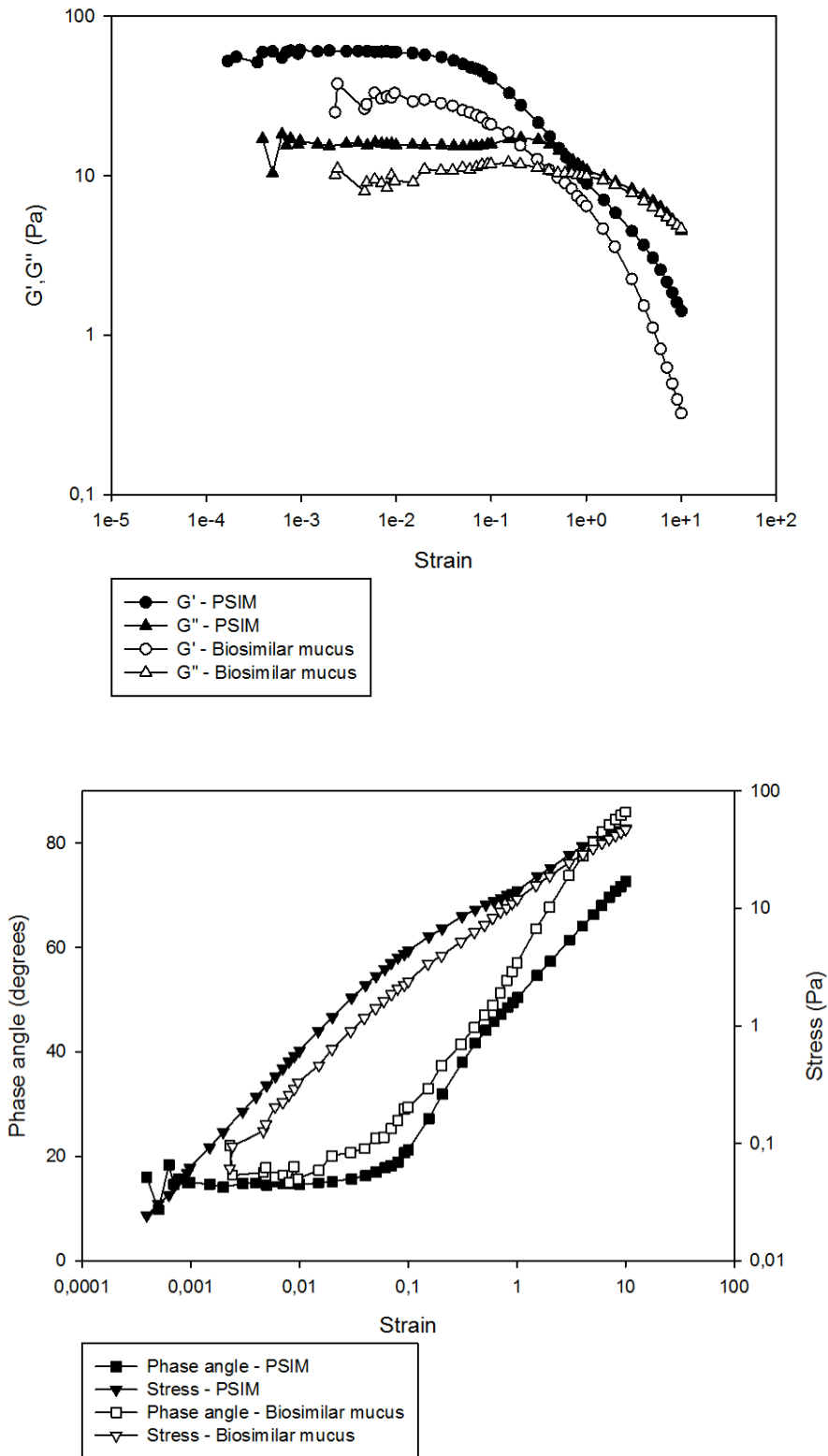
Figure 3.34 Strain sweeps with increasing strains, of PSIM (black graphs) and biosimilar mucus (white graphs). The fixed frequency of the measurements was 1 Hertz and the temperature set to 25 °C. The moduli values are presented in the upper plot, and the phase angle and stress values are presented in the bottom plot.

Data points in the strain region 0.00001-0.0004 of the PSIM measurements and the data points in the strain region 0.00001-0.002 of the biosimilar mucus are omitted because of noise.

As seen in Figure 3.34, the same trends are observed in the storage moduli (G') of PSIM and biosimilar mucus, with a smooth transition in behaviour from elastic-like to viscous-like, and with no signs of catastrophic failure. The loss moduli (G'') trends deviate somewhat more from each other in the two mucous systems. Nevertheless, the phase angles of the two systems are broadly similar, which implies a quite similar behaviour in the PSIM and biosimilar mucus when exposed to increasing strains. The behavioural transition occurs at nearly the same strain. The stability of the PSIM is seemingly somewhat higher than the stability of the biosimilar mucus, since the phase angle of the bioismilar mucus increases at lower strains and in a steeper manner, than the phase angle of the PSIM. This is not surprising as the gel matrix of the PSIM, which is mainly build up of mucins, is expected to be stronger and more stable than the gel matrix in biosimilar mucus, which consists of Sigma mucins supported by PAA. The stress curves of the two systems follow almost the same slopes, but deviates from each other in the strain range 5-10. There are differences in the absolute values of all the rheological variables presented, and with the exception of the phase angle all the variables are higher in the PSIM measurements.

The differences in the rheological profiles of PSIM and biosimilar mucus observed in the frequency sweeps and the strain sweeps, are probably due to the differences found in the structure of the gel network and components of the two systems. As the mucins found in the stomach and the mucins found in the small intestines are structurally related (Sellers et al., 1991) (Celli et al., 2005), one might expect that Sigma mucins, originating from the stomach of pigs, and PSIM should hold properties that are quite similar. The gastric mucus is in general somewhat more rigid than the small intestinal mucus (Mantle and Allen, 1981), and therefore one might expect the biosimilar mucus to comprise a more rigid gel than PSIM, and that differences in the rheological measurements reflects this. However, it is the opposite that is seen in the rheological measurements, and also observed in the distribution studies (section 3.1).

The reason for this is likely that the Sigma mucins of the biosimilar mucus do not have the same structure as when they were in the pig stomach. The isolation and purification process has most likely altered the physical and chemical properties of the Sigma mucin to the extent were reconstruction of the exact structure found in the pigs' stomach is not possible. This is supported by a study by Kočevar-Nared and colleagues (Kočevar-Nared et al., 1997). The Sigma mucin type II is a crude mixture of mucins, and the sugar and amino acid composition has not been determined (Sigma-Aldrich, 2011). The mucins found in mucus like PSIM are large molecules with molecular weights ranging from 10-40 MDa, linked together by mucin monomers of 0.3-0.5 MDa (Lai et al., 2009a). The result of the isolation and purification process of the Sigma mucins is likely fragmentation of the mucins, to a lower molecular weight than what is found in the PSIM. The purification process in it itself should not fragment the mucins, but it might occur if some of the non-mucin components in the Sigma mucin product are proteases naturally found in the mucus. Because of this, the Sigma mucins do not form a gel network when mixed into the HEPES buffer. They need the scaffolding properties of the PAA to form a proper gel network. The viscoelastic properties of biosimilar mucus is hence mainly a function of both the Sigma mucins and the PAA, but might be dependent on the lipids and bovine serum albumin as well (Bøgh et al., 2013), whereas the viscoelastic properties of the PSIM is predominantly a function of the mucin matrix (Lai et al., 2009b). Despite that the bisoimilar mucus is optimized to mimic the rheological profile of PSIM, it will be nearly impossible to get the exact same rheological profiles from the two systems when the components and the structure of the two systems deviate to this extent.

3.3.5 Control rheological measurements of Sigma mucin solutions

Control rheological measurements of Sigma mucin in 10 mM HEPES buffer containing 1 mM $MgSO_4$ and 1.3 mM $CaCl_2$ were run in order to verify the necessity of the non-Sigma mucin components of the biosimilar mucus. Solutions of three different concentrations were made; 5 % (w/v) – which is the same mucin concentration as the biosimilar mucus, 8 % (w/v) and 10 % (w/v). Different concentrations of the solutions enabled to check for concentration dependent behaviour.

The experimental set up differed somewhat from the set up of the biosimilar mucus and PSIM, as no proper rheological results were expected, since the solutions had a sol-like consistency. For each of the three Sigma mucin solutions six succeeding measurements were performed; strain sweep and frequency sweep at 15 °C, strain sweep and frequency sweep at 25 °C and strain sweep and frequency sweep at 37 °C. Different temperatures enabled to check for temperature dependent behaviour.

3.3.5.1 Strain sweeps

Strain sweeps in the strain range $1*10^{-5}$-100 with a fixed frequency of 1 Hertz, were run on 15 °C, 25 °C and 37 °C for each of the three Sigma mucin solutions. After each strain sweep a frequency sweep were run on the same temperature.

Some general trends could be seen in all the strain sweeps, presented in Appendix D. Three of the strain sweeps, one for each solution concentration at 15 °C, are presented in Figure 3.35.
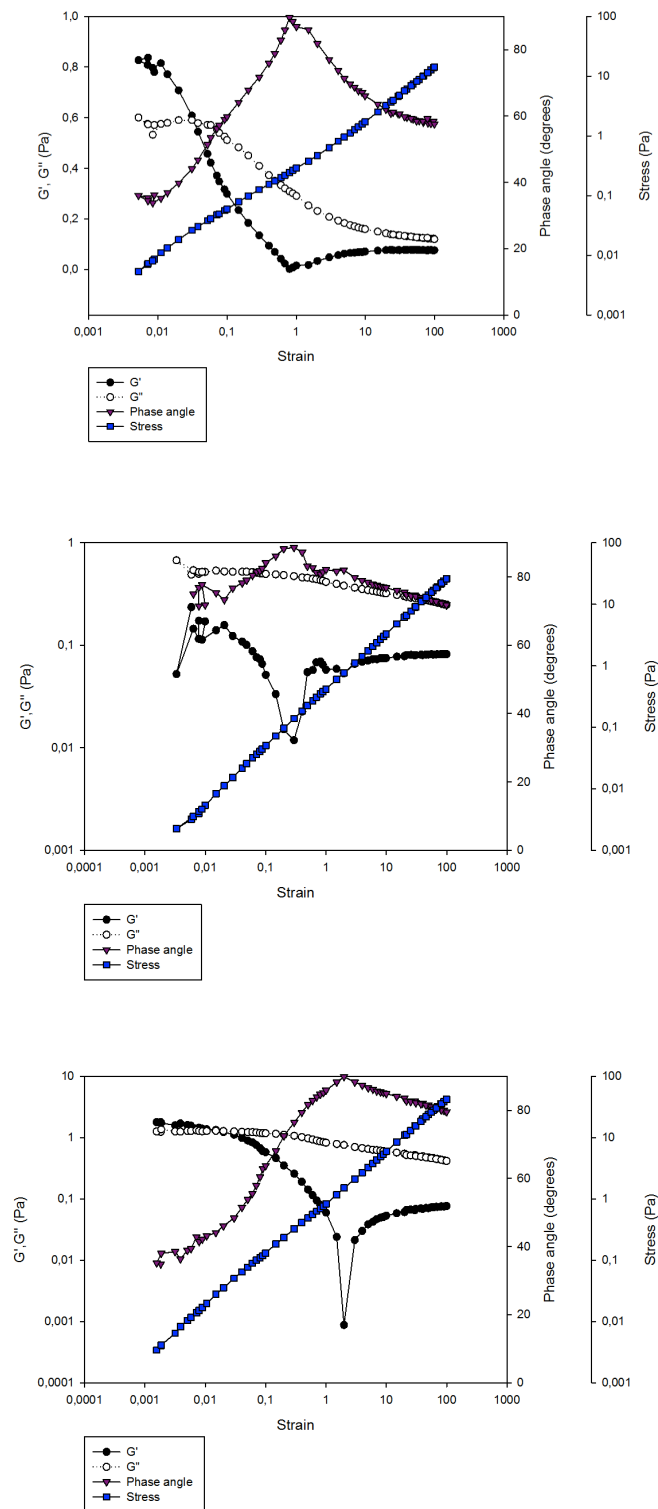
Figure 3.35 Strain sweeps of solutions of Sigma mucin dissolved in a 10 mM HEPES buffer containing 1.3 mM CaCl$_2$ and 1 mM MgSO$_4$. All the sweeps were run at a frequency of 1 Hertz. The upper plot is a sweep of the 5 % (w/v) solution, run at a temperature of 15 °C. The middle plot is a sweep of the 8 % (w/v) solution, run at a temperature of 15 °C. The bottom plot is a sweep of the 10 % (w/v) solution, run at a temperature of 15 °C.

In all the strain sweeps the values of the storage moduli (G') and the loss moduli (G'') are very low. This reflects the inability of the Sigma mucin to form a gel when dissolved in the buffer, and hence the absence of a characteristic viscoelastic behaviour, which were as expected. As discussed above, the inability to form a gel network is probably due to the low molecular weight of the Sigma mucins, which has been fragmented due to photolytic action of non-mucin proteins found in the Sigma mucin product.

Some general trends are observed in all the strain sweeps. The absolute values of the storage moduli (G') show no viscoelastic region at the lowest strains as it instantly starts to decrease when the strain increase, and hits a minimum when the strain is 1. At higher strains the absolute values starts to increase. This kind of behaviour is not expected as this implies that the behaviour becomes more elastic-like at the highest strains, but can be explained by that mucins can create interactions in shear (Corfield, 2000). New ordered structures might form by the glycosylated side chains of mucin, which is presumed to have been relatively well preserved, due to the inaccessibility of proteases naturally found in the Sigma mucin II.

The absolute values of the loss modulus (G'') decrease to some degree in the entire strain range. The phase angle of all the strain sweeps reaches a peak of 90 degrees at strains 1. The stress curves of the strain sweeps are quite linear, but some of them tend to level off at the highest strains, indicating that less stress needed to induce the strains in this region.

Except for the trend of the increasing storage modulus values at strains ~1 that diminishes with increasing Sigma mucin concentration, no distinctive temperature or concentration effects are seen in the strain sweeps of the Sigma mucin solutions.

3.3.5.2 Frequency Sweeps

Frequency sweeps of the three Sigma mucin soluitons were run, each at 15 °C, 25 °C and 37 °C. Three of the plots, one for each concentration at a temperature of 37 °C, is presented in Figure 3.36.
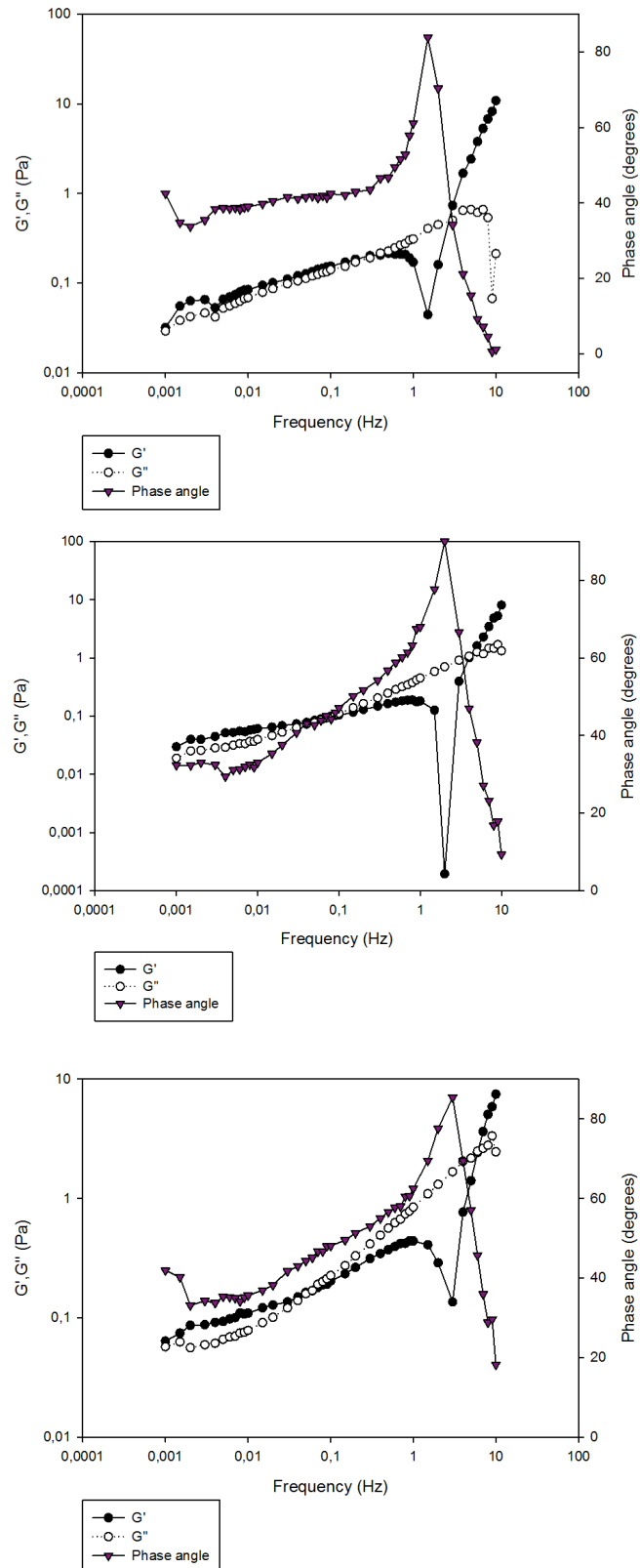
Figure 3.36 Frequency sweeps in the frequency range 0.001-10 Hertz of Sigma mucin dissolved in 10 mM HEPES buffer-solutions containing 1.3 mM $CaCl_2$ and 1 mM $MgSO_4$. The chosen fixed strain were 0.05. The upper plot represents a 5 % (w/v) solution, the middle represents a 8 % (w/v) solution, and the lower represent a 10 % (w/v) solution. All measurements were run at 37 °C.

In all the frequency sweeps some general trends are observed, independent of the Sigma mucin concentration or the temperature of the measurement. The absolute moduli values are very low, and both storage moduli (G') and loss moduli (G'') increase in the entire frequency range. The exception is when the storage moduli (G') hits a sudden minimum at ~5 Hertz. This is reflected in the phase angle which peaks at ~5 Hertz. According to theory the patterns of the storage modulus (G') and the loss modulus (G'') is consistent with a concentrated solution (Zhong and Daubert, 2013), which fits well here.

A U-shape is observed in the graphs of the phase angle, which is most dominant in the frequency sweeps of 15 °C and diminish at higher temperatures. This might be a temperature dependent effect, but can also be an effect of the experimental set-up, where the solutions exposed to the measurements of the highest temperatures previously have been exposed to the measurements of lower temperatures, which may have further weakened the system for the latter measurements.

The rheological measurements on the Sigma mucin solutions yielded results as expected, consistent with poor viscoelastic properties. Changing the temperature of the measurements or doubling of the concentration of Sigma mucin from 5 % (w/v), which is the concentration of the biosimilar mucus, to 10 % (w/v) had no effect. This has also been reported earlier (Kočevar-Nared et al., 1997).

The critical overlap concentration of the Sigma mucins is proportional to the molecular weigh of the molecules (Clasen et al., 2006). The Sigma mucins probably have such a low molecular weight that it does not support the formation of the mucin matrix found in native mucus. For creation of a gel like structure when utilizing Sigma mucins, the non-mucin components of the biosimilar mucus are necessary, in particular the PAA that contributes with scaffolding properties.

3.3.6 Conclusive remarks on the rheological measurements of PSIM, biosimilar mucus and Sigma mucin solutions

The results from the frequency sweeps and strain sweeps of PSIM showed that the PSIM has behaviour as expected for the maintenance of the protective barrier in the intestines and reuse of the mucus, with dominant elastic behaviour with increasing frequencies, and rheological reversibility, both shear thinning and thixotropic.

In general the biosimilar mucus show rheological behaviour as desired from an intestinal mucous model system. The frequency sweeps revealed a frequency dependent dominant elastic behaviour, but deviated from what was expected in the frequency range 7-10 Hertz, where the behaviour changed to more viscous-like. The strain sweeps showed a smooth transition from an elastic-like behaviour to a viscous-like behaviour and hence shear thinning properties. In addition time dependent thixotropic properties were verified by up-down strain sweeps.

Based on the comparison of the rheological profiles of PSIM and biosimilar mucus, an evaluation about the biosimilar mucus as an applicable small intestinal mucous model system can be done. The results of the rheological profile showed that overall the PSIM has somewhat higher mechanical properties than the biosimilar mucus, but that the behaviour is broadly similar if the strain and frequency are kept low. The biosimilar mucus was originally developed for compatibility with the Caco-2 cells, which are mainly utilized in intestinal drug absorption studies, since native mucus is not compatible with the cell line as it disrupts the cell monolayer (Boegh et.al, 2013). In nanoparticle drug delivery studies is not likely to apply very high frequencies or strains to the mucus, and in rheological terms the biosimilar mucus might be an applicable intestinal mucous model system.

Sigma mucin in HEPES buffer do not comprise a model system with rheological properties mimicking that of intestinal mucus, which emphasize the necessity of the non-mucin ingredients of the biosimilar mucus.

4. Future work

4.1 Distribution studies

It would have been interesting, if possible, to replicate the experiments were the distribution of nanoparticles were applied on top of mucus were investigated, but with Caco-2 cells coating the bottom of the glass chambers. By coating the wells with Caco-2 cells, it is likely that the mucus would have been more stable due to interactions with the glycocalyx (Lochner et.al, 2003). In this way perturbations might not have had such an impact on the distribution of the nanoparticles. Also, it might have been possible to add a thinner layer of mucus on top of the cells, which would make it easier for the laser of the confocal microscope to find and visualize the nanoparticles (assuming that the Caco-2 cells are readily penetrated by the laser).

4.2 The plate method

In the plate method it was discovered that the fluorescence intensity detected was wavelength dependent. It could have been interesting to investigate the background fluorescence intensity of PSIM and bisoimilar mucus on different wavelengths. If there had been found a wavelength area in the light spectra where the PSIM and biosimilar mucus did not yield any background fluorescence, it would have been interesting to further develop the method. This, however, requires the existence of fluorescent nanoparticles on the market with ex./em. maxima within the given wavelength area.

4.3 Further evaluation of the biosimilar mucus

An evaluation has been done on the applicability of the biosimilar mucus as a model system for small intestinal mucus in nanoparticle drug delivery/absorption studies. However, more studies should be made for a more thorough and complete evaluation. E.g. particle mobility in the biosimilar mucus could be tested by multiple particle tracking (MPT) or fluorescence recovery after photo bleaching (FRAP), and compared to similar measurements of PSIM.

5. Conclusion

The development of the plate method looked promising up until it was discovered that high background fluorescence was detected in PSIM and biosimilar mucus, which might be due to Raman scattering. The further development of the plate method was terminated.

The results form the distribution studies and comparison of the rheological profiles of PSIM and biosimilar mucus, suggest that the biosimilar mucus is an applicable intestinal mucus model system for studies of nanoparticle absorption through mucus and into cells. The distribution studies showed that different nanoparticles distribute in biosimilar mucus and PSIM in a comparable manner, and that the biosimilar mucus did not significantly aggregate or alter the nanoparticles, which could prevent the epithelial cells from nanoparticle uptake. It was also shown that the distribution pattern of nanoparticles in the two mucous model systems could not be predetermined based on the charge and/or size of the nanoparticle. Neither the biosimilar mucus or the PSIM were robust enough for the experimental conditions of studying the nanoparticle distribution and adsorption of nanoparticles on top of the mucus, and were also too dense for the laser of the confocal microscope to penetrate properly. The biosimilar mucus was shown to have broadly the similar viscoelastic properties as PSIM, as long as the strain and frequency were kept low.

6. References

ANTONI, L., NUDING, S., WELLER, D., GERSEMANN, M., OTT, G., WEHKAMP, J. & STANGE, E. F. 2013. Human colonic mucus is a reservoir for antimicrobial peptides. *Journal of Crohn's and Colitis,* 7**,** e652-e664.

ATUMA, C., STRUGALA, V., ALLEN, A. & HOLM, L. 2001. The adherent gastrointestinal mucus gel layer: thickness and physical state in vivo. *American Journal of Physiology - Gastrointestinal and Liver Physiology,* 280**,** G922-G929.

BANSIL, R. & TURNER, B. S. 2006. Mucin structure, aggregation, physiological functions and biomedical applications. *Current Opinion in Colloid & Interface Science,* 11**,** 164-170.

BARNES, H. A. 1997. Thixotropy—a review. *Journal of Non-Newtonian Fluid Mechanics,* 70**,** 1-33.

BHAT, P. G., FLANAGAN, D. R. & DONOVAN, M. D. 1995. The limiting role of mucus in drug absorption: Drug permeation through mucus solution. *International Journal of Pharmaceutics,* 126**,** 179-187.

BIOIMAGING. 2008. *Confocal microscopy - a brief explanation* [Online]. bioimaging.dk. Available: http://www.bioimaging.dk/index.php?id=71 [Accessed 01.04.14 2014].

BOEGH, M., BALDURSDÓTTIR, S. G., MÜLLERTZ, A. & NIELSEN, H. M. 2014. Property profiling of biosimilar mucus in a novel mucus-containing in vitro model for assessment of intestinal drug absorption. *European Journal of Pharmaceutics and Biopharmaceutics*.

BØGH, M., BALDHURSDOTTIR, S. G., NIELSEN, M. H., MÜLLERTZ, A. & NIELSEN, H. M. 2013. Developemt and rheological profiling of biosimilar mucus. *Nordic Rheology Society. Annual Transactions.,* 21**,** 233-240.

CELLI, J., GREGOR, B., TURNER, B., AFDHAL, N. H., BANSIL, R. & ERRAMILLI, S. 2005. Viscoelastic Properties and Dynamics of Porcine Gastric Mucin. *Biomacromolecules,* 6**,** 1329-1333.

CHAPLIN, M. 2012. *Hydrocolloid Rheology* [Online]. Available: http://www1.lsbu.ac.uk/water/hyrhe.html [Accessed 02.04.2014 2014].

CLASEN, C., PLOG, J. P., KULICKE, W.-M., OWENS, M., MACOSKO, C., SCRIVEN, L. E., VERANI, M. & MCKINLEY, G. H. 2006. How dilute are dilute solutions in extensional flows? *Journal of Rheology (1978-present),* 50**,** 849-881.

CONE, R. 2005. Mucus. *In:* AL., M. E. (ed.) *Mucosal Immunology.* London, UK Elsevier Academic Press.

CONE, R. A. 2009. Barrier properties of mucus. *Advanced Drug Delivery Reviews,* 61**,** 75-85.

CORFIELD, A. P. 2000. *Glycoprotein methods and protocols: the mucins,* Totowa, N.J., Humana Press.

CROMMELIN, D. J. A., STORM, G., VERRIJK, R., DE LEEDE, L., JISKOOT, W. & HENNINK, W. E. 2003. Shifting paradigms: biopharmaceuticals versus low molecular weight drugs. *International Journal of Pharmaceutics,* 266**,** 3-16.

D'HAENS, G. 2007. Risks and benefits of biologic therapy for inflammatory bowel diseases. *Gut,* 56**,** 725-732.

DAVIES, J. M. & VINEY, C. 1998. Water–mucin phases: conditions for mucus liquid crystallinity. *Thermochimica Acta,* 315**,** 39-49.

ENSIGN, L. M., CONE, R. & HANES, J. 2012. Oral drug delivery with polymeric nanoparticles: The gastrointestinal mucus barriers. *Advanced Drug Delivery Reviews,* 64**,** 557-570.

FLORENCE, A. 1997. The Oral Absorption of Micro- and Nanoparticulates: Neither Exceptional Nor Unusual. *Pharmaceutical Research,* 14**,** 259-266.

FURRER, P. & GURNY, R. 2010. Recent advances in confocal microscopy for studying drug delivery to the eye: Concepts and pharmaceutical applications. *European Journal of Pharmaceutics and Biopharmaceutics,* 74**,** 33-40.

FÖLDES-PAPP, Z., DEMEL, U. & TILZ, G. P. 2003. Laser scanning confocal fluorescence microscopy: an overview. *International Immunopharmacology,* 3**,** 1715-1729.

GALINDO-RODRIGUEZ, S. A., ALLEMANN, E., FESSI, H. & DOELKER, E. 2005. Polymeric Nanoparticles for Oral Delivery of Drugs and Vaccines: A Critical Evaluation of In Vivo Studies. 22**,** 419-464.

GIROD, S., ZAHM, J. M., PLOTKOWSKI, C., BECK, G. & PUCHELLE, E. 1992. Role of the physiochemical properties of mucus in the protection of the respiratory epithelium. *European Respiratory Journal,* 5**,** 477-487.

GRAZÚ, V., MOROS, M. & SÁNCHEZ-ESPINEL, C. 2012. Chapter 14 - Nanocarriers as Nanomedicines: Design Concepts and Recent Advances. *In:* JESUS, M. D. L. F. & GRAZU, V. (eds.) *Frontiers of Nanoscience.* Elsevier.

GROO, A.-C. & LAGARCE, F. 2014. Mucus models to evaluate nanomedicines for diffusion. *Drug Discovery Today*.

GUIOCHON, G. & BEAVER, L. A. 2011. Separation science is the key to successful biopharmaceuticals. *Journal of Chromatography A,* 1218**,** 8836-8858.

HENDERSON, R. K., BAKER, A., MURPHY, K. R., HAMBLY, A., STUETZ, R. M. & KHAN, S. J. 2009. Fluorescence as a potential monitoring tool for recycled water systems: A review. *Water Research,* 43**,** 863-881.

HEREDIA, R. B., DUEÑAS, S., CASTILLO, L., VENTURA, J. J., SILVA BRIANO, M., POSADAS DEL RIO, F. & RODRÍGUEZ, M. G. 2008. Autofluorescence as a tool to study mucus secretion in Eisenia foetida. *Comparative Biochemistry and Physiology Part A: Molecular & Integrative Physiology,* 151**,** 407-414.

HIDALGO, I. J., RAUB, T. J. & BORCHARDT, R. T. 1989. Characterization of the human colon carcinoma cell line (Caco-2) as a model system for intestinal epithelial permeability. *Gastroenterology,* 96**,** 736-49.

JAMESON, D. M. & ROSS, J. A. 2010. Fluorescence Polarization/Anisotropy in Diagnostics and Imaging. *Chemical Reviews,* 110**,** 2685-2708.

KOČEVAR-NARED, J., KRISTL, J. & ŠMID-KORBAR, J. 1997. Comparative rheological investigation of crude gastric mucin and natural gastric mucus. *Biomaterials,* 18**,** 677-681.

KWON, K.-C., VERMA, D., SINGH, N. D., HERZOG, R. & DANIELL, H. 2013. Oral delivery of human biopharmaceuticals, autoantigens and vaccine antigens bioencapsulated in plant cells. *Advanced Drug Delivery Reviews,* 65**,** 782-799.

LAI, S. K., O'HANLON, D. E., HARROLD, S., MAN, S. T., WANG, Y.-Y., CONE, R. & HANES, J. 2007. Rapid transport of large polymeric nanoparticles in fresh undiluted human mucus. *Proceedings of the National Academy of Sciences,* 104**,** 1482-1487.

LAI, S. K., WANG, Y.-Y. & HANES, J. 2009a. Mucus-penetrating nanoparticles for drug and gene delivery to mucosal tissues. *Advanced Drug Delivery Reviews,* 61**,** 158-171.

LAI, S. K., WANG, Y.-Y., WIRTZ, D. & HANES, J. 2009b. Micro- and macrorheology of mucus. *Advanced Drug Delivery Reviews,* 61**,** 86-100.

LAKOWICZ, J. R. 2006. *Principles of Fluorescence Spectroscopy,* Boston, MA, Springer Science+Business Media, LLC.

LARHED, A., ARTURSSON, P. & BJÖRK, E. 1998. The Influence of Intestinal Mucus Components on the Diffusion of Drugs. *Pharmaceutical Research,* 15**,** 66-71.

LAROUI, H., SITARAMAN, S. V. & MERLIN, D. 2012. Chapter six - Gastrointestinal Delivery of Anti-inflammatory Nanoparticles. *In:* NEJAT, D. (ed.) *Methods in Enzymology.* Academic Press.

LICHTENBERGER, L. M. 1995. The hydrophobic barrier properties of gastrointestinal mucus. *Annu Rev Physiol,* 57**,** 565-83.

LOCHNER, N., PITTNER, F., WIRTH, M. & GABOR, F. 2003. Preparation, characterization and application of artificial Caco-2 cell surfaces in the silver nanoparticle enhanced fluorescence technique. *Journal of Controlled Release,* 89**,** 249-259

MACADAM, A. 1993. The effect of gastro-intestinal mucus on drug absorption. *Advanced Drug Delivery Reviews,* 11**,** 201-220.

MANTLE, M. & ALLEN, A. 1981. Isolation and characterization of the native glycoprotein from pig small-intestinal mucus. *Biochem J,* 195**,** 267-75.

MOLLER, P. C. F., MEWIS, J. & BONN, D. 2006. Yield stress and thixotropy: on the difficulty of measuring yield stresses in practice. *Soft Matter,* 2**,** 274-283.

MØRK, P. C. 1999. *Overflate og kolloidkjemi: grunnleggende prinsipper og teorier,* Trondheim, Norges teknisk-naturvitenskapelige universitet, Institutt for kjemisk prosessteknologi.

NORRIS, D. A. & SINKO, P. J. 1997. Effect of size, surface charge, and hydrophobicity on the translocation of polystyrene microspheres through gastrointestinal mucin. *Journal of Applied Polymer Science,* 63**,** 1481-1492.

ORIVE, G., GASCÓN, A. R., HERNÁNDEZ, R. M., DOMÍNGUEZ-GIL, A. & PEDRAZ, J. L. 2004. Techniques: New approaches to the delivery of biopharmaceuticals. *Trends in Pharmacological Sciences,* 25**,** 382-387.

PICOUT, D. R. & ROSS-MURPHY, S. B. 2003. Rheology of Biopolymer Solutions and Gels. *TheScientificWorldJOURNAL,* 3**,** 105-121.

PONCHEL, G. & IRACHE, J.-M. 1998. Specific and non-specific bioadhesive particulate systems for oral delivery to the gastrointestinal tract. *Advanced Drug Delivery Reviews,* 34**,** 191-219.

RADER, R. A. 2013. FDA Biopharmaceutical Product Approvals and Trends in 2012. Up from 2011, but Innovation and Impact Are Limited. *BioProcess International,* 3.

ROSE, M. C. & VOYNOW, J. A. 2006. Respiratory Tract Mucin Genes and Mucin Glycoproteins in Health and Disease. *Physiological Reviews,* 86**,** 245-278.

SEKHON, B. S. 2010. Biopharmaceuticals: an overview. *Thai J. Pharm. Sci. ,* 34**,** 1-19.

SELLERS, L. A., ALLEN, A., MORRIS, E. R. & ROSS-MURPHY, S. B. 1991. The rheology of pig small intestinal and colonic mucus: weakening of gel structure by non-mucin components. *Biochim Biophys Acta,* 1115**,** 174-9.

SIGMA-ALDRICH. 2011. *What is the molecular weight of Product M2378, Mucin from porcine stomach?* [Online]. Available: http://sigma-aldrich.custhelp.com/app/answers/detail/a_id/3028/p/7,984 [Accessed 02.05. 2014].

SMART, J. D. 2005. The basics and underlying mechanisms of mucoadhesion. *Advanced Drug Delivery Reviews,* 57**,** 1556-1568.

SMIDSRØD, O. & MOE, S. T. 2008. *Biopolymer chemistry,* Trondheim, Tapir Academic Press.

SNIDER, J. 2013. *Fluorescent porbes* [Online]. © 2014 Thermo Fisher Scientific Inc. Available: http://www.piercenet.com/method/fluorescent-probes [Accessed 04.05. 2014].

SOCIETY OF PLASTICS ENGINEERS, T. A. M. U. 2012. *Introduction to Polymer Rheology* [Online]. Society of Plastics Engineers: Texas A&M University. Available: http://plastics.tamu.edu/class-resources/introduction-polymer-rheology [Accessed 02.04.2014 2014].

STAUB, A., GUILLARME, D., SCHAPPLER, J., VEUTHEY, J.-L. & RUDAZ, S. 2011. Intact protein analysis in the biopharmaceutical field. *Journal of Pharmaceutical and Biomedical Analysis,* 55**,** 810-822.

TAYLOR, C., ALLEN, A., DETTMAR, P. W. & PEARSON, J. P. 2003. The Gel Matrix of Gastric Mucus Is Maintained by a Complex Interplay of Transient and Nontransient Associations. *Biomacromolecules,* 4**,** 922-927.

TAYLOR, C., ALLEN, A., DETTMAR, P. W. & PEARSON, J. P. 2004. Two rheologically different gastric mucus secretions with different putative functions. *Biochimica et Biophysica Acta (BBA) - General Subjects,* 1674**,** 131-138.

TAYLOR, C., DRAGET, K. I., PEARSON, J. P. & SMIDSRØD, O. 2005a. Mucous Systems Show a Novel Mechanical Response to Applied Deformation. *Biomacromolecules,* 6**,** 1524-1530.

TAYLOR, C., PEARSON, J. P., DRAGET, K. I., DETTMAR, P. W. & SMIDSRØD, O. 2005b. Rheological characterisation of mixed gels of mucin and alginate. *Carbohydrate Polymers,* 59**,** 189-195.

TAYLOR NORDGÅRD, C. & DRAGET, K. I. 2011. Oligosaccharides As Modulators of Rheology in Complex Mucous Systems. *Biomacromolecules,* 12**,** 3084-3090.

TECAN AUSTRIA GMBH 2010. Optical system. *TECAN. Instructions for Use for Infinite 200 PRO.* Salzburg, Austria: Tecan Austria GmbH.

VERONESE, F. M. 2001. Peptide and protein PEGylation: a review of problems and solutions. *Biomaterials,* 22**,** 405-417.

VWR INTERNATIONAL. 2014. *Plater og moduler, FluoroNunc™ og LumiNunc™* [Online]. Available: https://no.vwr.com/app/catalog/Product?article_number=735-0004 [Accessed 01.05. 2014].

WAGNER JR, J. R., MOUNT III, E. M. & GILES JR, H. F. 2014. 20 - Polymer Rheology. *In:* WAGNER, J. R., MOUNT, E. M. & GILES, H. F. (eds.) *Extrusion (Second Edition).* Oxford: William Andrew Publishing.

WALSH, G. 2005. Biopharmaceuticals: recent approvals and likely directions. *Trends in Biotechnology,* 23**,** 553-558.

WASHINGTON UNIVERSITY IN ST.LOUIS DEPARTMENT OF EARTH AND PLANETARY SCIENCES. 2014. *in situ Planetary Raman Spectroscopy* [Online]. Available: http://epsc.wustl.edu/haskin-group/Raman/faqs.htm [Accessed 01.05. 2014].

WONG, T. W. 2010. Design of oral insulin delivery systems. *Journal of Drug Targeting,* 18**,** 79-92.

WYSS, H. M., LARSEN, R. J. & WEITZ, D. A. 2007. Oscillatory Rheology - Measuring the viscoelastic behaviour of soft materials. *G.I.T. Laboratory Journal,* 3-4**,** 68-70.

ZHONG, Q. & DAUBERT, C. R. 2013. Chapter 15 - Food Rheology. *In:* KUTZ, M. (ed.) *Handbook of Farm, Dairy and Food Machinery Engineering (Second Edition).* San Diego: Academic Press.

List of appendixes

Appendix A - Additional info to section 2 Materials & Methods

Appendix B – Calculations from section 3.1 Distribution studies of nanoparticles in and on mucus

Appendix C – Calculations and fluorescence intensity measurements from section 3.2 Development of the plate method

Appendix D – Rheological measurements from section 3.3.5 Control rheological measurements on Sigma mucin solutions

Appendix A - Additional info to section 2 Materials & Methods

A.1 Purification protocol of the pig gastric mucins

The purification protocol of pig gastric mucins was provided by Professor J.P. Pearson at the Institute for Cell and Molecular Biosciences, University of Newcastle upon Tyne.

Preparation of purified mucin samples

Pig gastric mucus gels were removed from the mucosa and immediately transferred into an ice cold cocktail of protease inhibitors in phosphate buffer (mucus to buffer ratio 1:4 v/v), pH 6.5, to prevent degradation by endogenous proteases. Mucus gel was solubilised in the inhibitor cocktail by high speed homogenisation in a Waring Blender for 1 minute. Soluble material was separated from insoluble cell debris by centrifugation (8000g, 1 hour, 4°C). The resulting supernatant was further purified to remove protein and nucleic acid by equilibrium density gradient ultracentrifugation in caesium chloride (CsCl) (Starkey *et al*., 1974). CsCl was added to give a starting density of 1.42 g/ml, and the solution centrifuged at 100,000g for 48 h at 4°C, using a fixed angle rotor.

The contents of each tube were removed as nine equal fractions with care being taken not to disturb the density gradient. The density of each fraction was measured, followed by exhaustive dialysis against distilled water at 4°C. Dialysed fractions were assayed for glycoprotein, protein and nucleic acid. Fractions rich in protein and nucleic acid were discarded, and those rich in glycoprotein were pooled, freeze dried and stored at –20°C.

Table A.1 Concentration and action of protease inhibitors within the proteolytic inhibitor cocktail

Protease inhibitor	Concentration (mM)	Mode of action
Phenylmethylsulphonyl fluoride (PMSF)	3	Inhibitor of serine proteases, e.g., elastase hydrolyses peptide bond at C-terminal side, and cathepsin and trypsin removes N-terminal dipeptides.

Sodium iodoacetate	1	Inhibitor of thiol-dependent proteases, e.g., cathepsin B and other disulphide dependent enzymes.
Benzamidine Hydrochloride	15	Specific inhibitor of trypsin and trypsin-like serine proteases (hydrolysis of proteins, peptides and amino acids).
Na_2 EDTA	10	Inhibitor of metallo-dependent proteases, e.g., Ca^{2+} dependent enzymes.
N-ethylmaleimide	10	Prevents disulphide group exchange.
a-amino caproic acid	100	Inhibitor of plasminogen activation to serine protease plasmin (hydrolyses peptide and ester bonds).

A.2 List of chemicals utilized in the thesis

Table A.2 A list of the chemicals utilized in the practical work of the master thesis.

Chemical	Producer	Lot number
Linoleic acid	Sigma Aldrich Co., St.Louis, USA	SLBB2791V
Cholesterol	Sigma Aldrich Co., St.Louis, USA	SLBC7554V
L-α-phosphatidylcholine	Sigma Aldrich Co., St.Louis, USA	BCBK8990V
Polysorbate 80	Sigma Aldrich Co., St.Louis, USA	BCBH5882V
Sigma porcine gastric mucin type II: crude	Sigma Chemical Co., St.Louis, USA	26H1004
Carbopol 934P /PAA	Reckitt & Colman Products, Kingston Upon Hull, UK	DS9068
Bovine Serum Albumin	Sigma Chemical Co., St.Louis, USA	108H0914
HEPES	Sigma Aldrich Co., St.Louis, USA	040M5432V
NaCl	Merck KGaA (Darmstadt, Germany	K42150704 116
$CaCl_2$	Merck KGaA (Darmstadt, Germany	K43533936 241
$MgSO_4$	Merck KGaA (Darmstadt, Germany	0076819
Dow Corning ® 200/100S fluid	VNR International LTD (Butterworth, UK	?
FluoSpheres® carboxylate modified microspheres, 0.2 µm, yellow-green fluorescent (505/515), 2 % solids	Invitrogen Ldt., Paisley, UK	714135

FluoSpheres® amine modified microspheres, 0.2 μm, yellow-green fluorescent (505/515), 2 % solids	Invitrogen Ldt., Paisley, UK	513683
FluoSpheres® carboxylate modified microspheres, 0.1 μm, yellow-green fluorescent (505/515), 2 % solids	Invitrogen Ldt., Paisley, UK	1173467
FluoSpheres® carboxylate modified microspheres, 0.1 μm, red fluorescent (580/605), 2 % solids	Invitrogen Ldt., Paisley, UK	483011
FluoSpheres® carboxylate modified microspheres, 0.2 μm, red fluorescent (580/605), 2 % solids	Invitrogen Ldt., Paisley, UK	646223
FluoSpheres® carboxylate modified microspheres, 1 μm, yellow-green fluorescent (505/515), 2 % solids	Invitrogen Ldt., Paisley, UK	468445
Dried agar	Becton Dickinson Company Sparks, USA	2011008

Appendix B - Calculations from section 3.1 Distribution studies of nanoparticles in and on mucus

B.1 Calculating the amounts of nanoparticles in 100 µL 200 nm sized particles and 100 µL 100 nm sized particles

The FluoSphere® nanoparticles has a concentration of 2 % (w/v), and a density of 1.05.

First the 2 % (w/v) nanoparticle solutions were mixed into the mucus into an end concentration of 0.08 % (w/v), using equation 1.

$$\frac{8\ \mu L}{200\ \mu L} * 2\ \% = 0.08\ \% \tag{1}$$

In order to obtain a 0.08 % (w/v) concentrated solution, 8 µL of the 2 % nanoparticle solution were mixed into 200 µL of mucus.

Equation 2 was used for calculating the amount of nanoparticles of the 0.08 % (w/v) solutions of 100 nm sized nanoparticles and 200 nm sized nanoparticles.

$$\frac{Number\ of\ microspheres}{mL} = \frac{6 * C * 10^{12}}{\rho * \pi \times \Phi^3} \tag{2}$$

were C = the concentration of suspended beads in g/mL

Φ = the diameter of micorspheres in µm

ρ = the density of the polymer in g/mL

The 200 nm sized nanoparticles;

$$\frac{Number\ of\ microspheres}{mL} = \frac{6 \times (0.02) * 10^{12}}{1.05 * \pi \times (0.2)^3} = 4.54 \times 10^{12}$$

$$\frac{Number\ of\ microspheres}{\mu L} = 4.54 * \frac{10^{12}}{1000} = 4.54 * 10^{9}$$

$$Number\ of\ microspheres\ in\ 8\ \mu L = 4.54 * \frac{10^{12}}{1000} \times 8 = 3.63 * 10^{10}$$

The number of particles in the 0.08 % (w/v) nanoparticle solution of 200 nm sized nanoparticles are 3.63 * 10^{10}, which is the desired number of particles of the solution of 100 nm sized nanoparticles.

The 100 nm sized nanoparticles;

$$\frac{Number\ of\ microspheres}{mL} = \frac{6 \times (0.02) * 10^{12}}{1.05 * \pi \times (0.1)^3} = 3.63 \times 10^{13}$$

$$\frac{Number\ of\ microspheres}{\mu L} = 3.63 * \frac{10^{13}}{1000} = 3.63 * 10^{10}$$

Hence, 1 µL of the 2 % (w/v) 100 nm nanoparticle solution needs to be mixed into 200 µL mucus in order to achieve the same amount of nanoparticles when 8 µL of the 2 % (w/v) nanoparticle solution of the 200 nm sized nanoparticels are mixed into 200 µL to an end concentration of 0.08 % (w/v).

With Equation 1 the end concentration of 1 µL of the 2 % nanoparticle solution in 200 µL were calculated to be 0.01 % (w/v).

B.2 Calculating the thickness of the mucus layers in the glass chambers

The area of each glass chamber was 0.8 cm^2, which equals 80 mm^2. The working distance of the chosen objective of the confocal laser were 1.7 mm, meaning that was the maximum height the mucus samples could have in the glass chambers, not accounting for meniscus formation.

With a maximum height of 1.7 mm, the maximum volume to be put in the glass chambers was calculated

$$80 \ mm^2 * 1.7 \ mm = 136 \ mm^3$$

$$136 \ mm^3 = 136 \ \mu L$$

Hence, 136 µL were the maximum volume to be put in the glass chamber wells.
When pipetting 100 µL in each glass chamber well, the height of the mucus were calculated

$$\frac{100 \ mm^3}{80 \ mm^2} = 1.25 \ mm$$

When 100 µL of mucus were put in each well and 100 µL nanoparticle solution put on top, also the height and volume of the nanoparticle solutions possible to visualise were calculated

$$1.7 \ mm - 1.25 \ mm = 0.45 \ mm$$

$$80 \ mm^2 * 0.45 \ mm = 36 \ mm^3 = 36 \ \mu L$$

Appendix C - Calculations and fluorescence intensity measurements from section 3.2 Development of the plate method

C.1 Calculation of the percentage mucus wet weight to evaporate during the drying procedure

The following is an example on how the percentage of wet weight to have evaporated from the mucus during drying, were calculated.

The measured weight of the microtitrer plate prior to addition of mucus: 50.37 g.

The measured weight of the microtitrer plate after addition of mucus: 51.97 g

The weight of the added mucus:

$$51.97\ g - 50.37\ g = 1.60\ g$$

The measured weight of the plate after the mucus has dried for 30 h: 50.91 g

The weight of the mucus that has evaporated:

$$51.97\ g - 50.91\ g = 1.06\ g$$

Percentage of the mucus wet weight that has evaporated during drying:

$$\frac{1.06\ g}{1.60\ g} \times 100\ \% = 66.25\ \%$$

Replicate experiments yielded results that lay within 65-70 %.

C.2 Fluorescence intensity measurements by the plate reader

C.2.1. Background fluorescence measurements on dried and fresh biosimialar mucus

The results from the first fluorescence intensity measurements on different states of biosimilar mucus are presented in Table C.1.

Table C.1 The background fluorescence intensity measurements of dried biosimilar mucus, dried biosimilar water with MQ-water on top and fresh biosimilar mucus. The ex./em. wave-lengths of the measurement were set to 495/535 nm. The lower row in the table resents the average values of the eight replicates.

Dried biosimilar mucus	Dried biosimilar mucus + MQ-water	Fresh bisoimilar mucus
35583	31064	30620
39320	30962	30955
40631	35032	30749
45187	33084	31246
45239	31978	30326
38986	32963	29429
42881	32449	30180
39680	30957	29354
40938.38	**32311.13**	**30357.38**

C.2.2 Additional background fluorescence measurements

For a more thorough investigation of the background fluorescence of different states of PSIM and biosimilar mucus, additional background fluorescence measurements were conducted. The results are presented in Table C.2, Table C.3, Table C.4 and Table C.5.

Table C.2 Fluorescence intensity measurements of eight replicates of fresh biosimilar mucus, fresh PSIM, 5% (w/v) Sigma solution, yellow-green FluoSpheres® (0.00001 % (w/v)), red FluoSpheres® (0.00001% (w/v)), MQ-water and empty wells. The fluorescence measurements are performed with ex./em. wave-lengths of 505/545 nm, and with 200 µL sample in each well. The values of the bottom row are average values of the eight replicate measurements.

Empty	MQ-water	Sigma mucin 5 %	Biosimilar mucus	PSIM	yellow-green (0.00001 %)	red (0.00001 %)
27	29	23396	31795	40309	572	34
17	36	24087	32250	44218	656	35
19	28	24804	32213	43286	635	35
17	25	24446	30025	42033	628	28
23	22	24354	31464	39585	664	36
26	45	24614	31860	37561	629	35
25	26	25077	31595	40659	570	32
29	28	23997	29449	39372	645	36
22,875	**29,875**	**24346,88**	**31331,38**	**40877,88**	**624,875**	**33,875**

Table C.3 Fluorescence intensity measurements of eight replicates of fresh biosimilar mucus, fresh PSIM, 5% (w/v) Sigma solution, yellow-green FluoSpheres® (0.00001 % (w/v)), red FluoSpheres® (0.00001% (w/v)), MQ-water and empty wells. The fluorescence measurements are performed with ex./em. wave-lengths of 580/625 nm, and with 200 µL sample in each well. The values of the bottom row are average values of the eight replicate measurements**.**

Empty	MQ-water	Sigma mucin 5 %	Biosimilar mucus	PSIM	yellow-green (0.00001 %)	red (0.00001 %)
28	46	7709	8532	39823	25	987
25	50	7919	8802	43913	42	1091
29	70	7866	8838	43828	41	1013
39	36	7974	8248	40532	56	965
62	34	8083	8415	37503	58	1046
27	48	7719	8340	31464	49	1131
36	52	8088	8841	40866	35	1157
47	62	7764	8164	40225	59	1060
36,625	**49,75**	**7890,25**	**8522,5**	**39769,25**	**45,625**	**1056,25**

Table C.4 Fluorescence intensity measurements of eight replicates of dried biosimilar mucus (BSM), dried biosimilar mucus and MQ-water, fresh biosimilar mucus, dried PSIM, 5% (w/v) Sigma solution, yellow-green FluoSpheres® (0.00001 % (w/v)), red FluoSpheres® (0.00001% (w/v)), MQ-water and empty wells. The fluorescence measurements is performed with ex./em. wave-lengths of 495/535 nm. The volume of sample in each well was 200 µL. The bottom row gives the average fluorescent intensity measurements of the eight replicate samples.

Empty	MQ-water	Dried biosimilar mucus	Dried biosimilar mucus + MQ-water	Fresh biosimilar mucus	Dried PSIM	Sigma mucin 5 %	Yellow-green (0.00001 %)	red (0.00001 %)
33	22	24724	35958	43923	39690	32483	2969	19
33	21	21226	36420	42028	41618	31549	2941	19
41	25	23172	34737	42859	36930	31453	2970	22
36	24	17794	32317	42561	32679	31468	2907	16
42	23	25298	35154	43115	32572	31292	2957	23
38	29	25414	34686	43800	26385	31061	2621	18
43	23	25906	28538	43802	29328	31016	3097	21
36	17	21507	33232	42580	26208	30561	2958	19
37,75	**23**	**23130,13**	**33880,25**	**43083,5**	**33176,25**	**31360,38**	**2927,5**	**19,625**

Table C.5 Fluorescence intensity measurements of eight replicates of dried biosimilar mucus (BSM), dried biosimilar mucus and MQ-water, fresh biosimilar mucus, dried PSIM, 5% (w/v) Sigma solution, yellow-green FluoSpheres® (0.00001 % (w/v)), red FluoSpheres® (0.00001% (w/v)), MQ-water and empty wells. The fluorescence measurements is performed with ex./em. wave-lengths of 580/615 nm. The volume of sample in each well was 200 µL. The bottom row gives the average fluorescent intensity measurements of the eight replicate samples.

Empty	MQ-water	Dried biosimilar mucus	Dried biosimilar mucus + MQ-water	Fresh biosimilar mucus	Dried native PSIM	Sigma mucin 5 %	Yellow-green (0.00001 %)	red (0.00001 %)
70	162	21046	30194	38760	47268	25099	148	3919
149	108	18959	29792	38734	45359	26427	154	4350
146	125	19908	31681	40539	45568	26143	135	4359
110	170	16454	32617	40567	43521	27023	151	4308
124	147	21091	33992	40195	39693	26875	167	4190
158	134	21875	33174	42464	35236	27191	146	4335
155	115	21646	29404	41050	32373	28480	121	4359
85	164	18592	30718	39455	34162	28035	159	4147
124,62	**140,62**	**19946,38**	**31446,5**	**40220,5**	**40397,5**	**26909,13**	**147,62**	**4245,87**

C.2.3 Sigma mucin gradient experiments

The results from the Sigma mucin gradient experiments are presented in Table C.6, Table C.7, Figure C.1 and Figure C.2.

Table C.6 The fluorescence intensity measured in three replicates of Sigma mucin solutions of different concentrations (indicated by the percentages (w/v)). The bottom row presents the average values of the three replicates. The ex./em. wave-length of the measurement was 495/535 nm.

Empty	MQ-water	0.05 %	0.1 %	0.5 %	1 %	5 %
38	46	505	844	4266	7629	41400
30	42	554	896	4360	8032	43138
31	38	539	925	4514	8347	43277
33	42	532.67	888.33	4380	8002.67	42605

Table C.7 The fluorescence intensity measured in three replicates of Sigma mucin solutions of different concentrations (indicated by the percentages (w/v)). The bottom row presents the average values of the three replicates. The ex./em. wave-length of the measurement was 580/615 nm.

Empty	MQ-water	0.05 %	0.1 %	0.5 %	1 %	5 %
140	249	620	912	4187	7285	41307
273	294	707	993	4041	7274	42071
210	222	536	1147	4110	7967	42399
207.67	255	621	1017.33	4112.67	7508.67	41925.67
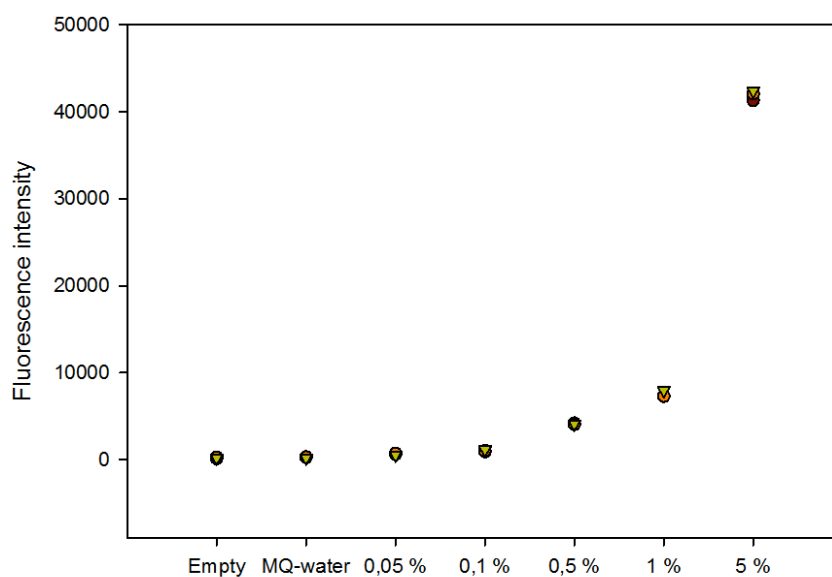
Figure C.1 The fluorescence intensity measured in three replicates of Sigma mucin solutions of different concentrations (indicated by the percentages (w/v)). The ex./em. wave-length of the measurement was 580/615 nm.
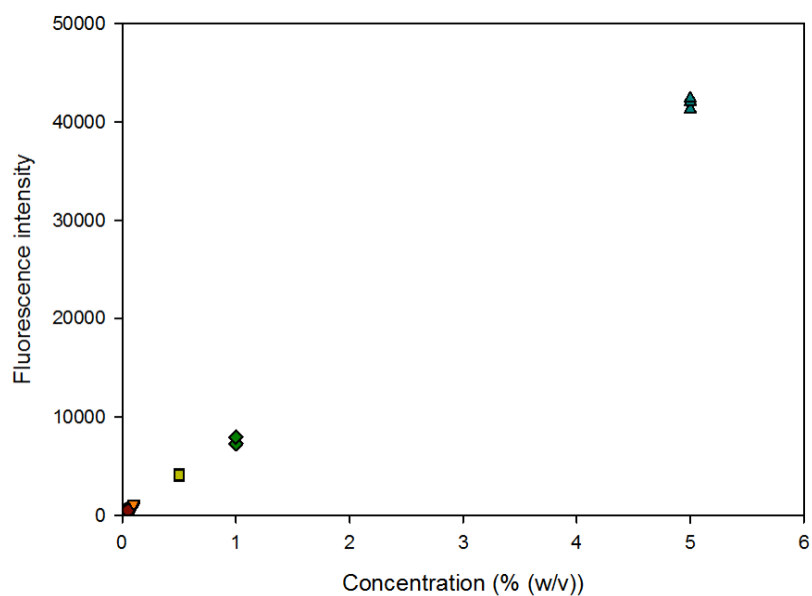
Figure C.2 Sigma mucin gradient The fluorescence intensity measured in three replicates of Sigma mucin solutions of different concentrations). The ex./em. wave-length of the measurement was 580/615 nm.

C.2.4 Fluorescence intensity measurements of differing amount of fresh PSIM and biosimilar mucus

The background fluorescence intensity were measured for differing amounts of fresh biosimilar mucus and fresh PSIM, and the results are presented in Table C.8, Table C.9 and Figure C.3.

Table C.8 Fluorescence intensity measurements of eight replicates of 100 µL amounts of fresh biosimilar mucus, 200 µL fresh biosimilar mucus, 100 µL fresh PSIM and 200 µL fresh PSIM. The ex./em. wavelengths of the measurements were 495/515 nm.

100 µL PSIM	100 µL Biosimilar mucus	200 µL PSIM	200 µL Biosimilar mucus
29727	16723	42902	25795
24973	18470	41400	24065
29029	14931	35491	25491
29820	14376	38088	25647
32701	16784	45496	26235
38626	15671	36721	25530
32040	18779	37397	25931
31191	15738	31638	24453
31013,38	**16434**	**38641,63**	**25393,38**

Table C.9 Fluorescence intensity measurements of eight replicates of 100 µL amounts of fresh biosimilar mucus, 200 µL fresh biosimilar mucus, 100 µL fresh PSIM and 200 µL fresh PSIM. The ex./em. wavelengths of the measurements were 580/615 nm.

100 µL PSIM	100 µL Biosimilar mucus	200 µL PSIM	200 µL Biosimilar mucus
34678	19865	37784	23881
30064	21864	36153	23846
33877	16858	31850	23732
36364	17615	33078	23052
36978	20371	37669	23604
43429	18118	31784	23583
38283	21037	32094	23619
35983	17823	27363	22468
36207	**19193,88**	**33471,88**	**23473,13**
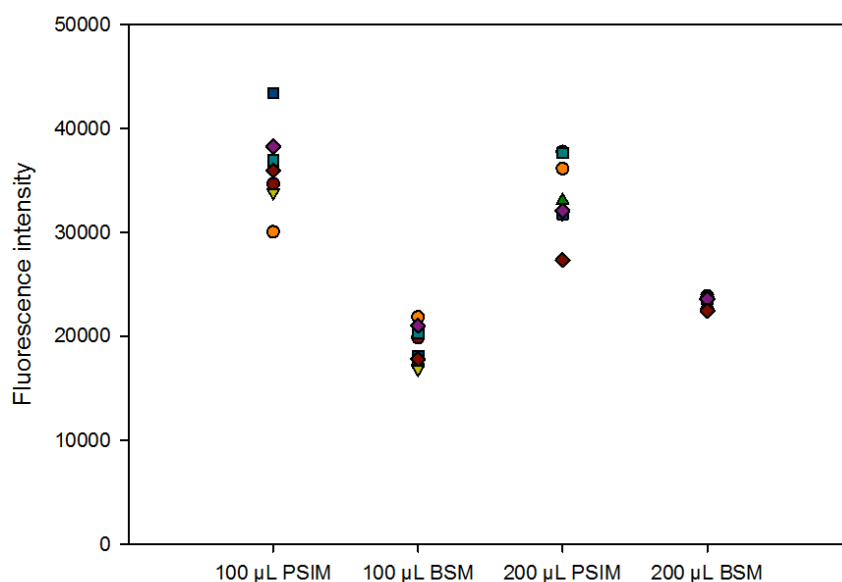
Figure C.3 Fluorescence intensity measurements of eight replicates of 100 µL amounts of fresh biosimilar mucus, 200 µL fresh biosimilar mucus, 100 µL fresh PSIM and 200 µL fresh PSIM. The ex./em. wavelengths of the measurements were 580/615 nm.

Appendix D – Rheological measurements from section 3.3.5 Control rheological measurements of Sigma mucin solutions

The results of the rheological measurements of the Sigma mucin solutions not presented in Results and Discussion section 3.3.5, is presented in this Appendix.

D.1 Rheolgical measurements of the Sigma mucin solutions – strain sweeps
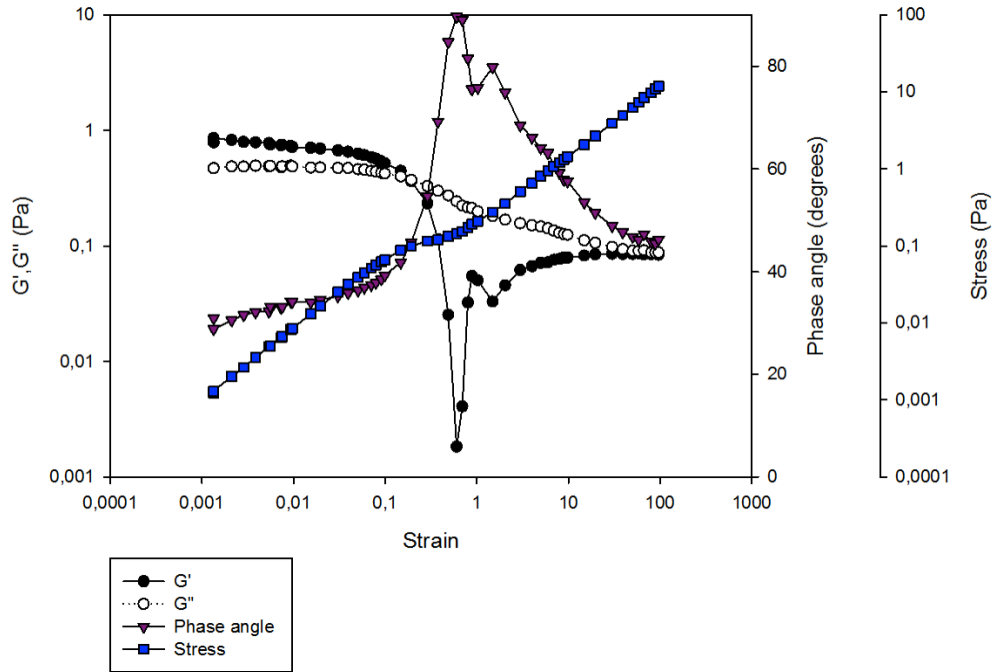
Figure D.1 Stain sweep of a 5 % (w/v) Sigma mucin solution in the strain range 0.001-100. The temperature of the measurement were 25 °C, and the frequency 1 Hertz.
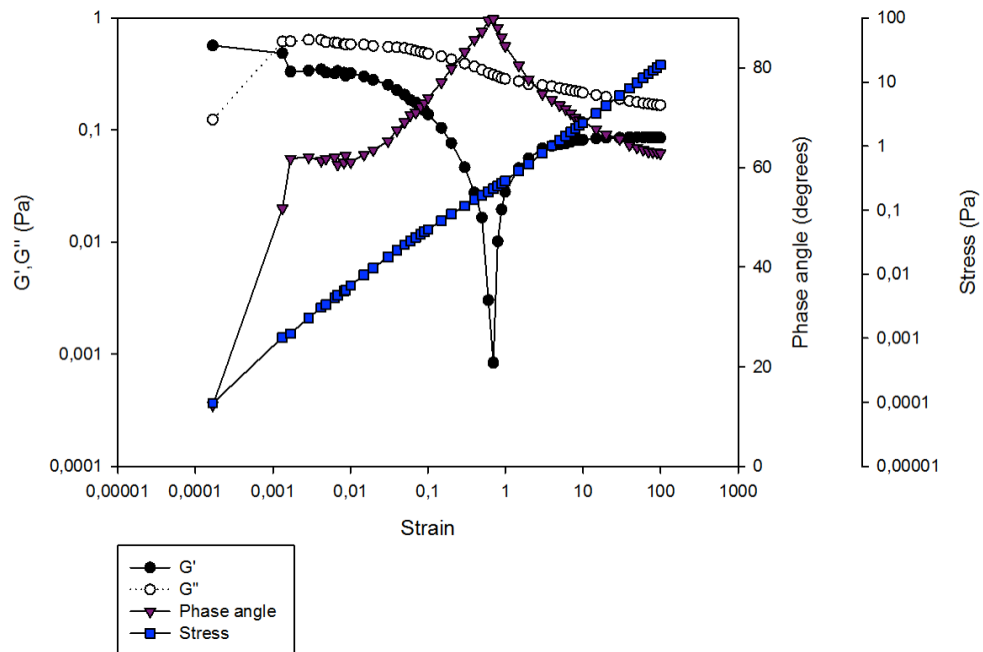

Figure D.2 Stain sweep of an 8 % (w/v) Sigma mucin solution in the strain range 0.001-100. The temperature of the measurement were 25 °C, and the frequency 1 Hertz.
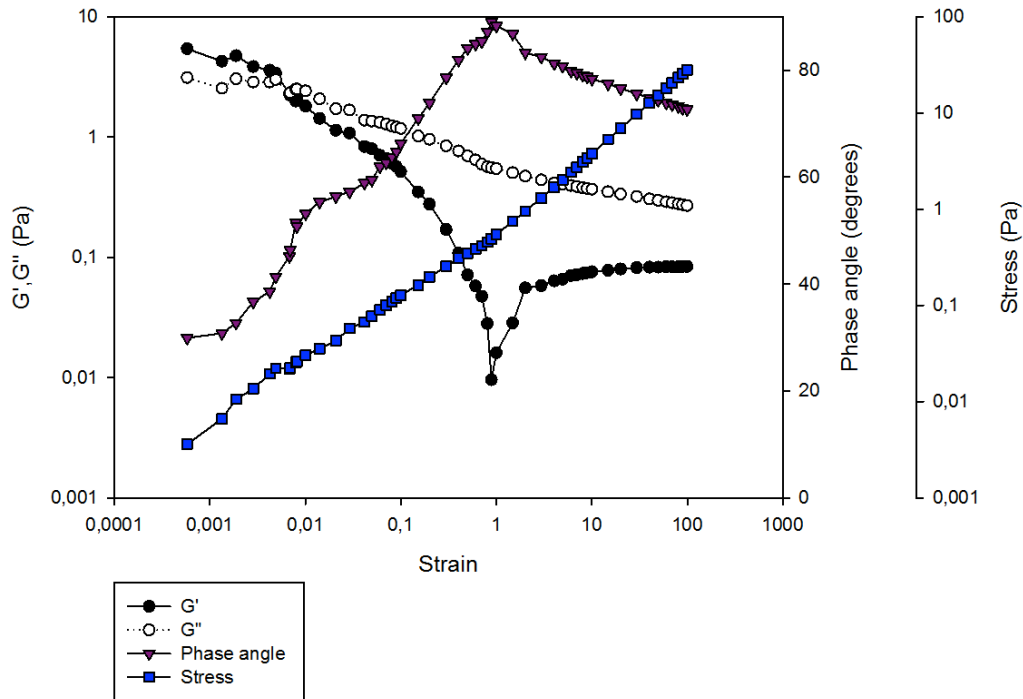
Figure D.3 Stain sweep of a 10 % (w/v) Sigma mucin solution in the strain range 0.001-100. The temperature of the measurement were 25 °C, and the frequency 1 Hertz.
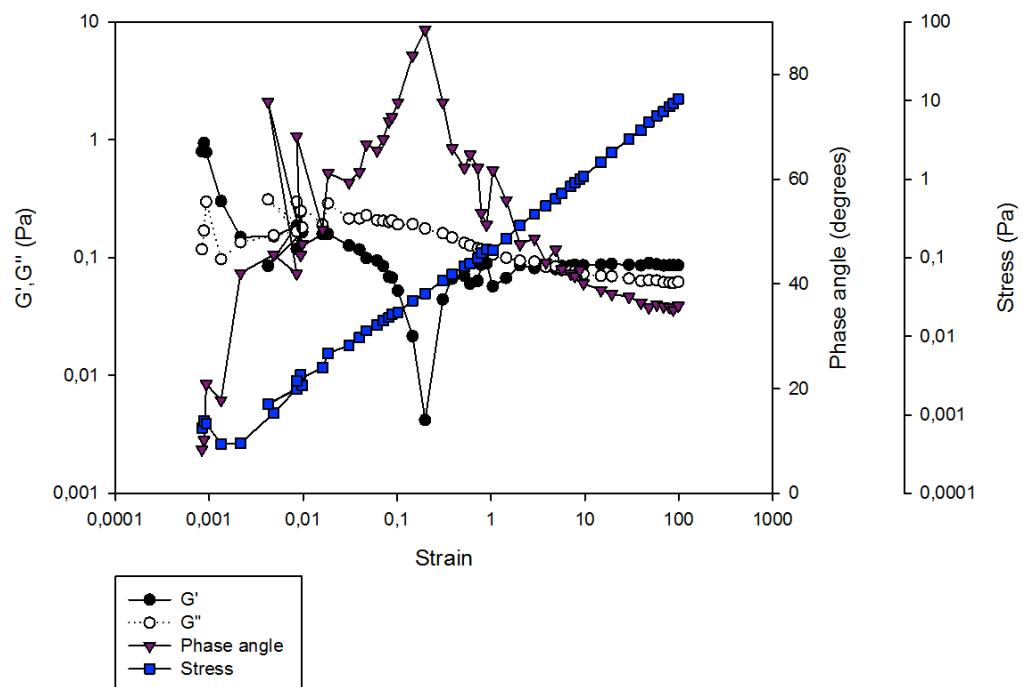
Figure D.4 Stain sweep of a 5 % (w/v) Sigma mucin solution in the strain range 0.001-100. The temperature of the measurement were 37 °C, and the frequency 1 Hertz.
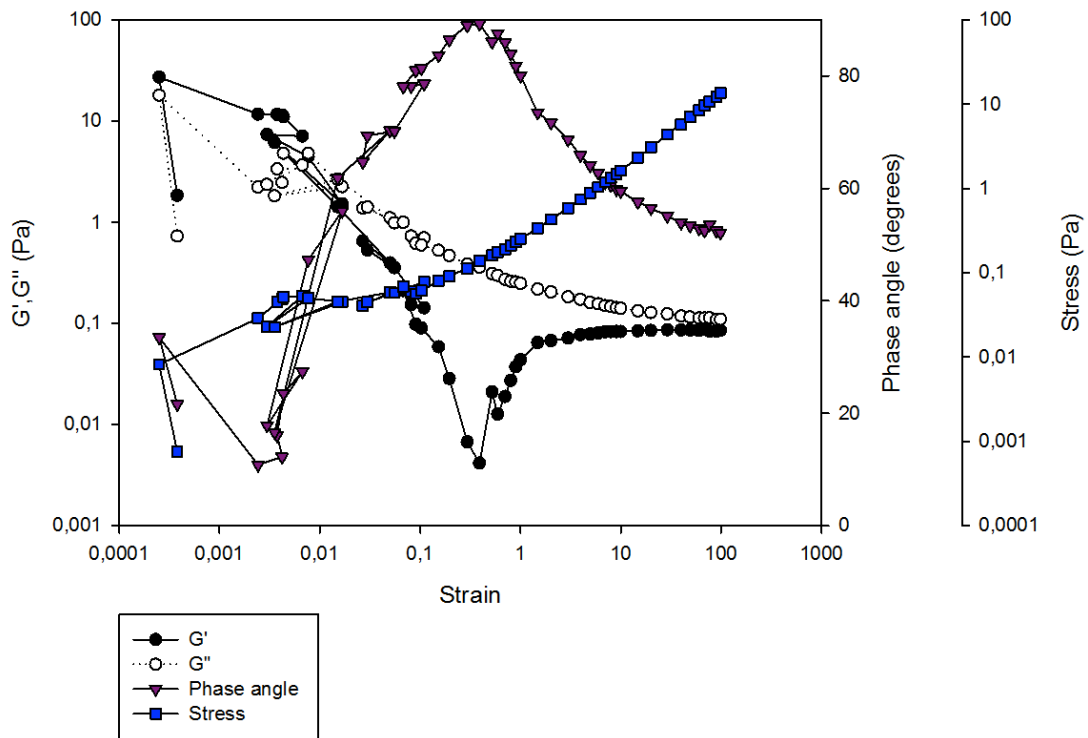
**Figure D.5** Stain sweep of an 8 % (w/v) Sigma mucin solution in the strain range 0.001-100. The temperature of the measurement were 37 °C, and the frequency 1 Hertz.
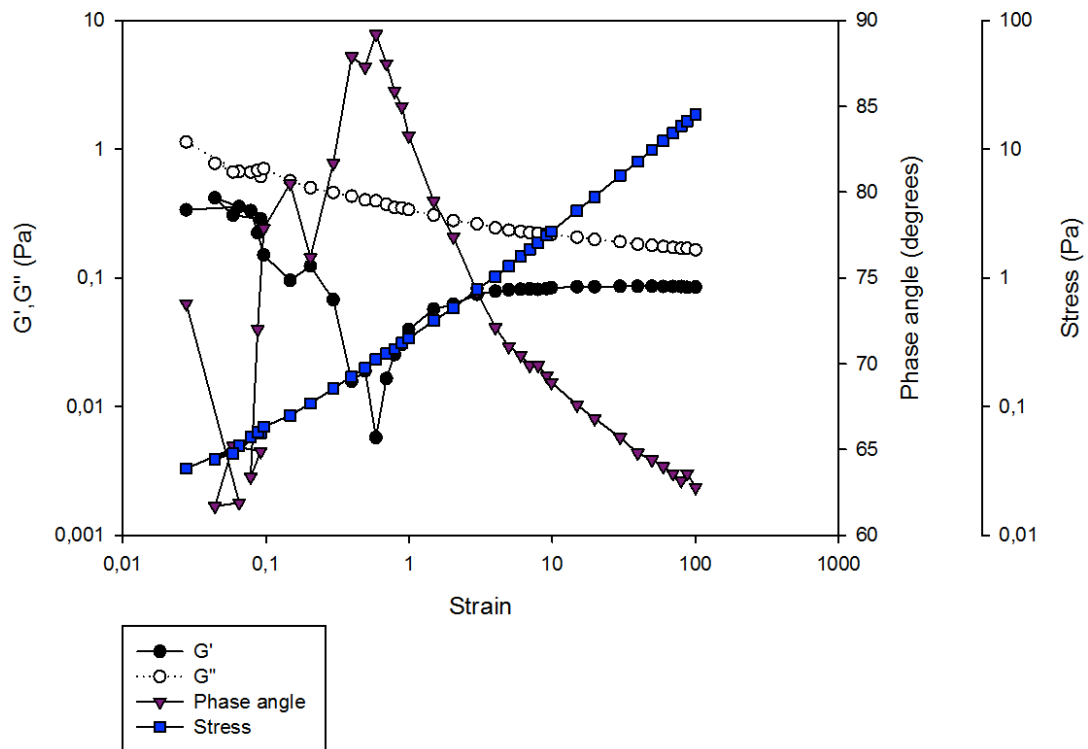
Figure D.6 Stain sweep of a 10 % (w/v) Sigma mucin solution in the strain range 0.001-100. The temperature of the measurement were 37 °C, and the frequency 1 Hertz.

D.2 Rheolgical measurements of the Sigma mucin solutions – frequency sweeps
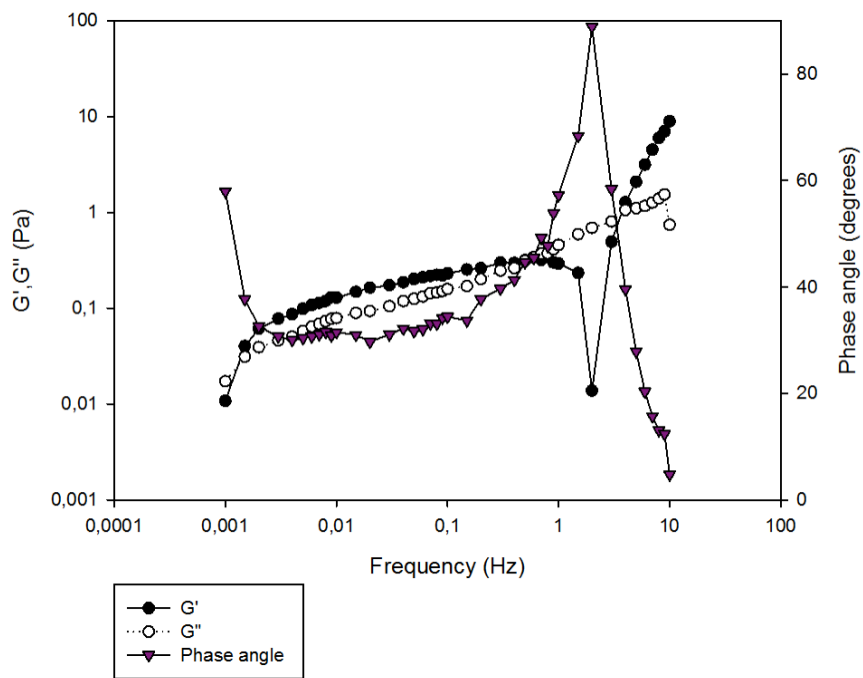
Figure D.7 Frequency sweep of a 5 % (w/v) Sigma mucin solution in the frequency range 0.001-100 Hertz. The temperature of the measurement were 15 °C, and the strain fixed to 0.05.
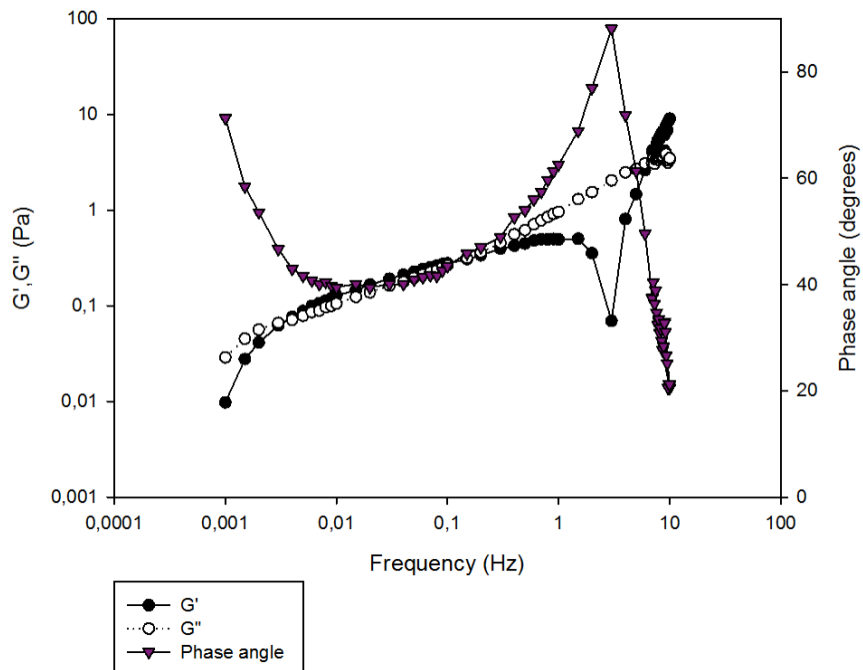

Figure D.8 Frequency sweep of an 8 % (w/v) Sigma mucin solution in the frequency range 0.001-100 Hertz. The temperature of the measurement were 15 °C, and the strain fixed to 0.05.
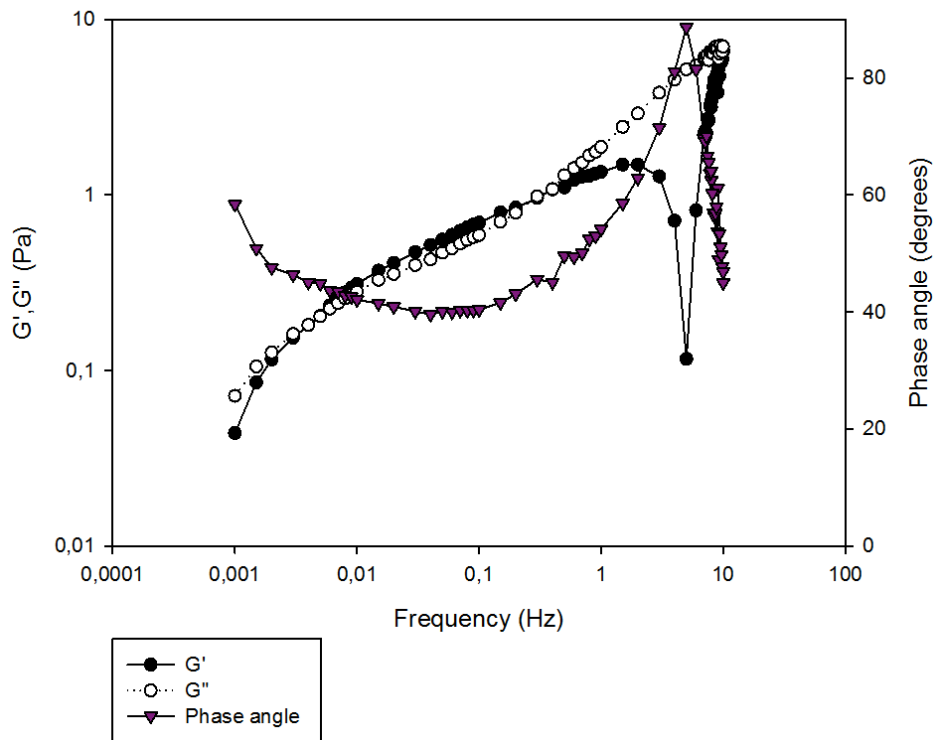
Figure D.9 Frequency sweep of a 10 % (w/v) Sigma mucin solution in the frequency range 0.001-100 Hertz. The temperature of the measurement were 15 °C, and the strain fixed to 0.05.
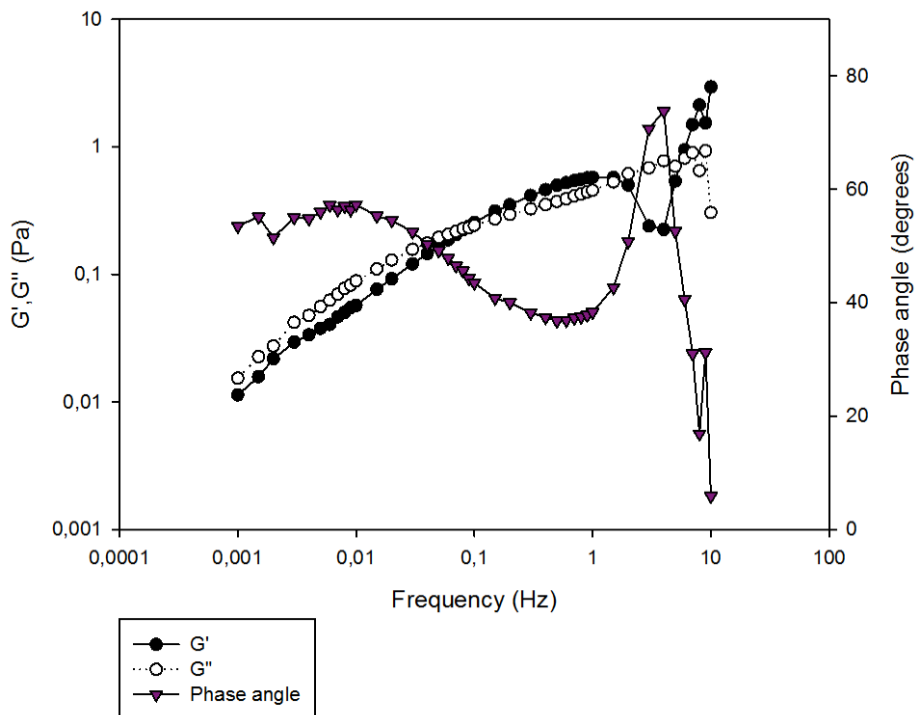

Figure D.10 Frequency sweep of a 5 % (w/v) Sigma mucin solution in the frequency range 0.001-100 Hertz. The temperature of the measurement were 25 °C, and the strain fixed to 0.05.
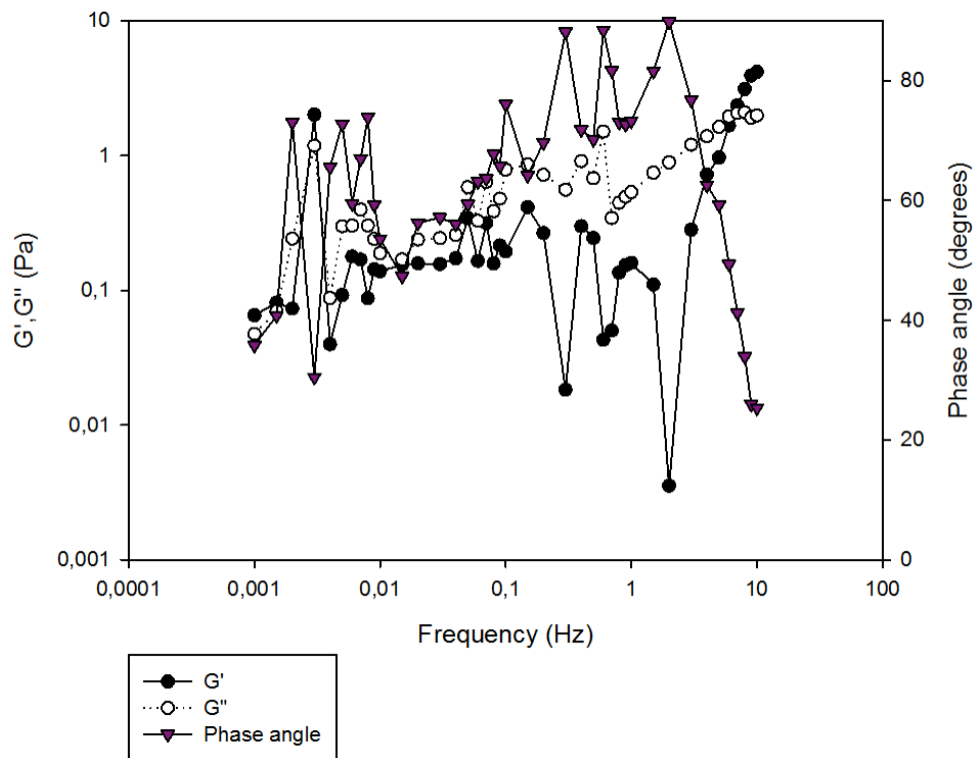
Figure D.11 Frequency sweep of an 8 % (w/v) Sigma mucin solution in the frequency range 0.001-100 Hertz. The temperature of the measurement were 25 °C, and the strain fixed to 0.05.
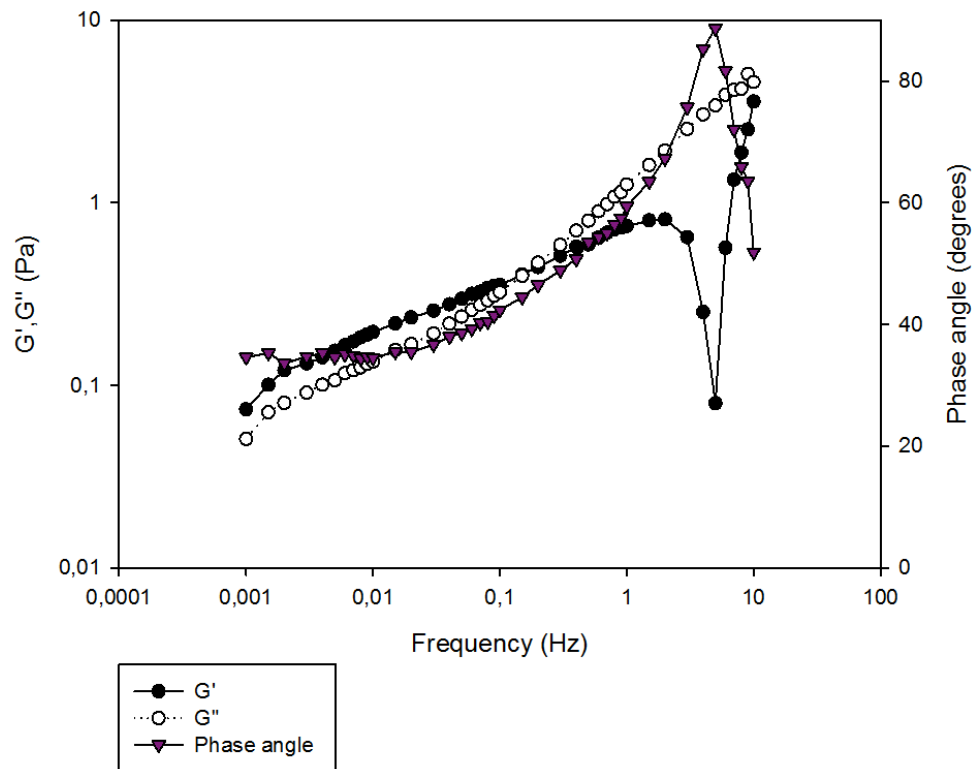
Figure D.12 Frequency sweep of a 10 % (w/v) Sigma mucin solution in the frequency range 0.001-100 Hertz. The temperature of the measurement were 25 °C, and the strain fixed to 0.05.

XXIV